

Simple, Environmentally Friendlier Materials

in Green Chemical Applications

by

Cody Nathaniel Sherren

A Thesis Submitted to Saint Mary's University, Halifax, Nova Scotia

in Partial Fulfillment of the Requirements for the Degree of

Master of Science in Applied Science

September, 2010, Halifax, Nova Scotia

Copyright Cody Nathaniel Sherren.

Approved: Dr. Jason Clyburne
Supervisor

Approved: Dr. Jason Masuda
Examiner

Approved: Dr. Christian
Suteanu
Examiner

Dr. Stephanie
MacQuarrie
External Examiner

Date: October 4, 2010

Abstract

Simple, Environmentally Friendlier Materials
in Green Chemical Applications

By Cody Nathaniel Sherren

November 1, 2010

Green chemistry is a popular class of chemistry in which certain principles are followed to minimize the negative impact of chemical processes. The principles focused on here include designing safer chemicals and the usage of catalysts. This work can be divided in four parts.

- 1) The ionic liquid 1-ethyl-3-methylimidazolium aluminum tetrachloride was reacted with lithium to produce a persistent radical that was characterized. This radical was similar to one detected in previous work involving the reaction of tetrakis(dimethylamino)ethylene with muonium.
- 2) Three novel carbonyl stabilized ylides were synthesized and, in one case, subsequently methylated in an attempt to produce a new C(0) compound.
- 3) Fatty acid-based ionic liquids were synthesized and tested as oil dispersants against Corexit™ 9500, a commercial product used in the cleanup of the Gulf of Mexico in 2010.
- 4) Amino sugar-based Schiff's bases were synthesized as potential alternatives to ubiquitous metal chelator ethylenediaminetetraacetic acid (EDTA).

Acknowledgements

I would like to begin by thanking Dr. Jason Clyburne. None of this work would have been accomplished without him, so I am deeply grateful. He has been an excellent supervisor and mentor, for matters both personal and professional, over the past two years.

Secondly, I would like to acknowledge the Clyburne group. Miller Makramalla, Luke Murphy and Jessica McClintick have been incredibly helpful in completing the experimentation for sections 3, 4 and 5 in this thesis and Dr. Katherine Robertson, who has been a great help in determining crystal structures, processing NMR and general review and editing. I would also like to thank Naomi Harper, not only for her camaraderie, but also for the decadent dishes she would prepare and share. It would have been a much less interesting couple of years if I had been the only member of the group going through this program. I would also like to acknowledge remaining Clyburne group members, both past and present for their assistance and friendship over the years.

Thirdly, I would like to thank my supervisory committee for taking the time to review my work, Dr. Cory Pye for all of his help with calculations, Dr. Marc Lamoureux for helping me figure out analytical techniques, Dr. Charles Walsby, Dr. Tim Storr and Changhua Mu at SFU for their hospitality and help with EPR, Dr. Paul Percival for his work at TRIUMF, Nick Giffin for the synthesis of TEMPOH (along with his infectious positive attitude), Arthur Hendsbee for all of his hard work with crystal structures, Tara Inman who has been indispensable in all matters administrative and is always up for a discussion, and the chemistry technicians Elizabeth McLeod, Darlene Goucher, John Tobin and Anna D'Intino who have been wonderful for procuring all of the materials I needed. Thank you also to Saint Mary's University and to NSERC for providing the funding necessary to complete these projects.

Finally I would like to thank my family. Katie Mills has been a wonderful source of support and understanding who is always trying her best to help me out. I always appreciate it. I would also like to thank my parents and brother for being so supportive, compassionate and proud.

Table of Contents:

Abstract.....	ii
Acknowledgements.....	iii
List of Figures	vii
List of Schemes	ix
List of Tables.....	xi
Table of Abbreviations.....	xii
1 Introduction to Ionic Liquids and Green Chemistry.....	2
2 The Generation and Characterization of a Radical in an Ionic Liquid.....	6
2.1 Ionic Liquids, NHCs and EROs.....	6
2.2 Synthesis of Ionic Liquid and Detection of Radical.....	8
2.3 Relation to Previous Muonium Work.....	13
2.4 Conclusion.....	13
2.5 Experimental	14
2.5.1 Preparation of ionic liquid.....	14
2.5.2 EPR measurements.....	15
2.5.3 Calculations.....	16
3 Synthesizing a C(0) Species with Carbonyl Stabilized Ylides.....	18
3.1 Phosphorus ylides.....	18
3.2 Properties and Reactivity of Ketenylidenetriphenylphosphorane	20

3.2	Results and Discussion	24
3.2.1	Synthesis of Three Carbonyl Stabilized Ylides	24
3.2.2	Methylation of a Carbonyl Stabilized Ylide	29
3.3	Conclusion.....	32
3.4	Experimental	33
3.4.1	Equipment and analysis	33
3.4.2	Preparation of compounds.....	34
4	Biodegradable Ionic Liquids as Oil Dispersants	38
4.1	Ionic Liquids, Surfactants and Oil Dispersants	38
4.2	Toxicity of Ionic Liquids	40
4.3	Biodegradable Ions	41
4.4	Results and Discussion	43
4.4.1	Preparation of Ionic Liquid Dispersants	43
4.4.2	Characterization of Ionic Liquids.....	44
4.4.3	Baffled Flask Test.....	45
4.4.4	Analysis of samples by GC/FID	47
4.5	Conclusion.....	50
4.6	Experimental Data – Ionic Liquids Characterization Data	51
5	Potentially Biodegradable Schiff's Bases as Chelating Agents	53
5.1	Chelating Agents	53

5.2	EDTA – Ethylenediaminetetraacetic Acid.....	54
5.2.1	Prevalence of EDTA	54
5.2.2	Concerns with EDTA	55
5.3	Amino Sugar Schiff's Bases	56
5.4	Stability constants	58
5.5	Results and discussion.....	59
5.5.1	Synthesis and Characterization Four Schiff's Base Ligands.....	59
5.5.2	Binding studies	65
5.6	Conclusion.....	73
5.7	Experimental	74
5.7.1	Equipment and analysis	74
5.7.2	Preparation of ligands.....	75
5.7.3	Preparation of solutions for the binding study.....	81
5.7.4	Binding study.....	82
6.	Conclusion.....	83
	References.....	84
	Appendix A	92
	Appendix B	125

List of Figures

Figure 1: Some commonly used ions in ionic liquids	3
Figure 2: Structures of imidazolium ion, N-heterocyclic carbene and EROs	6
Figure 3: Experimental and simulated EPR data	10
Figure 4: Structure and SOMO of generated radical	12
Figure 5: General formula for phosphacumulene and phosphallene ylide	19
Figure 6: Ketenyliidenetriphenylphosphorane drawn three ways	20
Figure 7: Thermal ellipsoid plot of trimethylphenol carbonyl stabilized ylide	26
Figure 8: Thermal ellipsoid plot of tert-butylhydroxytoluene CSY	27
Figure 9: Thermal ellipsoid plot of TEMPOH carbonyl stabilized ylide	28
Figure 10: HOMO of trimethylphenol carbonyl stabilized ylide	29
Figure 11: Thermal ellipsoid plot of methylated trimethylphenol product	31
Figure 12: GC calibration curve of Mesa oil standards	48
Figure 13: Concentration of Mesa oil in samples as determined by GC/FID	50
Figure 14: EDTA – ethylenediaminetetraacetic acid	54
Figure 15: General structure for a Schiff's base	56

Figure 16: D-glucosamine and salicylaldehyde	57
Figure 17: Reagents used to form the four Schiff's base ligands	60
Figure 18: Mechanism of amine aldehyde condensation	62
Figure 19: The synthesized amino sugar-based Schiff's bases	63
Figure 20: Thermal ellipsoid plot of glucosamine-salicylaldehyde Schiff's	64
Figure 21: Graph of voltage recorded during first Schiff's base titration	66
Figure 22: Graph of calibration curve for first Schiff's base titration	67
Figure 23: Graph of Cu^{2+} detected in first Schiff's base titration	67
Figure 24: Adam and Hall's metal-ligand chelate structure	69
Figure 25: Graph of Cu^{2+} detected in second Schiff's base titration	70
Figure 26: Graph of Cu^{2+} detected in third Schiff's base titration	72
Figure 27: Graph of Cu^{2+} detected in fourth Schiff's base titration	72
Figure 28: Graph of Cu^{2+} detected in first titration of deionized water	73

List of Schemes

Scheme 1: Postulated reaction mechanism producing the observed radical	9
Scheme 2: The addition of muonium to an electron rich olefin	13
Scheme 3: Synthesis of an alkene from a phosphorus ylide	18
Scheme 4: The reaction of ketylidetriphenylphosphorane with EI-Nu	21
Scheme 5: The formation of a Pt-substituted ketene	22
Scheme 6: The formation of a bisketene Pt cation	23
Scheme 7: Reaction of ketylidetriphenylphosphorane with a protic Nu	23
Scheme 8: Reaction of the three protic nucleophiles	25
Scheme 9: Proposed mechanism for methylation	30
Scheme 10: Experimental methylation of trimethylphenol CSY	30
Scheme 11: Synthesis of trimethylphenol carbonyl stabilized ylide	34
Scheme 12: Synthesis of tert-butylhydroxytoluene carbonyl stabilize ylide	35
Scheme 13: Synthesis of TEMPOH carbonyl stabilized ylide	36
Scheme 14: Synthesis of methylated trimethylphenol ylide	37
Scheme 15: Synthesis of glucosamine-salicylaldehyde Schiff's base	76

Scheme 16: Synthesis of glucosamine-pyridoxal Schiff's base	77
Scheme 17: Synthesis of tetraacetylglucosamine-salicylaldehyde Schiff's	79
Scheme 18: Synthesis of tetraacetylglucosamine-pyridoxal Schiff's base	80

List of Tables

Table 1: Important bond lengths and angles of several potential species	11
Table 2: Characteristics of synthesized carbonyl stabilized ylides	32
Table 3: Structures of choline, oleate, erucate, linoleate and laurate	42
Table 4: List of sample IDs for dispersant test	46
Table 5: Concentration of Mesa TM crude oil in calibration standards	47
Table 6: Concentration of Mesa TM crude oil in each sample	49
Table 7: List of IR peaks arising from imines	64

Table of Abbreviations

Abbreviation	Full name
[C ₆ mim]	1-hexyl-3-methylimidazolium
aCu ²⁺	Chemical activity of Cu ²⁺
CSY	Carbonyl stabilized ylide
d	Doublet (IR)
DFT	Density functional theory
E	Potential
E°	Standard potential
EA	Elemental Analysis
EDTA	Ethylenediaminetetraacetic acid
EPR	Electron paramagnetic resonance
ERO	Electron rich olefin
F	Faraday constant
FID	Flame ionization detector
GC	Gas chromatograph(y)

HOMO	Highest occupied molecular orbital
IR	Infrared
ISAB	Ionic strength adjustment buffer
IUPAC	International union of pure and applied chemistry
LD ₅₀	Median lethal dose
m	Multiplet (IR)
Me	Methyl
n	Number of moles
NHC	N-heterocyclic carbenes
NMR	Nuclear magnetic resonance
OAc	Acetoxy
PEG	Polyethylene glycol
ppm	Parts per million
R	Universal gas constant
RMSD	Root mean square deviation
rpm	Rotations per minute

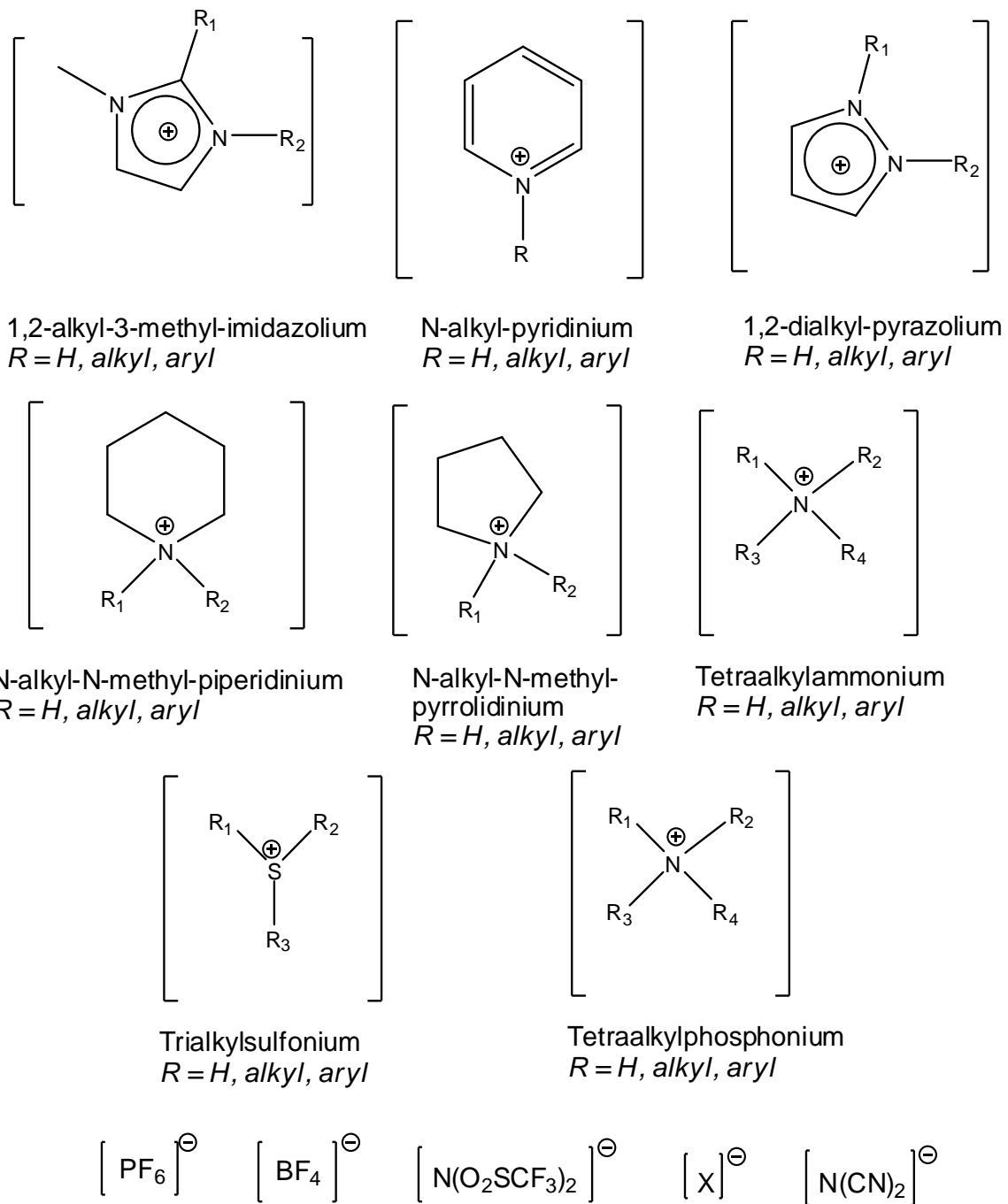
s	Singlet (IR)
SOMO	Singly occupied molecular orbital
t	Triplet (IR)
T	Absolute temperature
TEMPOH	1-hydroxyl-2,2,6,6-tetramethyl-piperidine
TMS	Tetramethylsilane

1 Introduction to Ionic Liquids and Green Chemistry

Ionic liquids are of high interest in many fields of chemistry, such as catalysis, biocatalysis, synthesis, analytical chemistry, electrochemistry, nanotechnology and separation technology.¹

Ionic liquids are also known as molten salts and they refer to any salt which is liquid at or below 100°C at atmospheric pressure.² Though it has been nearly a century since the first synthesis of an ionic liquid, it is only recently that ionic liquids have become popular for use as solvents.³ It is quite astonishing how quickly work with ionic liquids has progressed from the determination of physical properties⁴, to academic experimentation⁵, to industrial promise⁶ and finally to actual industrial application.⁷

Ionic liquids make for very versatile solvents as a particular ionic liquid can be “tailor-made” for a particular reaction. That is to say that an appropriate cation and/or anion can be selected to activate or somehow interact with one or more reagents, resulting in an optimized reaction. Considering the number of cations and the number of anions available to paired, there are millions of different ionic liquids which could be formed (Figure 1).⁷ One may hypothesize that many of the reactions commonly done in conventional solvents may be paired with unique ionic liquids to optimize the speed and/or yield.



X = Br, Cl, I

Figure 1: Some commonly used ions in ionic liquids.

Furthermore, ionic liquids are garnering attention because they are viewed as environmentally friendlier solvents.¹ Although the toxicity of ionic liquids can vary greatly (according to the cation and anion selected), the overwhelming majority of ionic liquids are non-volatile at standard atmospheric pressure.⁷ This non-volatility eliminates the potential for air pollution and provides a safer environment for individuals handling the substance. Additionally, ionic liquids can be reused for future reactions.⁸ This recycling is not only greener, but also helps to offset their higher costs (relative to the many inexpensive conventional solvents), making ionic liquids more appealing to the realm of industry in addition to academia. Finally, depending on the composition of the ionic liquid, it can sometimes be tuned to increase biodegradability.⁹

Contrarily, ionic liquids do also have a number of problems. Due to their recent popularity and vast number of possible combinations, studies which quantify their stability, purity, biodegradability and toxicity are sorely lacking. Additionally, there is a real difficulty in using ionic liquids as reengineering existing processes to take advantage of the ionic liquid's properties can be quite challenging. For a full discussion of the neglected issues, one should be referred to the review by Scammells, Scott and Singer.¹⁰

Though ionic liquids were the original focus, this body of work grew to encompass several aspects of green chemistry by following some of the principles put forth by Anastas and Warner¹¹. With the principle in mind to "Design Safer Chemicals", we endeavored to design biodegradable oil

dispersants and metal chelators. Furthermore, staying true to the principle of catalytic reagents being superior to stoichiometric reagents, the chemistry of carbonyl stabilized ylides and imidazolium radicals, both potential catalysts, were examined. This body of work is separated into four distinct sections with each section existing as a self-contained manuscript ready for publication.

2 The Generation and Characterization of a Radical in an Ionic Liquid

2.1 Ionic Liquids, NHCs and EROs

Imidazolium ions have numerous applications in modern chemistry. First, they are important components in ionic liquids which are promising solvents for a variety of industrial applications⁷. These solvents are particularly attractive due to their low volatility, low flammability, and thermal stability, all features that are important in their successful industrial introduction¹². Secondly, imidazolium ions, specifically 1,3-dialkylimidazolium ions, are precursors to *N*-heterocyclic carbenes (NHC)¹³. These highly basic and extremely reactive compounds are important components in organocatalysts as well as transition metal complexes which often exhibit high catalytic behavior¹⁴.

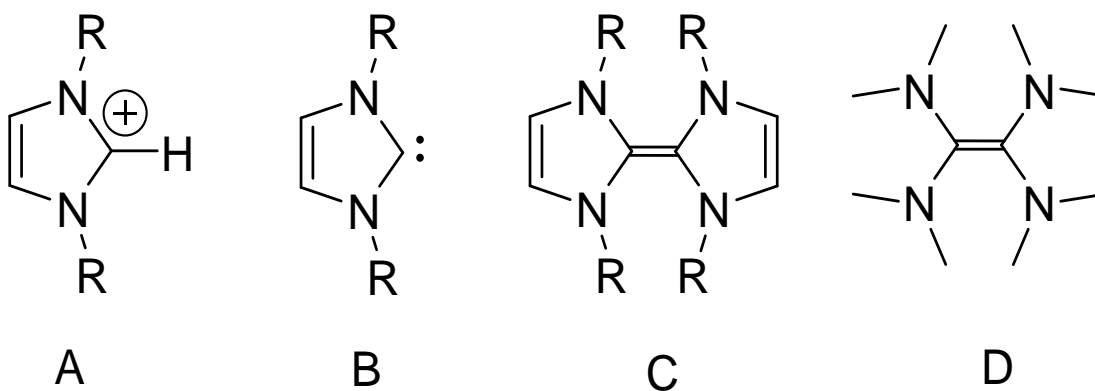


Figure 2: Imidazolium ion **A**, *N*-heterocyclic carbene **B**, electron-rich olefin **C** and tetrakis(dimethylamino)ethylene **D**.

The interplay between imidazolium ions **A** and N-heterocyclic carbenes **B** is, at first glance, simple. Related by the addition/removal of a mere proton, the chemistry of this type of reaction is only in its infancy. Simple protonation studies of NHCs have revealed the formation of numerous types of adducts, including neutral and ionic alternatives depending upon both the nature of the E-H bond (E = C, N, O) as well as the carbene.^{15,16} Also salient to this discussion is the relationship between NHCs **B** and the broad class of molecule known as the electron rich olefin (ERO) **C**. Almost fifty years ago Wanzlick and Buchler proposed that an equilibrium exists between imidazol-2-ylidenes and their tetraamino substituted “dimers”.¹⁷ The important work from Arduengo¹⁸ on the synthesis and isolation of stable free NHCs subsequently facilitated experimental confirmation of this phenomenon.¹⁹ NHCs can be converted to ERO derivatives through a proton catalyzed reaction although there is considerable debate on the mechanism.²⁰ We were interested in identifying whether it would be possible, in broadly basic conditions, to identify a coupling reaction as was recently reported to occur in the radiation damage of ionic liquids.^{21,22,23,24} Here we report the identification of a radical formed in the reaction of lithium metal with a simple imidazolium ion as well as the reaction of a hydrogen atom surrogate (muonium) with an electron rich olefin **D**. The radicals identified may be important in long term use of some ionic liquids in a variety of electron rich applications, including batteries^{25,26} and solar cells.^{27,28}

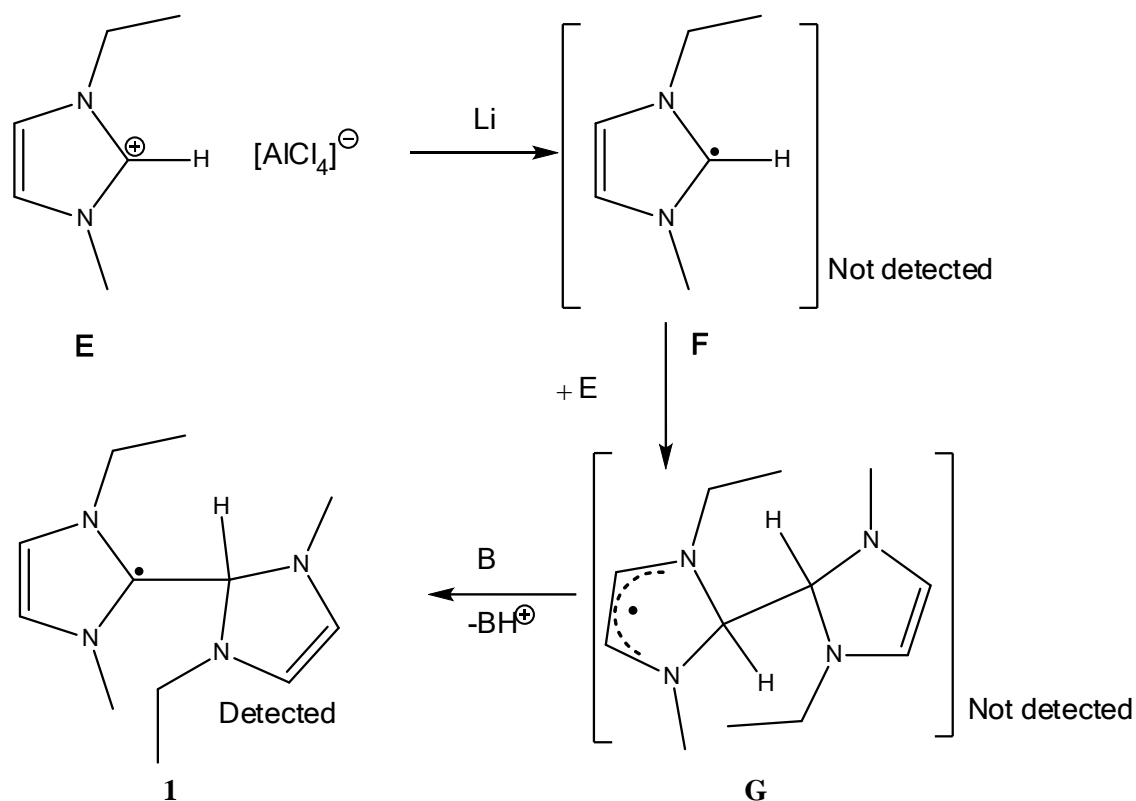
2.2 Synthesis of Ionic Liquid and Detection of Radical

Recognizing the potentially high moisture sensitivity of the radicals we were seeking to prepare we chose to examine the highly moisture sensitive tetrachloroaluminate salts. Generally shunned due to the aforementioned moisture sensitivity, we felt that in this case it would be an asset. The selected IL was composed of 1-ethyl-3-methylimidazolium chloride mixed with 40% AlCl_3 .²⁹ This material is a liquid at room temperature, and the presence of AlCl_3 aids to ensure that the system is anhydrous. The stoichiometry ensures that the mix is basic, with an excess of chloride ion relative to AlCl_3 .

Addition of lithium beads to the solution and subsequent stirring for 24 hours resulted in the formation of a clear, rusty red-brown solution. The unreacted Li beads were removed by filtration. The color of this IL was persistent over several weeks in solution, with decay of the color only when exposed to moist air. A portion of this material was placed inside a 5 mm quartz tube and electron paramagnetic resonance studies were performed on the solution. The data obtained from the study is shown in Figure 3. Our first instinct was to assign the structure to the radical **F** (Scheme 1) but, as seen in Table 1, the observed data is clearly inconsistent with that structure. This led us to consider dimerized carbenes as the mechanisms for such structures have been previously studied.³⁰ The lack of a large ^1H hyperfine coupling constant is consistent with the formation of the radical **1**.

Based upon the careful works of Rouzo³¹ and Shkrob³² examining radiation damage to ionic liquids, we explored alternative structures and calculated their anticipated EPR spectra. Presented in Table 1, several structural alternatives were explored and the major anticipated EPR data for three possible radical structures are reported.

The spectrum, shown in Figure 3, was reproduced accurately by simulation of the generated species. It contains radical-spin coupling to four nitrogen atoms (14N , $I = 1$) and five inequivalent hydrogen atoms (1H , $I = 1/2$).



Scheme 1: Postulated reaction mechanism producing the observed radical. The postulated mechanism invokes the "charge trapping" mechanism proposed by Wishart.²³

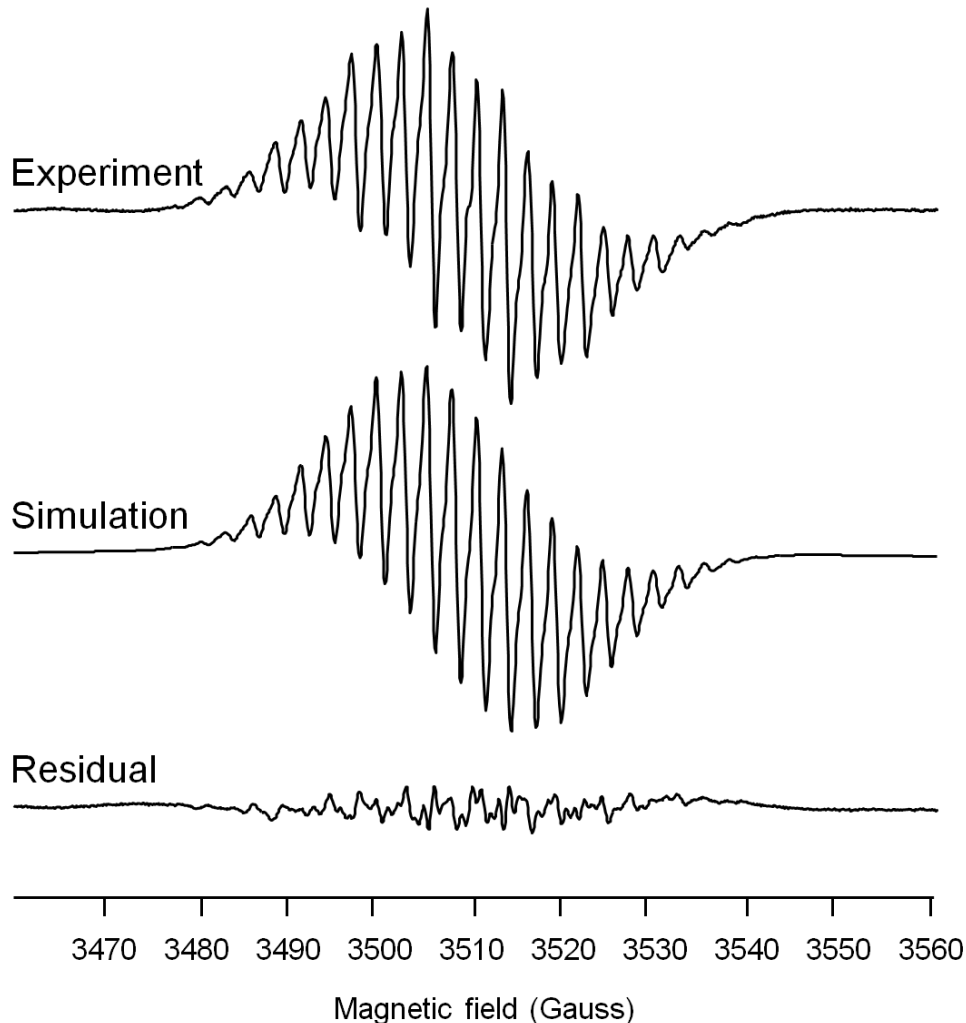


Figure 3: Experimental (top) and simulated (bottom) EPR spectra of the solution formed after treatment of an imidazolium ionic liquid with lithium. **Experimental spectral parameters:** frequency = 9.8383 GHz, modulation amplitude = 1.0 G, time constant = 5.12 ms, sweep time = 20 s, average of 200 scans. **Simulation parameters:** $g = 2.00279$, $a(^{14}\text{N}) = 5.3$ G, $a(^{14}\text{N}) = 5.4$ G, $a(^{14}\text{N}) = 5.4$ G, $a(^{14}\text{N}) = 1.6$ G, $a(^1\text{H}) = 8.4$ G, $a(^1\text{H}) = 5.4$ G, $a(^1\text{H}) = 5.6$ G, $a(^1\text{H}) = 2.8$ G, $A(^1\text{H}) = 2.7$ G, $A(^1\text{H}) = 2.8$ G. Peak-to-peak line-width = 1.3 G, Lorentzian line shapes.

C ₂ -H (Å)	1.077	1.091	1.096			
C ₂ -N ₁ (Å)	1.334	1.420	1.428	1.413	1.487	1.334
C ₂ -N ₃ (Å)	1.335	1.417	1.426	1.435	1.482	1.335
C ₁ -N ₅ (Å)	1.380	1.396	1.386	1.376	1.411	1.380
C ₃ -N ₄ (Å)	1.380	1.391	1.387	1.403	1.413	1.380
C=C (Å)	1.359	1.348	1.351	1.349	1.337	1.359
N-C-N (°)	108.93	104.84	104.33	104.58	102.12	108.93
C ₂ -C _{2'} (Å)	N/A	N/A	1.726		1.496	
EPR Data predicted (Gauss)	N/A	H:26.77, 6.03, 5.04, 2.51, 1.01 N ₁ :2.67, N ₃ :2.38	H: 22.56, 20.98, 8.14, 5.39, 4.40, 2.75, 2.46, 2.25, 1.40 N ₁ :26.47, N ₃ : 7.77, N ₁ :25.62, N ₃ : 13.80		H: 8.48, 4.79, 4.68, 1.52, 1.27, 1.19 N ₁ :3.00, N ₃ : 2.95, N ₁ :1.60, N ₃ : 5.93	

Table 1: Important bond lengths and angles of several species potentially found in reaction mixture.

The structure of radical **1** was probed using computational methods as well. Shown in Figure 4 is the structure of the optimized radical, with important bond lengths and angles included in Table 1. Also shown in Figure 4 is a diagram of the SOMO of **1** illustrating the delocalized nature of the radical. Most interesting is the potential of **1** to behave as a hydrogen atom source, a base, and an oxidant or a reductant. This suggests that if such a species is generated in a working IL solution that the function of the IL may not be decreased as one may have anticipated. In fact, the function could even increase due to advantageous behavior of the detected radical.

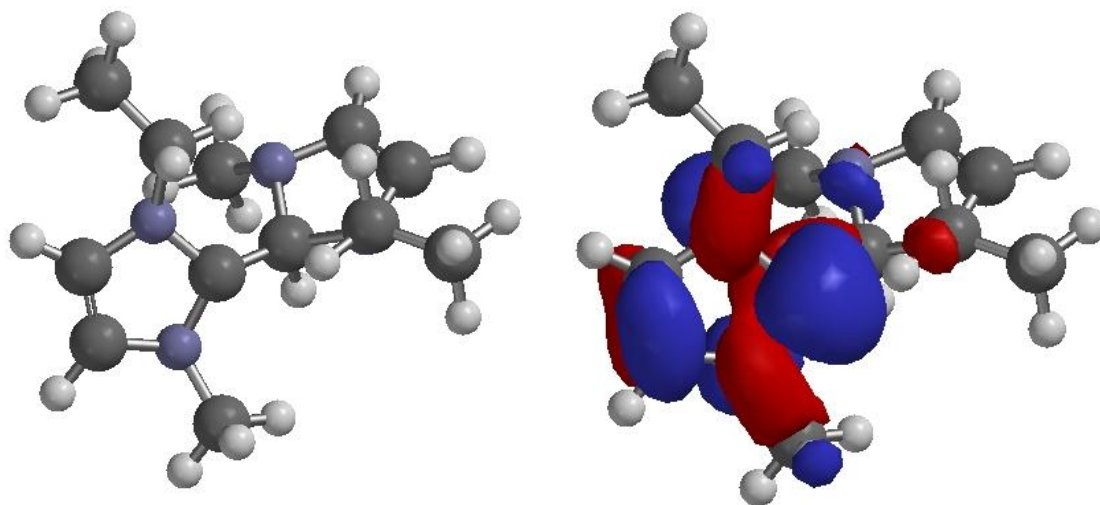
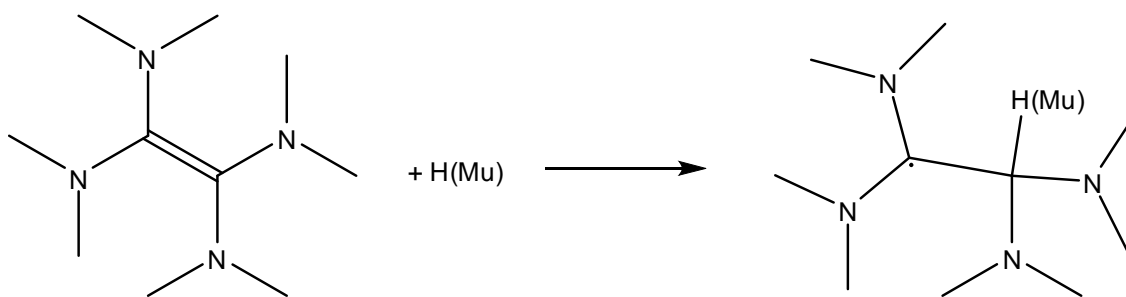


Figure 4: Structure of **1** (left) and diagram of its SOMO (right). Density functional B3LYP/6-31+g* calculations were performed using Spartan '06 for Windows.³³

2.3 Relation to Previous Muonium Work

It is interesting to note that radical **1** is related to a broad class of molecules known as electron rich olefins. Understanding the chemistry of EROs is central to our understanding of NHC chemistry since EROs are formally considered dimers of NHCs. The ERO **C** is unknown, but some EROs are conveniently available. Tetrakis(dimethylamino)ethylene is one such derivative. Previous work by the Clyburne group involved the addition of muonium to this ERO, generating a radical structurally similar to **1** (Scheme 2).



Scheme 2: The addition of muonium to an electron rich olefin generating a radical which is structurally similar to the radical generated in an ionic liquid and detected by EPR.

2.4 Conclusion

A hydrogen atom adduct of an electron rich olefin was generated in an ionic liquid and subsequently detected by EPR spectroscopy. Though the

detected radical seemed unusual at first, the Clyburne group had previously observed the generation of a structurally similar radical through the addition of muonium to an electron rich olefin.

2.5 Experimental

2.5.1 Preparation of ionic liquid

In a nitrogen atmosphere, N,N'-methyl-ethyl-imidazolium chloride (9.89 g) was weighed and added into a 50 mL round-bottom flask. Aluminum(III) chloride (5.96 g) was added to the flask in small increments over the course of ninety minutes using a Teflon[®] coated micro-spatula. At first the solids were stirred using a glass stirring rod, eventually forming a paste. At this point, the exothermic nature of the reaction has the potential to char the materials and thus, the aluminum chloride was added particularly slowly and cautiously. Upon further addition the paste loosened to a liquid, at which point a magnetic stir bar was used to stir the mixture henceforth. Upon completion of the reaction, the resulting product was a mildly viscous green-yellow colour. The composition of the ionic liquid was 40 mole % aluminum chloride, making it somewhat basic.

Lithium beads (20-30 beads) were then added to the ionic liquid. The flask was sealed and left to stir for 24 hours. The liquid became rusty red in colour.

2.5.2 EPR measurements

EPR spectra were collected at room temperature with a Bruker EMXplus EPR spectrometer operating at X-band (~9.5 GHz). Samples were loaded into 4 mm outer-diameter quartz tubes under an inert atmosphere and the tubes were sealed with O-ring needle valves. Sample volumes were ~300 μL .

The EPR spectrum detected after treatment of the imidazolium ionic liquid with lithium was simulated using the MatLab-based simulation package, EasySpin.³⁴ Accurate simulation of the spectrum was surprisingly difficult due to contributions from several partially resolved hyperfine couplings. Furthermore, it was hard to assess using traditional manual simulation methods whether a particular model for the hyperfine structure was significantly better than any other. To address these problems we used the iterative fitting procedure available in EasySpin to find the optimum set of g-value, line-width and hyperfine splitting parameters for simulation of the spectrum. This was performed in two stages using a genetic algorithm initially, followed by further refinement using a simplex least-squares refinement. The fitting procedure produced a calculation of RMSD between the experimental and simulated spectra. This was key for unbiased comparison of different models. For our work, the best simulation possible with two ^{14}N atoms gave an RMSD more than double that of the best fitting with four ^{14}N nuclei. Comparison of the two simulated spectra showed that the two ^{14}N model produced spectral line shapes, defined by partially resolved

hyperfine splitting, that did not match well with the experimental spectrum, whereas the four ^{14}N model agrees very well with experimental spectrum.

The iterative fitting procedure not only gave an unbiased assignment of the spectrum but also allowed simulation with a minimal set of hyperfine interactions. Potentially, a large number of ^1H nuclei can contribute to the hyperfine structure seen in the EPR spectrum. Simply counting lines to determine multiplicity in this case was not sufficient due to the complexity arising from the partially resolved structure. Using iterative spectral fitting, followed by comparison of calculated hyperfine couplings relative to the fitted line width and comparison of the RMSD it was determined that, in addition to four ^{14}N hyperfine interactions, only five ^1H hyperfine couplings provided resolved contributions to the spectrum.

Armed with the hyperfine couplings determined from the EPR simulation, it was then possible to identify the radical species responsible for the spectrum, based both on general predictions from the size and multiplicity of the hyperfine couplings and DFT calculations.

2.5.3 Calculations

Geometry optimizations (opt=tight) were performed using the Gaussian 09 program (Revision A.02),³⁵ the B3LYP functional,³⁶ and a 6-311+g* basis set on all atoms. Frequency calculations at the same level of theory confirmed that the

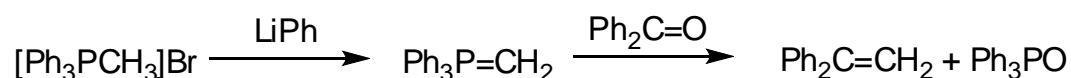
optimized structures were located at a minimum on the potential energy surface. Single point calculations specifically for hyperfine coupling were completed with the B3LYP functional and the EPR-III basis set of Barone³⁷ on all atoms.

The hyperfine couplings calculated for the deprotonated dimer radical are in very good agreement with experiment (Table 1). As demonstrated by spin-density calculations, the absence of a large hyperfine coupling is due to the absence of a proton at principal spin-bearing carbon.

3 Synthesizing a C(0) Species with Carbonyl Stabilized Ylides

3.1 Phosphorus ylides

Phosphorus ylides were originally described in the late 18th century. However it was not until 1919 that $\text{Ph}_3\text{P}=\text{CH}_2$ was synthesized and properly characterized.³⁸ And it was not until the work of Wittig³⁹ that the reaction (Scheme 3) was studied and its full potential was realized.



Scheme 3: Synthesis of an alkene from a phosphorus ylide.

This simple method of synthesizing substituted alkenes resulted in the synthesis of many novel molecules. In fact, the Wittig reaction led to the industrial synthesis of a variety of biologically active molecules, including Vitamin A, which was one of the reasons Wittig was awarded the Nobel Prize in Chemistry in 1979.⁴⁰ Though the Wittig reaction is incredibly useful and versatile, from a green chemistry perspective it does not fare well. The reaction exhibits an incredibly poor atom economy by producing a molar equivalent of triphenylphosphine oxide as a byproduct. Fortunately there have been several attempts at increasing the “greenness” of the Wittig reaction in recent years.^{41,42}

One class of phosphorus ylides, which is of particular interest, is the one containing cumulated double bonds (two double bonds on the same carbon). Chief among those are the phosphacumulene ylides (**H**) and phosphallene ylides (**I**) as shown in Figure 5. A vast amount of work has been done with these ylides as outlined in the 1977 review by Bestmann⁴³ as well as the more recent works by Bertani *et al.*³⁸ and Schobert⁴⁴.

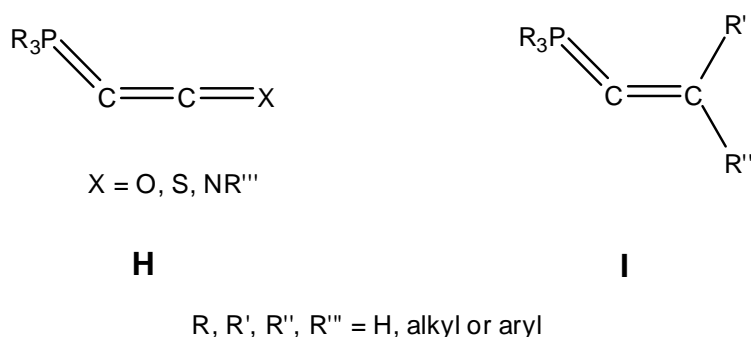


Figure 5: General formula for phosphacumulene ylide **H** and phosphallene ylide **I**.

Of particular interest to our research group is the phosphacumulene ylide $Ph_3P=C=C=O$. This compound will be referred to as *ketenylidenetriphenylphosphorane*, the most commonly used name in the literature. The proper IUPAC name is *triphenylphosphonium ketenide* or *ketene ylide*³⁸, and chemical suppliers often sell the product under the name (*triphenylphosphoroanylidene*)ketene.

3.2 Properties and Reactivity of Ketenylidenetriphenylphosphorane

Ketenylidenetriphenylphosphorane is interesting in that, though it is often presented as the ylene structure, it can also be considered as an ylide (Figure 6). The crystal structures of the compound⁴⁵ indicates that the P=C=C angle is not linear, but has an angle of 145.5° thus suggesting the importance of the ylide contribution. Additionally, the bond length of phosphorus to the ylidic carbon is 1.648 Å, shorter than the average bond length of phosphorus to the phenyl carbons of 1.80 Å. It is possible that this indicates partial double bond character in the P-C bond, giving credence to the importance of the ylene structure. However this bond shortening could also be due to coulombic force arising from the charge difference between P and C. Finally, an alternative and much less common way of looking at the compound is to see it as a triphenylphosphine adduct of C=C=O (Figure 6 - L).

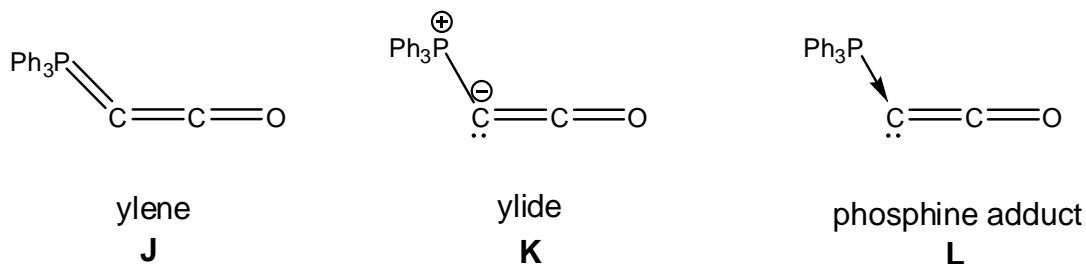
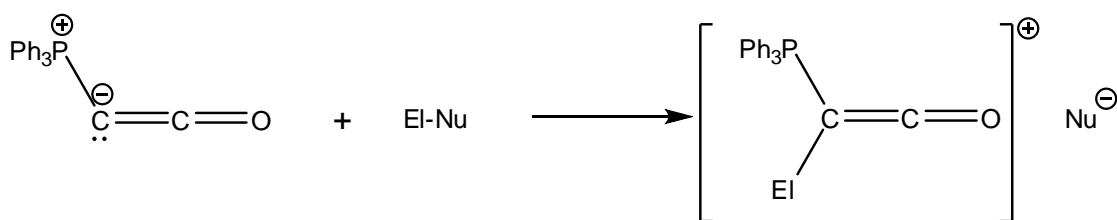


Figure 6: Ketenylidenetriphenylphosphorane drawn as an ylene **J**, ylide **K** and phosphine adduct **L**.

Though $\text{Ph}_3\text{P}=\text{C}=\text{C}=\text{O}$ appears to be a ketene, its reactivity is distinctly different. The difference lies in the occupancy of its orthogonal π -orbitals. In $\text{Ph}_3\text{P}=\text{C}=\text{C}=\text{O}$ the π -orbitals in the plane of the molecule have the same occupancy as the π -orbitals perpendicular to the plane. In contrast, ketenes have orthogonal π -orbitals which are not equivalently filled³⁸ resulting in the reactivity typical of ketenes (dimerization, cycloaddition etc.) which is not observed in ketenylidenetriphenylphosphorane.⁴⁶

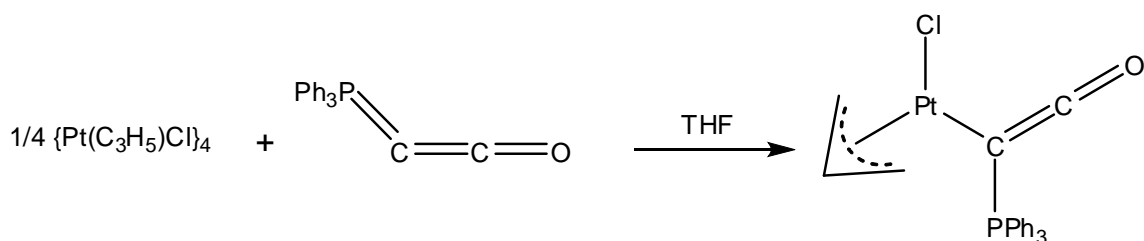
The orbital occupancy of ketenylidenetriphenylphosphorane allows it to react with general electrophile-nucleophile type compounds to produce phosphonium salts (Scheme 4). The resulting phosphonium cation exhibits the same charge density distribution as a typical ketene and thus can participate in the “typical ketene reactions” which were previously mentioned. For an extensive overview of this type of reactivity, refer to the review by Bestmann.⁴³



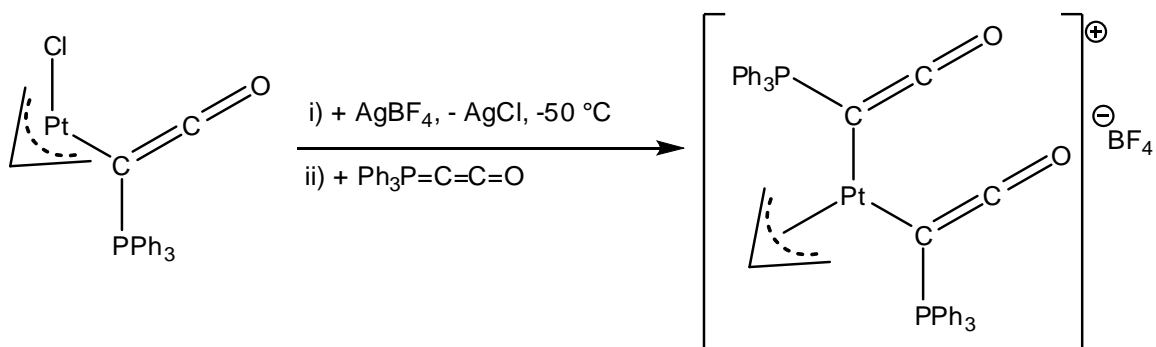
Scheme 4: The reaction of ketenylidenetriphenylphosphorane with a general electrophile-nucleophile compound to produce a phosphonium salt.

It is the basicity on the ylidic carbon which allows $\text{Ph}_3\text{P}=\text{C}=\text{C}=\text{O}$ to react with compounds of the type $\text{E}^{\text{I}}\text{-Nu}$ and it is the same basicity which allows $\text{Ph}_3\text{P}=\text{C}=\text{C}=\text{O}$ to coordinate to transition metals. Assuming the transition metal center is not coordinatively saturated, it can act as an isolated electrophilic site. This allows for an attack by the ylidic carbon, resulting in an easily isolated metal-substituted ketene. Bertani³⁸ has produced an excellent review covering the properties of these unique ketenes.

Stable metal-substituted ketenes have been produced using a variety of transition metals, including $\text{Cr}(0)$, $\text{Mo}(0)$, $\text{Mn}(\text{I})$, $\text{W}(\text{II})$ and more³⁸. Of particular interest are the Pt based metal-substituted ketenes (Scheme 5) as they have been shown to be able to form bisketenes as both stable neutral compounds and as unstable cations (Scheme 6).

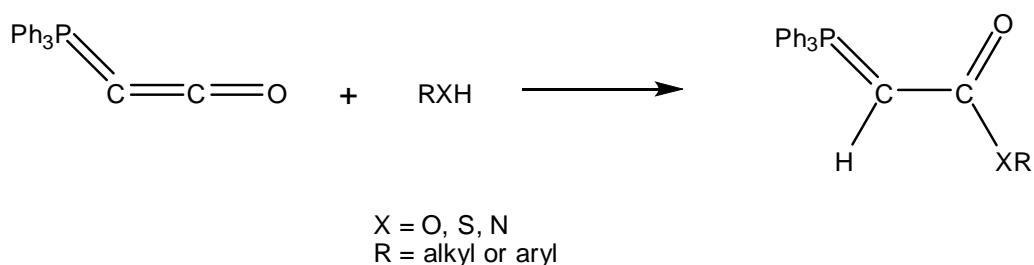


Scheme 5: The formation of a Pt-substituted ketene.



Scheme 6: The formation of a bisketene Pt cation.

Though the reactivity of Ph₃P=C=C=O with an EI-Nu compound was previously described in Scheme 7, the compound can react via a different mechanism under certain circumstances. In fact, if the nucleophile is strong enough, as in the case of protic nucleophiles, an attack on the carbonyl carbon will occur resulting in formation of a carbonyl stabilized ylide. This general procedure has resulted in the isolation of a number of carbonyl stabilized ylides which would otherwise have been synthetically challenging.^{43,47,48}

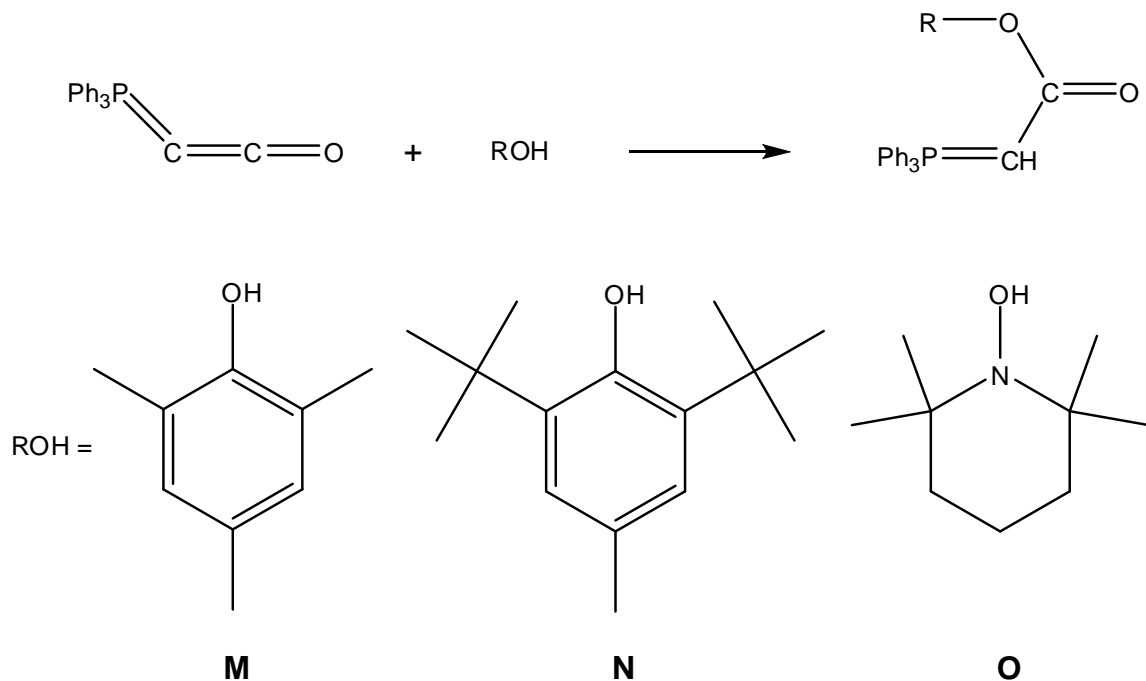


Scheme 7: Reaction of ketenylidetriphenylphosphorane with a protic nucleophile.

3.2 Results and Discussion

3.2.1 Synthesis of Three Carbonyl Stabilized Ylides

Three protic nucleophiles (2,4,6-trimethylphenol, tert-butylhydroxytoluene and 1-hydroxyl-2,2,6,6-tetramethyl-piperidine) were reacted with ketylidetriphenyl-phosphorane to form carbonyl stabilized ylides (Scheme 8). Under an argon atmosphere, 1.0 mmol ketylidetriphenylphosphorane was dissolved in dichloromethane. To this, 1.0 mmol of the protic nucleophile was added. The solution was swirled and a small amount of benzene was added to prevent evaporation to dryness. The flask was left uncovered overnight and clear, beige crystals were collected the next day. The structures were confirmed by NMR (Appendix A p. 2-14), IR (Appendix B p. 2-4) and X-ray crystallography (Figures 7, 8 and 9). The formation of a new product was evident by the shifting of a peak in the IR from 2110 cm^{-1} assigned to the C=C=O functionality, to 1600 cm^{-1} - 1700 cm^{-1} assigned to the C=O group. Furthermore, the ^{31}P peak around 5 ppm (in CD_2Cl_2 and CDCl_3) shifted downfield (Table 2, page 30). It should be noted that in the ^1H NMR spectrum, the peak from the ylide proton in **3** gives the expected doublet while the multiplicity of the peak for **5** is unclear as it is obscured by methyl peaks. **2** and **4** however display broad singlets. Such peak broadening has been observed before in ylides.⁴⁹



Scheme 8: Reaction of the three protic nucleophiles (2,4,6-trimethylphenol **M**, tert-butylhydroxytoluene **N**, and 1-hydroxyl-2,2,6,6-tetramethyl-piperidine **O**) with ketenylidetriphenylphosphorane to form products **2**, **3** and **4**, respectively.

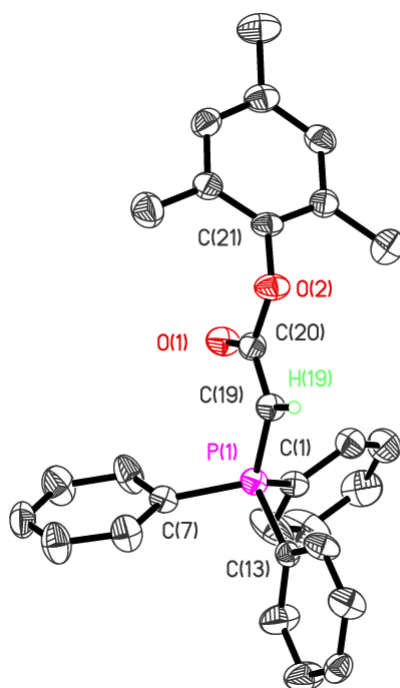


Figure 7: Thermal ellipsoid plot (50% probability ellipsoids) of **2**. Hydrogen atoms (except for H19) have been omitted for clarity. Only one of two unique molecules in the asymmetric unit is shown. Selected bond distances (Å) and angles (°): P1-C13 1.798(3), P1-C7 1.803(3), P1-C1 1.807(3), P1-C19 1.701(3), C19-H19 0.89(3), C19-C20 1.393(4), O1-C20 1.226(3), O2-C20 1.391(3), O2-C21 1.409(3), C20-O2-C21 116.2(2), O1-C20-O2 119.9(3), O1-C20-C19 126.4(3), O2-C20-C19 113.6(3), C20-C19-P1 116.2(2), C20-C19-H19 122.2(19), P1-C19-H19 121.2(18), C19-P1-C13 109.80(15), C19-P1-C7 114.67(14), C13-P1-C7 106.16(13), C19-P1-C1 112.88(15), C13-P1-C1 106.56(13), C7-P1-C1 106.25(14).

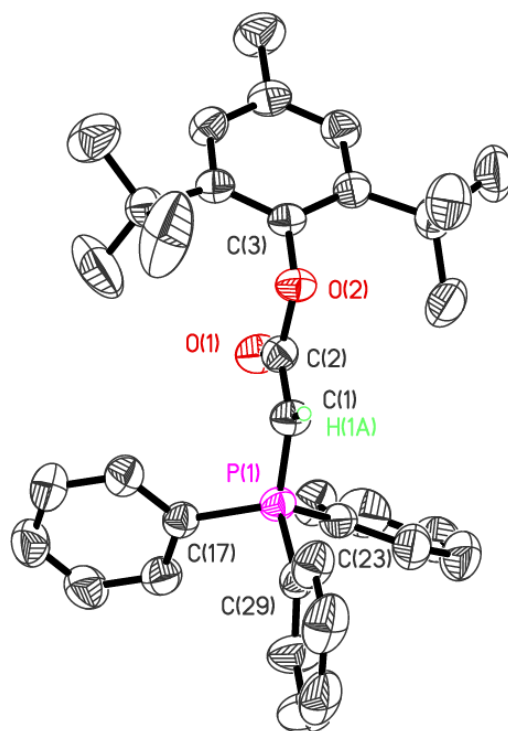


Figure 8: Thermal ellipsoid plot (50% probability ellipsoids) of **3**. Hydrogen atoms (except for H1A) have been omitted for clarity. Selected bond distances (Å) and angles (°): P1-C1 1.698(2), P1-C17 1.815(2), P1-C23 1.812(2), P1-C29 1.803(2), C1-H1A 0.9300, C1-C2 1.392(3), O1-C2 1.222(3), O2-C2 1.407(3), O2-C3 1.398(3), C1-P1-C29 109.82(12), C1-P1-C23 114.37(11), C29-P1-C23 106.97(11), C1-P1-C17 113.30(11), C29-P1-C17 105.70(11), C23-P1-C17 106.14(11), C3-O2-C2 114.70(17), C2-C1-P1 116.48(18), C2-C1-H1A 121.8, P1-C1-H1A 121.8, O1-C2-C1 126.4(2), O1-C2-O2 120.6(2), C1-C2-O2 113.0(2).

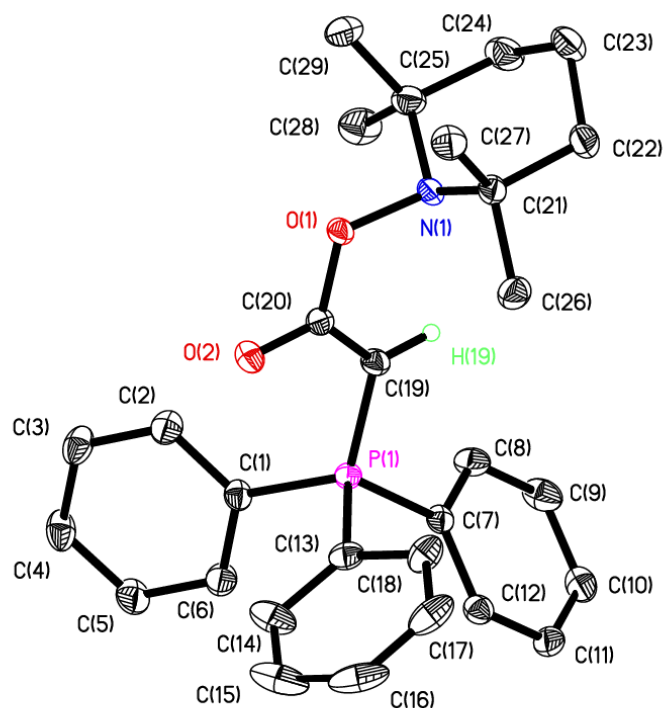


Figure 9: Thermal ellipsoid plot (50% probability ellipsoids) of **4**. Hydrogen atoms (except for H19) have been omitted for clarity. Selected bond distances (Å) and angles (°): P1-C1 1.8065(15), P1-C7 1.8085(14), P1-C13 1.8086(15), P1-C19 1.7075(14), C19-H19 0.966(18), C19-C20 1.4046(19), O1-C20 1.3944(16), O2-C20 1.2315(17), N(1)-O(1) 1.4562(15), N(1)-C(21) 1.4950(19), N(1)-C(25) 1.4955(19), C(20)-O(1)-N(1) 115.58(9), O1-C20-O2 112.77(11), O1-C20-C19 120.89(13), O2-C20-C19 126.32(13), C20-C19-P1 116.19(11), C20-C19-H19 123.8(11), P1-C19-H19 119.5(10), C19-P1-C1 117.21(7), C19-P1-C7 108.03(7), C1-P1-C7 106.02(6), C19-P1-C13 113.19(7), C1-P1-C13 105.79(7), C7-P1-C13 105.83(7).

3.2.2 Methylation of a Carbonyl Stabilized Ylide

The next step for this project was to methylate the ylides which had been synthesized. Calculations were performed⁵⁰ on product **2**. The resulting HOMO (Figure 10) displayed a large amount of charge density around the ylidic carbon, but also displayed reasonably large electron density on the carbonyl oxygen. It was hoped that this charge density would be enough to have the methylation occur at the carbonyl O site. This would result in a more labile H on the formerly ylidic carbon (Scheme 9), the reactivity of which could then be examined.

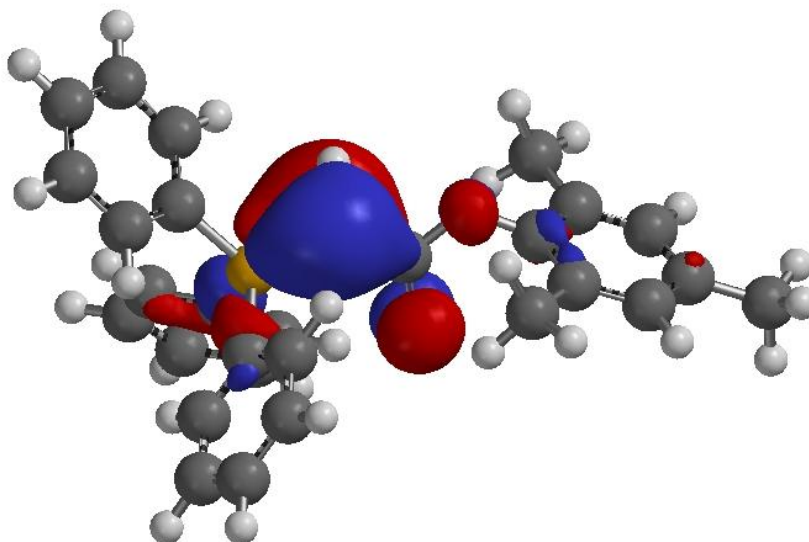
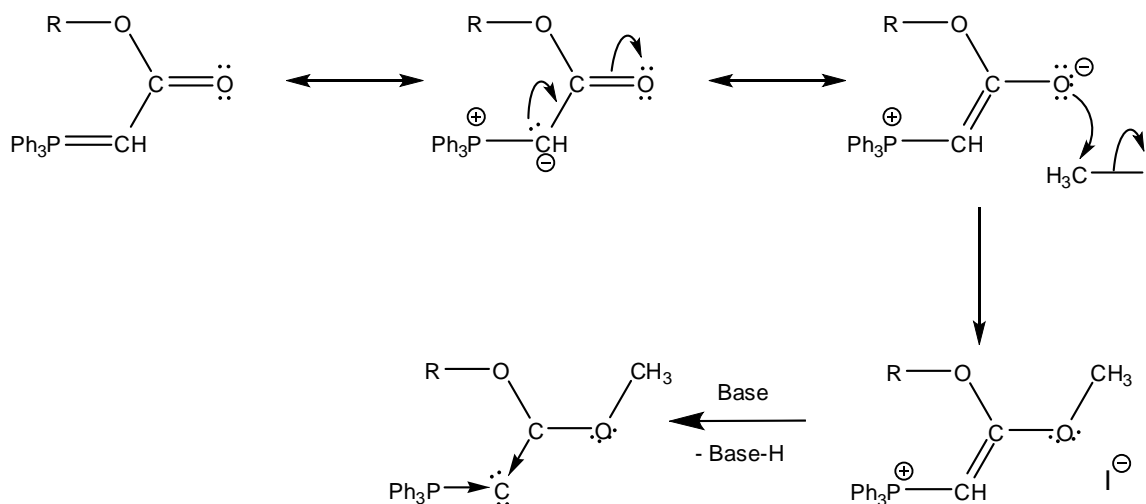
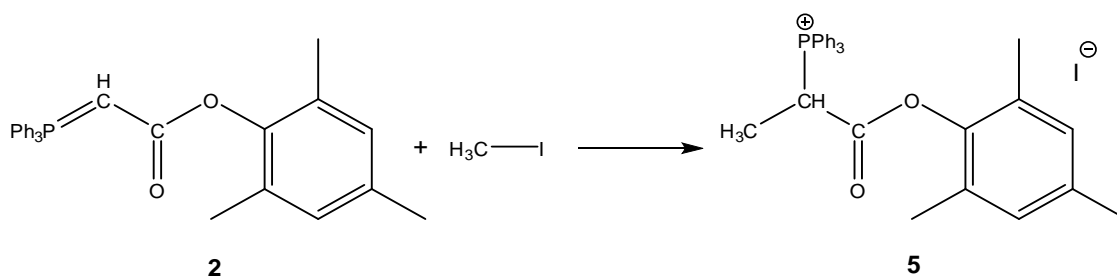


Figure 10: HOMO of **2** calculated at the density functional B3LYP/6-31+g* level using Spartan '06 for Windows³³.



Scheme 9: Proposed mechanism for the methylation reaction of carbonyl stabilized ylides.⁵¹

The methylation was only successful with product **2** (Scheme 10). For the reaction, 1 mmol of **2** was dissolved in dichloromethane. To this, 1 mmol of methyl iodide was added. The solution was swirled, a small amount of benzene was added and the flask was left uncovered overnight. The next day, clear beige crystals were collected. The structure was confirmed by NMR (Appendix A p. 15-18), IR (Appendix B p. 5) and X-ray crystallography (Figure 11).



Scheme 10: Experimental methylation of **2** to produce **5**.

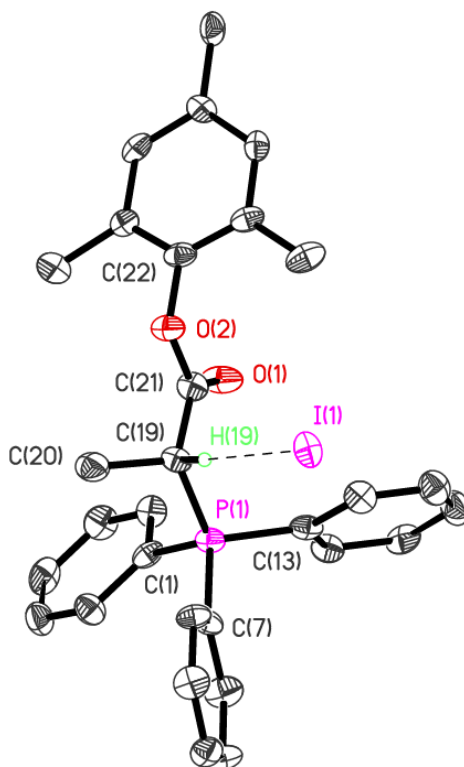


Figure 11: Thermal ellipsoid plot (50% probability ellipsoids) of one of the two crystallographically non-equivalent ion pairs in **5**. Hydrogen atoms (except for H19) have been omitted for clarity. The C-H \cdots I hydrogen bond (one of two in the structure) is indicated by the dashed line. Selected bond distances (Å) and angles (°): P1-C1 1.787(7), P1-C7 1.794(6), P1-C13 1.796(6), P1-C19 1.833(6), C19-C20 1.514(8), C19-C21 1.494(8), C21-O1 1.188(7), C21-O2 1.349(8), O2-C22 1.408(6), C1-P1-C7 109.4(3), C1-P1-C13 110.7(3), C1-P1-C19 109.4(3), C7-P1-C13 108.1(3), C7-P1-C19 106.9(3), C13-P1-C19 112.2(3), C21-C19-C20 110.8(5), C21-C19-P1 110.7(4), C20-C19-P1 111.3(4), O1-C21-O2 124.1(5), O1-C21-C19 126.2(6), O2-C21-C19 109.7(5), C21-O2-C22 116.4(5). Hydrogen bond (C19-H19...I1) distances (Å) and angles (°): C19-H19 0.980, H19...I1 2.962, H19...I1 3.934, C19-H19...I1 171.5.

Product	C=O stretch (cm ⁻¹)	¹ H ylide proton (ppm)	³¹ P (ppm)
2	1638	3.17	19.1, 15.4
3	1653	3.36 (² J _{H-P} = 23.5 Hz)	18.8
4	1605	3.61	19.4
5	1740	1.84	27.8

Table 2: Identifying characteristics of synthesized products

One peculiarity from Table 2 worth discussing is the appearance of two peaks in the ³¹P spectrum of **2**. At the time of writing, two students have repeated the reaction and in both cases the NMR data showed two peaks in the ³¹P spectrum. Surprisingly, when **2** is methylated to produce **5** only one peak is observed in the ³¹P spectrum. This phenomenon will be investigated further in the future.

3.3 Conclusion

Three novel carbonyl stabilized ylides were synthesized and characterized. Crystal structures of **2**, **3** and **4** were obtained. Product **2** was then methylated. Although methylation did not occur at the desired site, it did result in another new product, **5**, which was also crystallographically characterized. This approach was not successful for the preparation of new C(0) compounds with mixed PR₃ and CR₂ ligands.

3.4 Experimental

3.4.1 Equipment and analysis

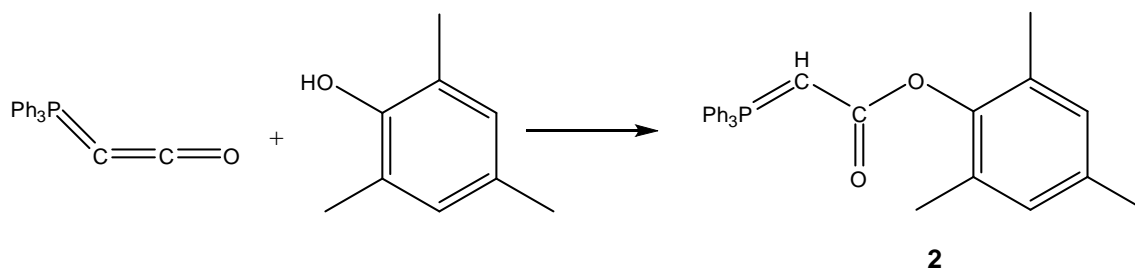
An argon atmosphere drybox was used for the preparation of these compounds. UltraHighPurity 5.0 GP-529323 type argon gas was used in all cases. The drybox used was an *MBraun* Unilab UL07-023. Anhydrous solvents were fed directly into the box from an *MBraun* MB-SPS solvent system. Vacuum pumps attached to manifold were *Welch* 1399 & 1380 DuoSeal. Masses were determined using an *OHAUS* Adventurer Pro AV412C balance. The oven used to dry glassware was a *Thermo Electron Corporation* Model #6528. NMR spectra were obtained on a *Bruker Avance* 500 MHz spectrophotometer. IR spectra were taken on a *Bruker Vertex* 70 infrared spectrometer as an evaporated dichloromethane solution between potassium bromide plates. Elemental analysis was obtained on a *Perkin Elmer 2400 Series II* CHN analyzer.

The NMR data collection was performed by Dr. Michael Lumsden of the Atlantic Region Magnetic Resonance Centre. ^1H spectral shifts were reported in relation to either known residue solvent peaks or TMS, when available. ^{31}P spectral shifts were taken without calibration. Elemental analysis data was collected by Jessica McClintick using the equipment in the Centre for Environmental Analysis and Remediation (CEAR) at Saint Mary's University. Crystal structures were determined by Arthur Hendsbee and Dr. Katherine Robertson at Saint Mary's University.

3.4.2 Preparation of compounds

Preparation of (2)

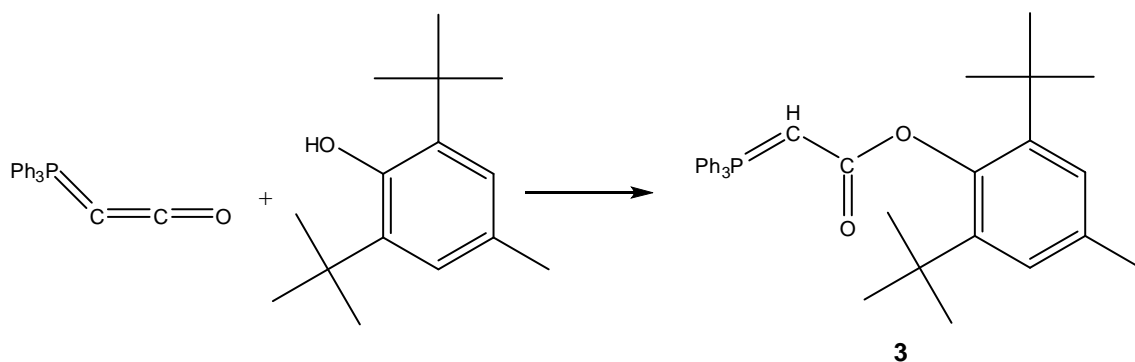
Ketenylidetriphenylphosphorane (0.30 g) was weighed out and put in a clean 50 mL Schlenk flask and ~15 mL of dichloromethane was added to dissolve the solid. Upon dissolution, 2,4,6-trimethylphenol (0.14 g) was added. The flask was swirled to ensure mixing and dissolution and then ~1 mL of benzene was added (Scheme 11). The flask was left uncovered in the dry box overnight. In the morning the crystals were collected and dried under vacuum. The crystals were then characterized as **2** using infrared, NMR, melting point, elemental analysis and crystallographic data.



Scheme 11: Synthesis of **2**. Product **2** was collected as beige crystals. Yield = 0.41g, 94%. m.p. = 159-161°C. ^1H NMR (500 MHz, CDCl_3) δ (ppm): 7.60 (m, 15H, Ar-H), 6.80 (m, 2H, Ar-H), 3.17 (s, 1H, CH), 2.23 (m, 6H, CH_3), 1.74 (s, 2H, CH_3), 1.62 (s, 1H, CH_3). ^{13}C NMR (500 MHz, CDCl_3) δ (ppm): 132.3, 132.2, 132.0, 127.8, 127.7, 127.6, 19.7, 15.7. ^{31}P NMR (500 MHz, CDCl_3) δ (ppm): 19.1, 15.4. See Appendix A (p. 2-4), IR: See Appendix B (p. 2), E.A. $\text{C}_{29}\text{H}_{27}\text{O}_2\text{P}$: Calculated C 79.43, H 6.21. Found C 78.90, H 6.07.

Preparation of (3)

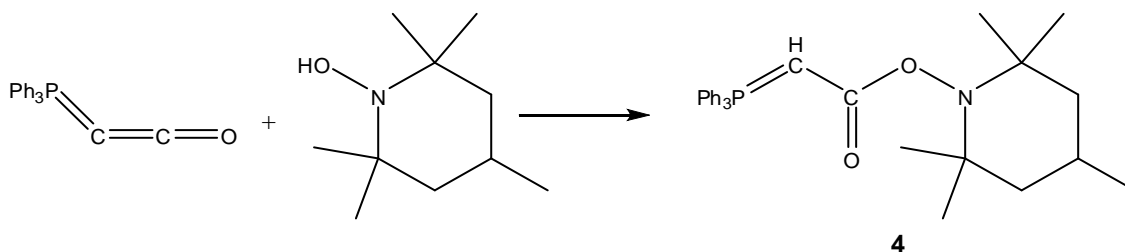
In a dry box, ketylidetriphenylphosphorane (0.30 g) was weighed out and put in a clean 50 mL Schlenk flask, ~15 mL of dichloromethane was added to dissolve the solid. Upon dissolution, tert-butylhydroxytoluene (0.22 g) was added. The flask was swirled to ensure mixing and dissolution and then ~1 mL of benzene was added (Scheme 12). The flask was left uncovered in the dry box overnight. In the morning the crystals were collected and dried under vacuum. The crystals were then characterized as **3** using infrared, NMR, melting point and crystallographic data.



Scheme 12: Synthesis of **3**. Product **3** was collected as beige crystals. Yield = 0.43g, 82%. m.p. = 168-170°C. ^1H NMR (500 MHz, CDCl_3) δ (ppm): 7.74 (m, 6H, Ar-H), 7.56 (m, 3H, Ar-H), 7.45 (m, 6H, Ar-H), 7.04 (s, 2H, Ar-H), 3.36 (d, $^2J_{\text{P-H}} = 23.5\text{Hz}$, 1H, CH), 2.27 (s, 3H, CH_3), 1.39 (s, 18H, CH_3). ^{13}C NMR (500 MHz, CDCl_3) δ (ppm): 133.1, 131.8, 128.5, 128.4, 127.3, 126.2, 35.3, 31.5, 30.3, 21.4. ^{31}P NMR (500 MHz, CDCl_3) δ (ppm): 18.8. See Appendix A (p. 5-9). IR: See Appendix B (p. 3).

Preparation of (4)

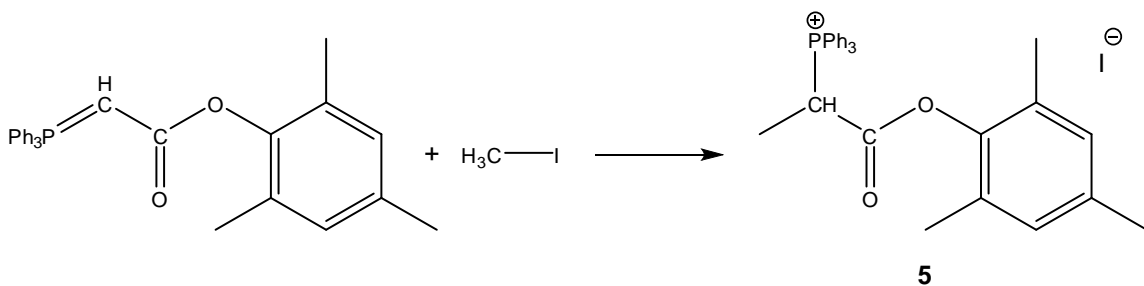
In a dry box, ketylidetriphenylphosphorane (0.30 g) was weighed out and put in a clean 50 mL Schlenk flask, ~15 mL of dichloromethane was added to dissolve the solid. Upon dissolution, 1-hydroxyl-2,2,6,6-tetramethyl-piperidine (0.17 g) was added. The flask was swirled to ensure mixing and dissolution and then ~1 mL of benzene was added (Scheme 13). The flask was left uncovered in the dry box overnight. In the morning the crystals were collected and dried under vacuum. The crystals were then characterized as **4** using infrared, NMR, melting point, elemental analysis and crystallographic data.



Scheme 13: Synthesis of **4**. Product **4** was collected as beige crystals. Yield = 0.39g, 82%. m.p. = 163-166°C. ^1H NMR (500 MHz, CD_2Cl_2) δ (ppm): 7.68 (m, 6H, Ar-H), 7.55 (m, 3H, Ar-H), 7.47 (m, 6H, Ar-H), 3.61 (s, 1H, CH), 1.58 (m, 5H, CH_2), 1.38 (m, 1H, CH_2), 1.24 (m, 12H, CH_3). ^{13}C NMR ((500 MHz, CD_2Cl_2) δ (ppm): 133.2, 131.9, 128.8, 128.0, 60.0, 40.0, 32.6, 20.6, 17.4. ^{31}P (500 MHz, CD_2Cl_2) δ (ppm): 19.4. See Appendix A (p. 10-14). IR: See Appendix B (p. 4). E.A. $\text{C}_{30}\text{H}_{36}\text{NO}_2\text{P}$: Calculated C 76.08, H 7.66, N 2.96. Found C 74.63, H 7.26, N 2.68.

Preparation of (5)

In a dry box, product **1** (0.44 g) was weighed and put in a clean 50 mL Schlenk flask, ~15 mL of dichloromethane was added to dissolve the solid. Iodomethane (0.14 g) was added to a vial along with ~5 mL of dichloromethane. The contents of the vial were then added to the flask and the flask was swirled to ensure mixing. Subsequently, ~1 mL of benzene was added (Scheme 14). The flask was left uncovered in the dry box overnight. In the morning the crystals were collected and dried under vacuum. The crystals were then characterized as **5** using infrared, NMR, melting point and crystallographic data.



Scheme 14: Synthesis of **5**. Product **5** was collected as beige crystals. Yield = 0.36g, 79%. m.p. = 172-176°C. ^1H NMR (500 MHz, CDCl_3) δ (ppm): 8.00 (m, 6H, Ar-H), 7.67 (m, 3H, Ar-H), 7.60 (m, 6H, Ar-H), 6.68 (s, 2H, Ar-H), 2.10 (m, 6H, CH_3), 1.84 (m, 7H, CH_3 , CH). ^{13}C NMR (500 MHz, CD_2Cl_2) δ (ppm): 166.4, 144.4, 134.0, 133.5, 133.4, 129.4, 129.3, 116.3, 37.0, 36.6, 24.0, 19.7, 12.3. ^{31}P (500 MHz, CDCl_3) δ (ppm): 27.8. See Appendix A (p. 15-18). IR: See Appendix B (p. 5).

4 Biodegradable Ionic Liquids as Oil Dispersants

4.1 Ionic Liquids, Surfactants and Oil Dispersants

With the increased world demand for oil, marine oil spills due to accidents in transportation or offshore drilling have become a serious concern. These oil spills have a major detrimental effect on marine life which in turn impacts the industries relying on this marine life as a source of income, such as the fisheries industry. It is more economical to treat an oil spill in open water, as opposed to waiting for the oil to reach the shore and then performing the cleanup.⁵²

Dispersants are one of the few available chemical remedies for marine oil spills. Dispersants are chemical compounds containing one or more surfactants, or surface active reagents. Surfactants contain both hydrophobic and hydrophilic components which allow them to break up oil slicks into oil droplets which are dispersed throughout the body of water. This dispersed oil has less of an environmental impact as microorganisms are better able to biodegrade the smaller droplets.⁵³ Many commercially available surfactants are ionic compounds, making ionic liquids interesting candidates to act as oil dispersants.

The now rapidly growing field of ionic liquids began with the synthesis and characterization of ethylammonium nitrate by Paul Walden in 1914.⁷ Today, the applications of ionic liquids are many and growing rapidly. Ionic liquids offer a potentially 'green' alternative to molecular solvents, their use in microwave chemistry and as catalysts has also been convincingly demonstrated.^{54,55,56}

An important quality of ionic liquids in this regard is their potential to act as surfactants.⁵⁷ Certain ionic liquids have shown the ability to form multilamellar vesicles which parallel surfactant micelles.⁵⁸ This is an attractive feature since the potential ability for these amphiphilic ionic liquids to dissolve both polar and non-polar substances could greatly increase their utility as a 'green' alternative to organic solvents.⁵⁹ Merrigan, *et al.* report the synthesis of an imidazolium-based ionic liquid that, when mixed with [C6mim]PF₆ can emulsify perfluorohexane.⁶⁰ With the ability of some ionic liquids to act as surfactants proven, another question is posed - can ionic liquids act as oil dispersants, and if so how well?

Boukherissa *et al.* tested several different ionic liquids for their ability to act as dispersants of petroleum asphaltene, and reported very promising results.⁶¹ The current study outlines the dispersant abilities of several ionic liquids, measured in comparison to Corexit™ 9500⁶². This composition of this dispersant was previously confidential, however as it was used to such an overwhelming extent in treatment of the Gulf of Mexico, the Environmental Protection Agency has released the ingredient list. Corexit™ 9500 contains a variety of sorbitan derivatives, a butanedioic acid sodium salt, propanol and petroleum distillates.⁶³ Our ionic liquids were synthesized from oleic acid, erucic acid, linoleic acid or lauric acid as the anion source and choline hydroxide as the cation in every instance.

4.2 Toxicity of Ionic Liquids

In order to consider ionic liquids as a safer, environmentally friendlier alternative, their toxicity and biodegradability must be thoroughly assayed. Investigation into the 'green' aspects of ionic liquids has been explored, though as it is with anything, further study is always needed. This is particularly true when considering the biodegradability of ionic liquids, since the amount of research done in this field is lacking. Boethling *et al.* have outlined several factors that seem to affect the overall biodegradability of ionic liquids, though these are simply general observations. Incorporation of benzene rings, long unsubstituted alkyl chains, hydroxyl groups and carbonyl groups seem to cause an increase in the biodegradability of ionic liquids. Furthermore, decreased biodegradability seems to follow with the inclusion of halogens, fused aromatic rings, heterocycles and aliphatic ether groups.⁶⁴ With the large number of ion pairs available for synthesis of ionic liquids, it is possible to fine-tune the functional groups present in each ion in order to emphasize biodegradability (or some other desired property) of the ionic liquid.

The work by Wells and Coombe shows that great care must be taken when working with some ionic liquids. Their biodegradation and freshwater ecotoxicity studies showed that some common ionic liquids have the potential to be quite damaging to the environment if released into the water.⁶⁵ Conversely, Gathergood *et al.* identified several readily biodegradable ionic liquids after performing closed bottle tests and CO₂ headspace tests.⁶⁶ These differing results

simply emphasize the vast variety of ionic liquids available and the amount of research that is needed in the field of biodegradation of ionic liquids. It is important to consider the effect the dispersant itself may have on the environment; use of biodegradable oil dispersants should avoid additional contamination throughout the degradation process.

4.3 Biodegradable Ions

Oleic acid and erucic acid are long-chained unsaturated aliphatic carboxylic acids and are known to be biodegradable. One study by Erhan *et al.* showed that in an environment containing a mixed culture of *Penicillium verucosum*, *Mucor racemosus* and *Enterobacter aerogenes*, both oleic acid and erucic acid were over 99% degraded in ten days.⁶⁷ Similar anaerobic degradation studies performed on linoleic acid showed that after 25 days it was no longer detectable.⁶⁸ Lauric acid, which constitutes a large portion of coconut oil, is well known to be biodegradable⁶⁹. Choline is an important nutrient that plays a role in the formation of membrane phospholipids and the neurotransmitter acetylcholine⁷⁰; as a result it is also biodegradable.⁷¹

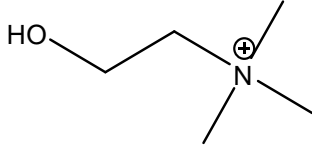
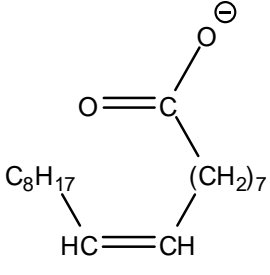
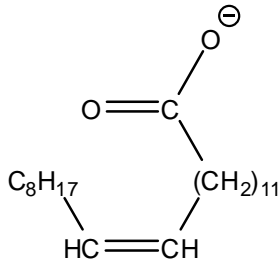
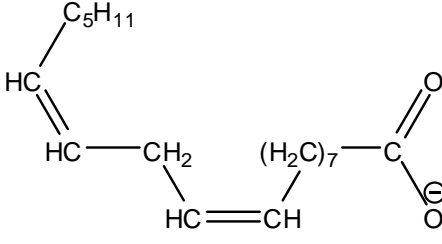
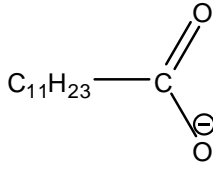
Ion	Structure
Choline	
Oleate	
Erucate	
Linoleate	
Laurate	

Table 3: Structures of choline, oleate, erucate, linoleate and laurate ions. Choline was paired with each of the anions to form the four ionic liquids studied.

Table 3 shows the structures of choline and the four anions present in the ionic liquids studied. The long aliphatic hydrocarbon chains of the carboxylates and the hydroxyl group on the choline ion respectively constitute the hydrophobic and hydrophilic components necessary in a surfactant. As expected⁷², the ionic liquids composed of unsaturated fatty acids are much less viscous than the saturated choline laurate.

4.4 Results and Discussion

4.4.1 Preparation of Ionic Liquid Dispersants

The ionic liquids were prepared initially in small amounts; 5 mL of a 45 wt% solution of choline hydroxide in methanol was used for preparation of each ionic liquid. Equivalent amounts of each acid were added to the choline hydroxide in separate round-bottom flasks (5.87 mL of oleic acid, 5.80 mL of linoleic acid, 7.32 mL of erucic acid and 3.73 g of lauric acid). The lauric acid was heated on a hotplate until melted before addition to the choline hydroxide. Each solution was stirred and the methanol present was removed on a rotary evaporator. The resulting ionic liquids were dried under reduced pressure. Each of these reactions produced viscous orange-brown ionic liquids, similar in colour to the choline hydroxide solution used.

This same procedure was used in an attempt to form an ionic liquid with sodium lauryl sulfate. Sodium lauryl sulfate (5.40 g) was added to 5 mL of a 45

wt% solution of choline hydroxide in methanol. The sodium lauryl sulfate remained solid, so ~15 mL of water was added, dissolving the solid and forming a white soapy liquid.

4.4.2 Characterization of Ionic Liquids

The ionic liquids, choline hydroxide and each of the fatty acids were characterized using ^1H NMR, ^{13}C NMR and infrared spectroscopy.

Changes in the ^1H NMR spectra (Appendix A p. 19-26) demonstrated the loss of a proton on going from the free acid to the ionic liquid. The formation of the carboxylates of the fatty acids was indicated by the lack of a hydroxyl proton peak in the 12 ppm range. The infrared spectra further confirm this with the disappearance or diminishment of OH bends in the spectra of all the ionic liquids synthesized.

Integrations in the ^1H NMR spectra were also used to confirm a 1:1 ratio of fatty acid anion to choline cation for each synthesized ionic liquid. ^{13}C NMR was also employed to confirm the correct number of carbon signals. Peaks corresponding to methanol were observed in both spectra. Overall, this data correlates well with that in the literature.^{73, 74, 75}

4.4.3 Baffled Flask Test

For the baffled flask tests 100 μL of MESA™, a dark and viscous recycled oil product, was added to 120 mL filtered cold seawater (from the Bedford Basin in Bedford, NS) in a baffled flask. 4 μL of each dispersant was added to the separate flasks containing the seawater and oil mixtures. The dispersants were used in their purified form (some methanol was found to be present by ^{13}C NMR, but this amount was small). The flasks were shaken at 200 rpm for 10 minutes on an orbital shaker and then allowed to stand for a further 10 minutes before 80 mL samples were extracted. To prevent bacterial growth over the storage period, 0.1 mL of 6 M hydrochloric acid was added to each sample.⁷⁶

ID	Sample
CL020	Choline oleate
CL021	Choline laurate
CL022	Choline linoleate
CL023	Choline erucate
CL024	Choline oleate with PEG
CL025	Choline linoleate with PEG
CL026	Oleic Acid
CL027	Linoleic Acid
CL028	Choline Hydroxide
CL029	Choline + sodium lauryl sulfate
CL030	Glycerol
BL010	Seawater
BL011	Seawater and MESA
CX010	Corexit™ 9500

Table 4: CL020-CL025 are the ionic liquid dispersants used in the baffled flask tests. BL010 and BL011 are blank samples and CX010 is a dispersant used industrially, used in this experiment for comparison. PEG = Polyethylene glycol.

4.4.4 Analysis of samples by GC/FID

Each sample was analyzed by gas chromatography with flame ionization detection. Seven standard solutions containing the MesaTM crude oil were made. The data for the calibration is presented in Table 5 and a plot of this data (Figure 12) shows the anticipated linear response.

Standard #	MESATM Concentration ($\mu\text{g}/\text{mL}$)
1	50.4
2	100.8
3	252
4	504
5	1008
6	1512
7	3024

Table 5: Concentration of MesaTM crude oil in each of the seven standards used for calibration. Samples were prepared using water from the Bedford Basin.

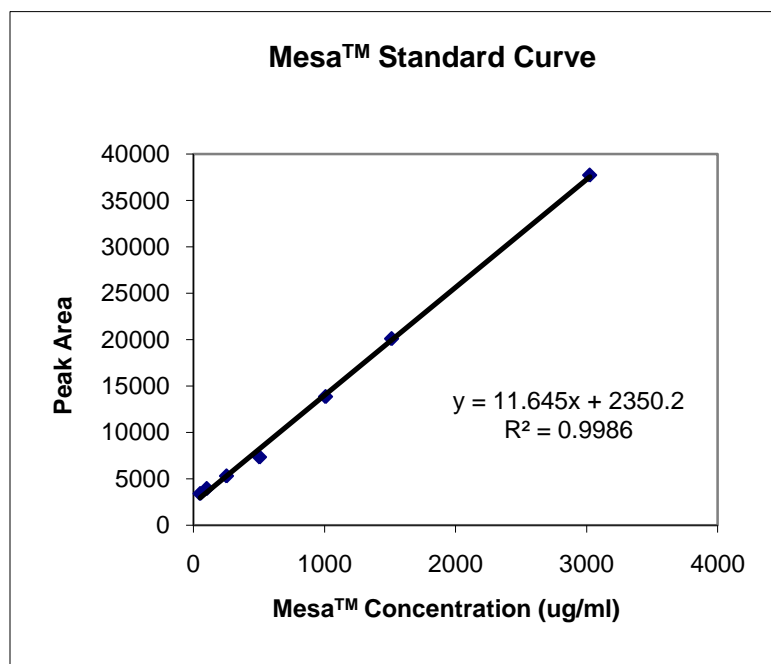


Figure 12: GC calibration curve of the seven Mesa™ crude oil standards showing the concentrations listed in Table 5 (x) vs. peak area (y).

The dispersed oil in sea water samples (80 mL) were extracted with 10 mL of dichloromethane using a roller extractor.⁷⁷ The solvent was separated from the water layer and the extracts were concentrated to 1 mL. These sample extracts were analyzed by GC/FID to determine the concentration of Mesa™ crude oil in solution, thus giving a good approximation of the dispersant abilities of the ionic liquids in comparison to Corexit™ 9500. With the exception of the two blanks, BL010 and BL011, it was found that dilution of the samples was necessary since much of the data obtained lay well outside the standard curve shown in Figure 12. A two-fold dilution was required for glycerol. Four-fold dilutions were required for choline oleate, choline laurate, choline linoleate, choline erucate, choline

oleate in PEG as well as oleic acid and linoleic acid. Ten-fold dilutions were required for choline linoleate in PEG, choline hydroxide and choline lauryl sulfate. A twenty-fold dilution was required for Corexit™ 9500. After accounting for the dilutions made, the following concentrations of Mesa™ crude oil in each analyzed sample were recorded (Table 6).

Sample ID	MESA Concentration (µg/mL)
CL020	100.44
CL021	108.27
CL022	106.26
CL023	124.77
CL024	134.90
CL025	155.48
CL026	105.52
CL027	106.62
CL028	257.80
CL029	313.91
CL030	49.47
CX010	539.95

Table 6: Concentration of Mesa™ crude oil in each sample, determined by analysis with GC/FID.

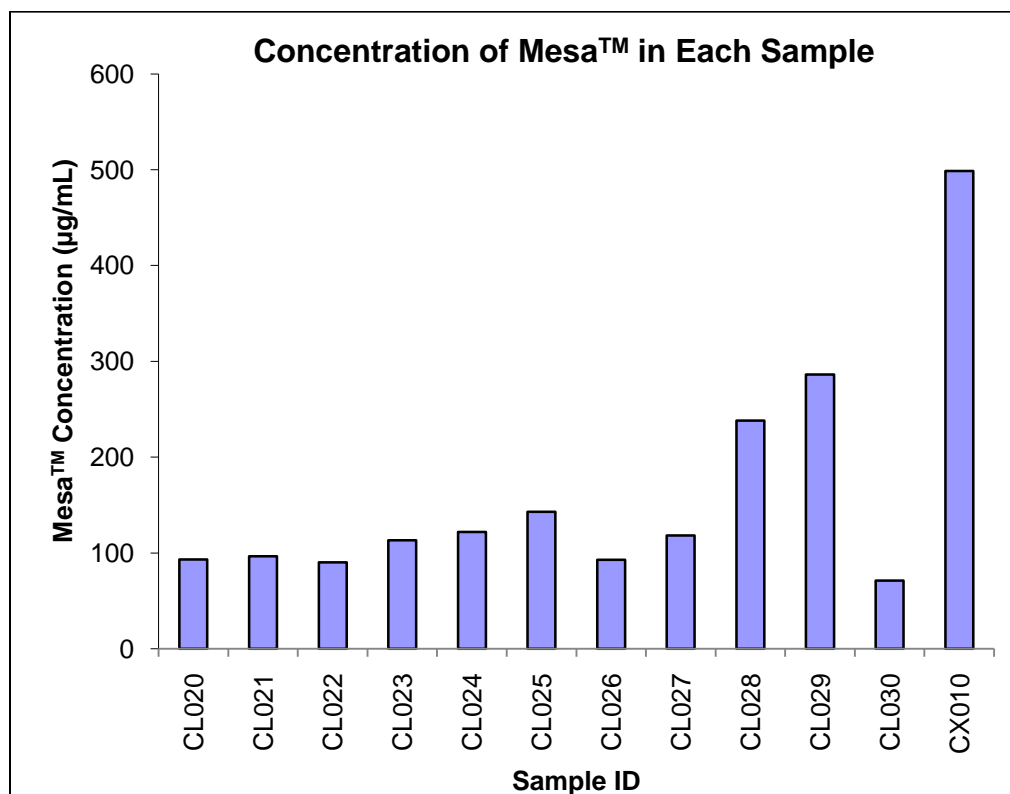


Figure 13: Concentration of Mesa™ crude oil in each sample, as determined by GC/FID.

4.5 Conclusion

The data in Table 6 and Figure 13 show that although the synthesized ionic liquids do not act as dispersants to the degree Corexit™ does, they do show some ability to act as oil dispersants. Interestingly CL028 (choline hydroxide) and CL029 (choline lauryl sulfate) show impressive results in comparison to Corexit™ 9500. Equal volumes of each sample were taken, however because of their similar densities and differing molecular weights, this equates to a greater number of choline molecules being present in these

samples compared to the others. Assuming choline is responsible for more of the observed dispersaion than the fatty acids, this would result in a greater ability for an equal volume of choline hydroxide to disperse the Mesa™ crude oil as dispersant ability is a colligative property. The data shows the great potential for ionic liquids, with proper adjustments and formulations, to play an integral role in the future as an alternative to conventional oil dispersants.

4.6 Experimental Data – Ionic Liquids Characterization Data

Choline oleate:

^1H NMR (CDCl_3 , 500 MHz) δ (ppm): 5.58 (s, 2H), 5.26 (m, 2H), 3.97 (m, 2H), 3.55 (m, 2H), 3.30 (s, 3H), 3.22 (s, 9H), 2.07 (t, $J = 7.8$ Hz, 2H), 1.93 (m, 4H), 1.49 (m, 2H), 1.25 (m, 20H), 0.81 (t, $J = 7.0$ Hz, 3H). ^{13}C (CDCl_3 , 500 MHz) δ (ppm): 129.7, 129.6, 68.0, 55.7, 54.1, 49.3, 38.5, 31.7, 29.7, 29.6, 29.5, 29.5, 29.4, 29.3, 29.2, 29.1, 27.0, 27.0, 26.7, 22.4, 13.9. See Appendix A (p. 19-20).
IR: See Appendix B (p. 5). E.A. $\text{C}_{23}\text{H}_{47}\text{NO}_3$: Calculated C 71.64, H 12.28, N 3.63. Found C 67.48, H 12.16, N 4.22.

Choline erucate:

^1H NMR (CDCl_3 , 500 MHz) δ (ppm): 5.33 (m, 1H), 4.08 (m, 2H), 3.62 (m, 2H), 3.37 (s, 2H), 3.30 (s, 8H), 2.10 (m, 4H), 1.58 (s, 2H), 1.26 (m, 20H), 0.87 (m, 3H).
 ^{13}C (CDCl_3 , 500 MHz) δ (ppm): 129.8, 68.2, 55.8, 54.3, 38.9, 31.8, 30.0, 29.7, 29.7, 29.7, 29.6, 29.4, 29.3, 29.2, 29.2, 27.1, 27.1, 27.0, 14.1. See Appendix A

(p. 21-22). IR: See Appendix B (p. 6). E.A. $C_{27}H_{55}NO_3$: Calculated C 73.41, H 12.55, N 3.17. Found C 66.68, H 12.10, N 4.17.

Choline linoleate:

1H NMR ($CDCl_3$, 500 MHz) δ (ppm): 5.30 (m, 6H), 4.01 (m, 2H), 3.58 (m, 2H), 3.35 (s, 4H), 3.26 (s, 9H), 2.73 (m, 2H), 2.10 (m, 2H), 2.03 (m, 4H), 1.29 (m, 16H), 0.87 (m, 3H). ^{13}C ($CDCl_3$, 500 MHz) δ (ppm): 130.1, 130.1, 127.8, 127.8, 68.1, 55.8, 54.2, 49.6, 38.6, 31.4, 29.8, 29.6, 29.5, 29.3, 29.2, 27.1, 27.1, 27.0, 26.8, 25.5, 22.4, 13.9. See Appendix A (p.23-24). IR: See Appendix B (p. 7). E.A. $C_{23}H_{45}NO_3$: Calculated C 72.01, H 11.82, N 3.65. Found C 65.51, H 11.67, N 3.81.

Choline laurate:

1H NMR ($CDCl_3$, 500 MHz) δ (ppm): 5.36 (m, 2H), 3.91 (m, 2H), 3.48 (m, 2H), 3.25 (s, 2H), 3.17 (s, 9H), 2.00 (m, 2H), 1.44 (m, 2H), 1.18 (m, 16H), 0.78 (t, J = 7.0 Hz, 3H). ^{13}C ($CDCl_3$, 500 MHz) δ (ppm): 67.8, 55.6, 54.0, 49.2, 38.5, 31.7, 29.8, 29.5, 29.5, 29.5, 29.4, 29.1, 26.7, 22.4, 13.8. See Appendix A (p. 25-26). IR: See Appendix B (p. 8). E.A. $C_{17}H_{37}NO_3$: Calculated C 67.28, H 12.29, N 4.62. Found C 61.97, H 12.12, N 6.32.

5 Potentially Biodegradable Schiff's Bases as Chelating Agents

5.1 Chelating Agents

In many current industrial processes, metal ions can be major contaminants resulting in numerous disadvantageous effects. These metal ions may be introduced through the raw materials used in the process as well as via the erosion and degradation of equipment and machinery while in use. These metal ions can initiate a number of different chemical processes, such as corrosion or catalytic degradation, depending on which metals are present.⁷⁸ Furthermore these metal contaminants may end up in the final product which, in the case of consumables, is detrimental. Additionally the prospect of contamination of effluent, and eventually a water supply, is nearly inevitable.

To effectively mitigate the dangers posed by metal ion contamination, chelating agents are often used. A chelating agent is essentially any polydentate ligand which binds to a single atom through two or more of its binding sites. By design, these chelating agents tend to have a much stronger affinity for one or more specific metal ions than an atomically similar monodentate ligand.⁷⁹ By far the most heavily used chelating agent, with regards to industrial or household use, is EDTA (ethylenediaminetetraacetic acid) (Figure 14).⁸⁰

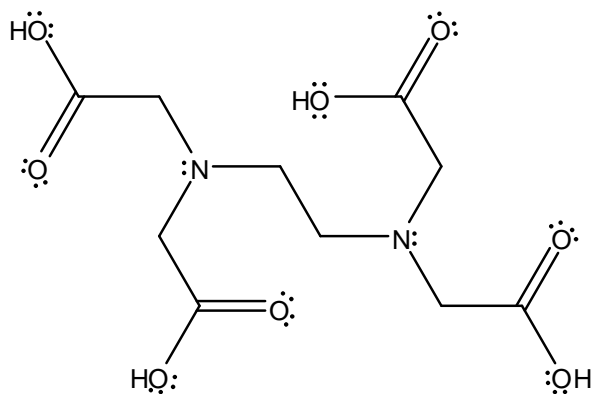


Figure 14: EDTA – ethylenediaminetetraacetic acid

5.2 EDTA – Ethylenediaminetetraacetic Acid

5.2.1 Prevalence of EDTA

EDTA has been in commercial use for nearly 75 years. It is used both in its pure form and also as salts composed with sodium, potassium, calcium and/or ammonium. It is a strong complexing agent and a very stable molecule, and thus lends itself to a variety of industrial and household applications. The compound is able to chelate to a myriad of metals including Al, Ba, Ca, Co, and Cu.⁸¹ EDTA is used in one third of detergents produced worldwide, and is also used in large amounts in water treatment, the pulp and paper industry and to a lesser extent in a variety of other industries such as textiles, agrochemicals and the production of cosmetics and foodstuffs.⁸⁰ Due to the prevalence of EDTA in both detergents and water treatment, it should come as no surprise that in our environment EDTA

is by far the most prevalent in the aqueous medium. Its presence in soils is rather minimal and is due largely to the disposal of EDTA-containing products in waste landfills, as well as any agrochemical applications for which EDTA is used. It is unlikely to find EDTA in the air as it is a non-volatile compound. Any trace amounts of EDTA in the air system are due to aerial application of EDTA for agrochemical use.⁷⁸

EDTA has found such wide industrial use because it is generally considered to be a rather safe material. This is because the LD₅₀ of EDTA salts in rats is roughly 2-10 g/kg. Given the small amounts of EDTA used in products and processes, acute toxicity due to oral dosing, is not a genuine concern. Additionally, EDTA is not metabolized by the body, nor is it retained. Nearly all EDTA consumed is excreted through urine such that bioaccumulation is not a risk.⁸²

5.2.2 Concerns with EDTA

EDTA, however, also causes some concerns. Studies have shown that EDTA may form complexes with heavy metals already settled in the sediment.⁸³ This effectively redissolves these heavy metals and mobilises them throughout the water system. Of particular concern is the complexation and increased mobilisation of radioactive ions.⁸⁴ EDTA has also been shown to complicate pregnancies in rats. Administration of 380 mg/kg of disodium EDTA daily to

pregnant rats resulted in weakness, drowsiness, and loss of appetite among other symptoms. The most concerning symptom was the increased rate of fetal resorption, likely due to mineral deprivation of the embryos as caused by metal chelation and subsequent excretion.⁸²

The largest concern with EDTA lies in its persistence. As it is used so commonly and is so persistent⁸⁵, it has become a major pollutant in our water systems. Though its health effects may actually be relatively innocuous, the long-term effects of an increasing concentration of EDTA in our environment are unknown.⁷⁸ As such, it may be beneficial to look into more biodegradable chelating agents in order to find compounds robust enough to complete the desired task while not lasting indefinitely.

5.3 Amino Sugar Schiff's Bases

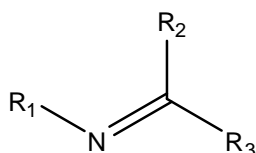


Figure 15: Schiff's base (R₁=aryl or alkyl group).

Schiff's bases (Figure 15), having formed a number of stable chemical species with a number of different metals, have been an important and widely

studied class of coordination chemistry. Furthermore, it has been known for over 100 years that sugars and sugar-based compounds can form complexes with metals. It was in 1922 that a group first discovered that amino sugars could readily form Schiff's bases. Schiff's bases of sparing water-solubility were formed with D-glucosamine and salicylaldehyde (Figure 16) as well as with structurally similar aromatic aldehydes.⁸⁶ Surprisingly, it wasn't until the work of Adam and Hall⁸⁷ sixty years later that groups began exploring metal complexation to these amino sugar-based Schiff's bases. The main interest in these amino sugar ligands is in the development of new metal chelators for use in a clinical setting⁸⁸ and for use in catalysis⁸⁹, though other more general applications may also be feasible.

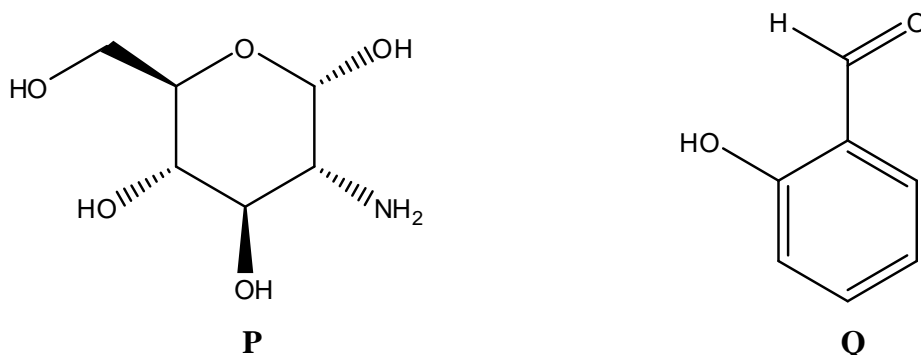


Figure 16: D-glucosamine **P** and salicylaldehyde **Q**.

5.4 Stability constants

A stability constant (alternatively referred to as a formation constant or binding constant) is an equilibrium constant for the formation of a metal-ligand complex in a solution. A stability constant is an effective way to measure a ligand's affinity for a metal ion in solution. This, in essence, quantifies the failure or success for the complexation of a designed ligand.⁹⁰

There are several different ways of determining a stability constant. In this study the ability of amino sugar Schiff's base ligands to form complexes with copper was examined. Thus, a solid-state copper(II) ion-selective electrode was used to perform a potentiometric titration. The most important property of the electrode is that it maintains a Nernstian response over a specified copper concentration (pCu) range. That is to say, the electrode potential must obey the equation:

$$E = E^\circ + (RT/nF)\ln(a_{\text{Cu}^{2+}})$$

where E is the potential, E° is a standard potential which varies according to the electrode in use, R is the universal gas constant, T is absolute temperature, n is the number of moles of electrons transferred, F is the Faraday constant and $a_{\text{Cu}^{2+}}$ is the chemical activity of Cu^{2+} . At 25°C and a specific ionic strength the equation becomes⁹¹:

$$E = E^\circ + (0.0296)\log[\text{Cu}^{2+}]$$

To actually begin using the copper(II) ion-selective electrode, one must first create a calibration curve using standards of known copper ion concentration in aqueous solution. As previously mentioned, the electrode response can vary depending on ionic strength, so an ionic strength adjustment buffer (ISAB) is added both to the calibration standards and later to the samples. Once the calibration curve is complete sample measurement can begin. The electrode system is set up in a beaker with an aqueous solution (100 mL) containing a known concentration of ligand (~1.00 mM). To this solution, a known concentration of copper ion solution (1.60 mM) is slowly added via burette. The electrode will not detect copper ions if they are bound to the ligand upon addition. Once enough copper ion solution has been added that equilibrium has been achieved, any further addition will result in excess free copper ion in solution which is detected by the electrode. The recorded data allows for calculation of the stability constant.⁹²

5.5 Results and discussion

5.5.1 Synthesis and Characterization Four Schiff's Base Ligands

Adam and Hall reported some of their metal-ligand chelates to be crystalline, yet they never obtained any X-ray crystal structure. The original goal of this project was to obtain crystal structures of one or more of the synthesized

Schiff's base ligands. We would then attempt to prepare and structurally characterize metal-ligand chelates with these ligands.

Four different ligands were synthesized. Following the work of Adam and Hall, one compound was made using D-glucosamine and salicylaldehyde, while another was made using 1,3,4,6-tetra-O-acetyl-2-amino-2-deoxy- β -D-glucosamine and salicylaldehyde. Similarly, two more compounds were made using the same amino sugars, but substituting pyridoxal (Vitamin B6) in lieu of salicylaldehyde (Figure 17).

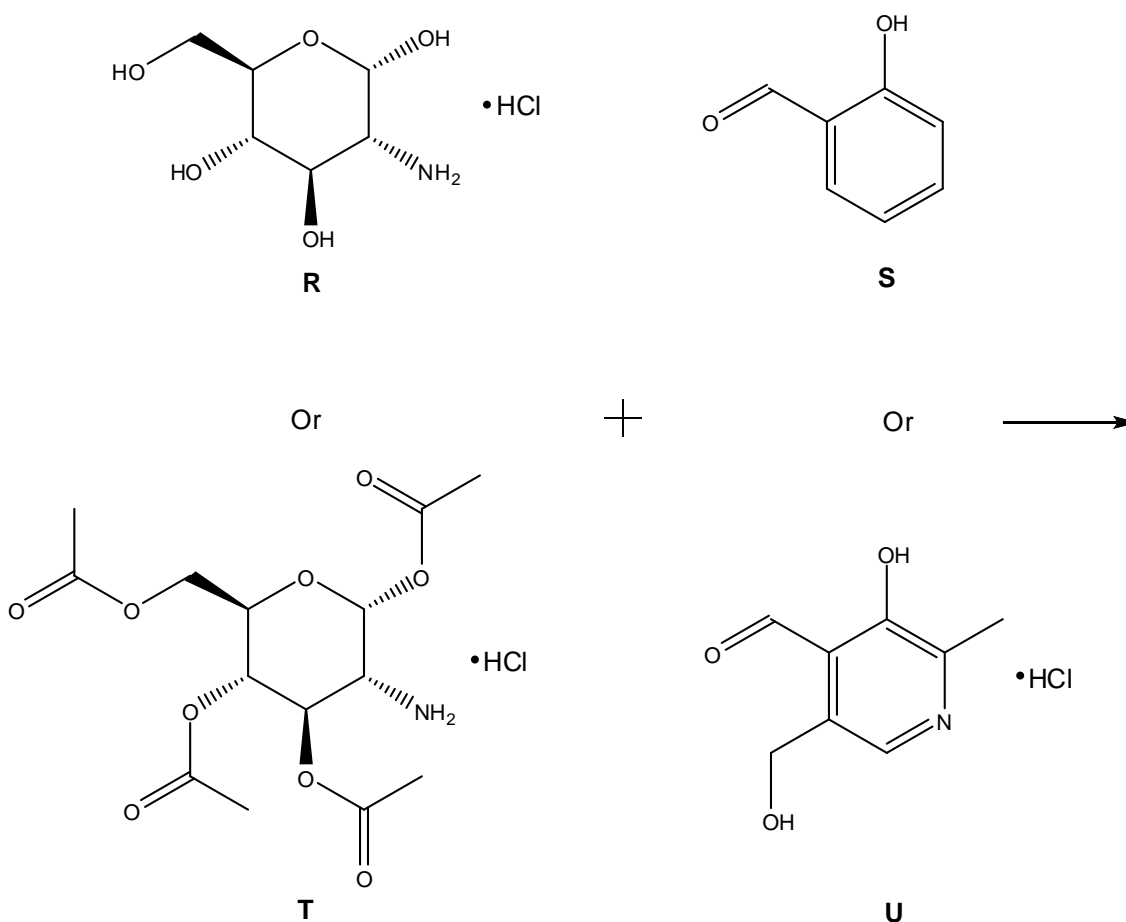


Figure 17: Reagents used to form the four amino sugar-based Schiff's bases. D-glucosmine hydrochloride **R**, salicylaldehyde **S**, 1,3,4,6-tetra-O-acetyl-2-amino-2-deoxy- β -D-glucopyranose hydrochloride **T** and pyridoxal hydrochloride **U**.

To prepare these ligands, 1.00 mmol of amino sugar hydrochloride was dissolved in 50% by volume methanol/water. To this, 1.00 mmol of sodium bicarbonate was added to react with the hydrochloride and free the amino sugar. 1.00 mmol of salicylaldehyde (or 1.00 mmol pyridoxal hydrochloride + 1.00 mmol sodium bicarbonate) was added (Figure 18). Upon addition, each of the solutions became yellow. They were stirred for two hours, left to sit overnight and the precipitate was filtered off and dried in the morning. The structures (Figure 19) were confirmed by NMR (Appendix A p. 27-33) and IR (Appendix B p. 10-13) spectroscopy. The simplest indication of a successful reaction was the appearance of a peak in the IR spectrum between 1640 cm^{-1} and 1643 cm^{-1} (Table 7). This is assigned to an imine bond, indicating the successful synthesis of the ligands. A crystal structure of one of the ligands was also obtained (Figure 20).

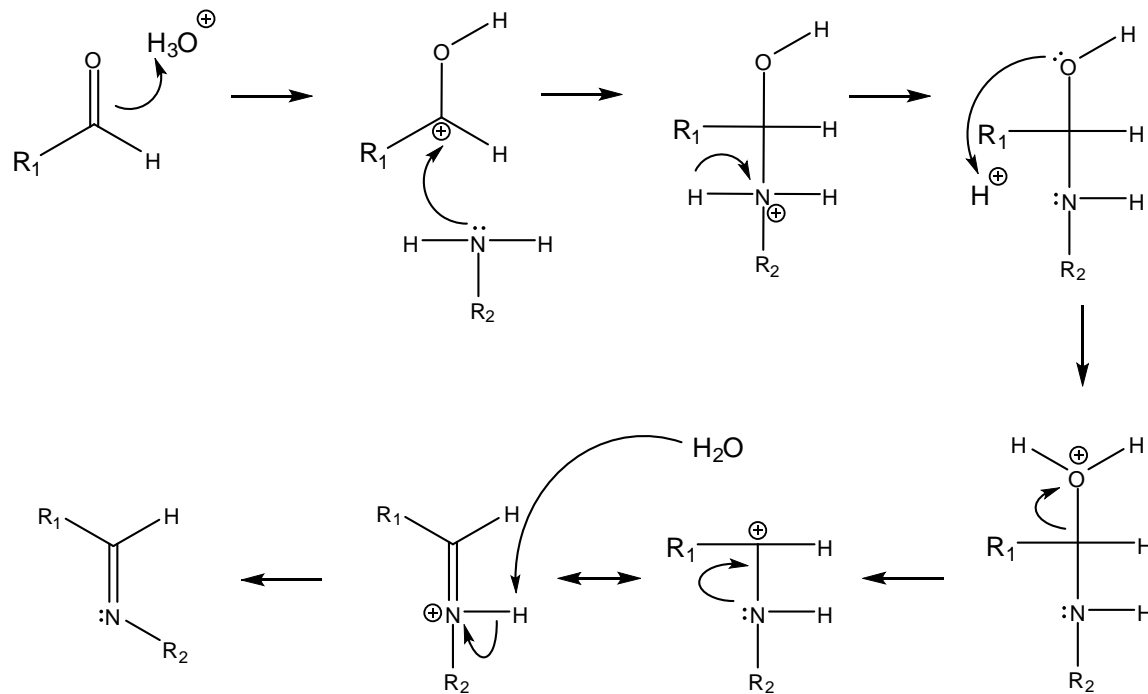


Figure 18: Mechanism of the amine aldehyde condensation which produces the amino sugar-based Schiff's bases.

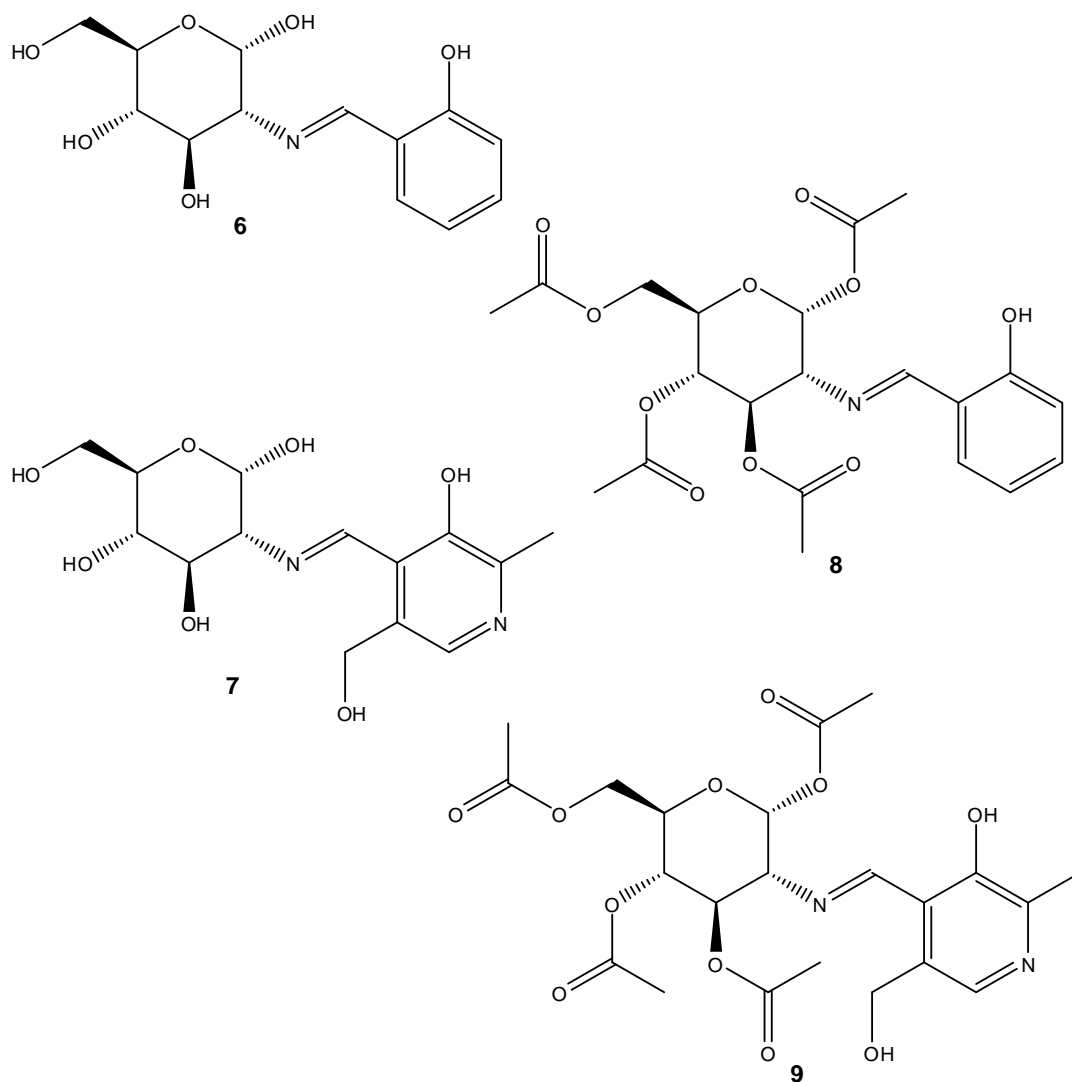


Figure 19: The synthesized amino sugar-based Schiff's bases. Glucosamine-salicylaldehyde Schiff's base **6**, glucosamine-pyridoxal Schiff's base **7**, tetraacetylglucosamine-salicylaldehyde Schiff's base **8** and tetraacetylglucosamine-pyridoxal Schiff's base **9**. Compounds **6** and **7**, which are soluble in water and alcohols, were originally synthesized but were difficult to crystallize once chelated. Compounds **8** and **9**, which are soluble in acetone and alcohols and sparingly soluble in water, were synthesized. These compounds would be more likely to crystallize out of a water-alcohol mixture due to their lower solubility in said solvents.

Product	Peak (cm ⁻¹)
6	1632
7	1645
8	1632
9	1632

Table 7: List of IR peaks arising from imines, indicating successful synthesis of products **6**, **7**, **8** and **9**.

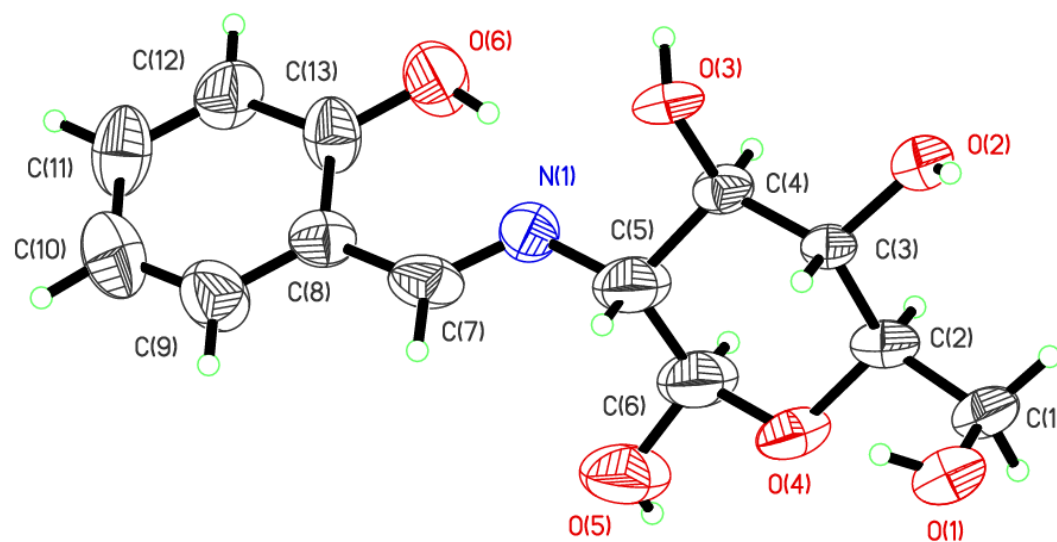


Figure 20: Thermal ellipsoid plot (50% probability ellipsoids) of **6**. Selected bond distances (Å) and angles (°): N1-C7 1.268(9), N1-C5 1.485(10), C8-C7 1.428(11), C5-C4 1.509(11), C5-C6 1.572(13), C8-C9 1.354(11), C8-C13 1.404(11), C9-C8-C13 119.0(8), C9-C8-C7 121.5(8), C13-C8-C7 119.5(7), N1-C7-C8 124.3(8), C7-N1-C5 120.3(8), N1-C5-C4 111.3(7), N1-C5-C6 108.5(7).

The produced Schiff's bases were dissolved in an ethanol-water mixture and to these, 0.5 molar equivalents of $\text{Cu}(\text{OAc})_2$ were added. The solutions were stirred for several hours and then cooled. When using ligand **9**, small green crystals were isolated after filtering or by rotary evaporation. These crystals were mounted on the X-ray diffractometer, but did not diffract, thus no data could be collected. Infrared spectroscopy showed a shift in the imine peak, attributed to new coordination at the nitrogen site. The compound was believed to be paramagnetic and upon attempting to collect NMR data, no meaningful results were obtained. Consequently, NMR characterization was abandoned. Chelates formed by the other three ligands were not isolable. At this point, it was decided that a binding study would be performed in lieu of collecting crystal data.

5.5.2 Binding studies

Binding studies were performed in duplicate on all four ligands. Not all ligands were tested on the same day, but a new calibration curve was produced for each day. For each experiment, 100 mL of a 1 mM solution of ligand (with 2% v/v ionic strength adjustment buffer added) was titrated with a 100 ppm (1.6 mM) solution of copper (II) (also with added ISAB) at a pH of 6. Figure 21 shows the plot of the data collected when titration was performed on the glucosamine-salicylaldehyde Schiff's base.

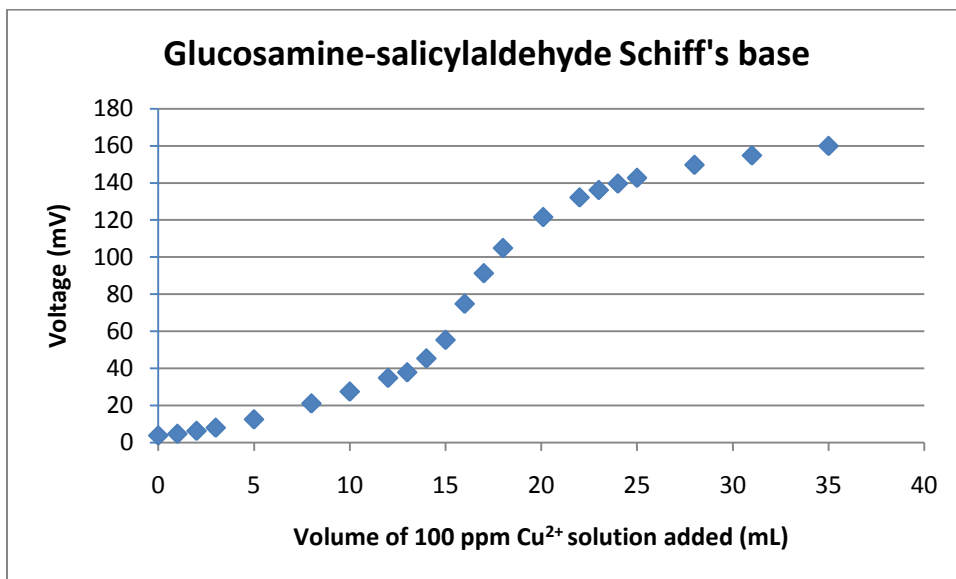


Figure 21: A graph of the voltage recorded during the titration of the glucosamine-salicylaldehyde Schiff's base.

Using the equation from the linear regression of the calibration curve (Figure 22)

-

where x = voltage (in mV), the pCu can be determined. By taking the inverse log of this number, the concentration of copper ion (in ppm) was found and plotted against the volume of copper solution added (Figure 23).

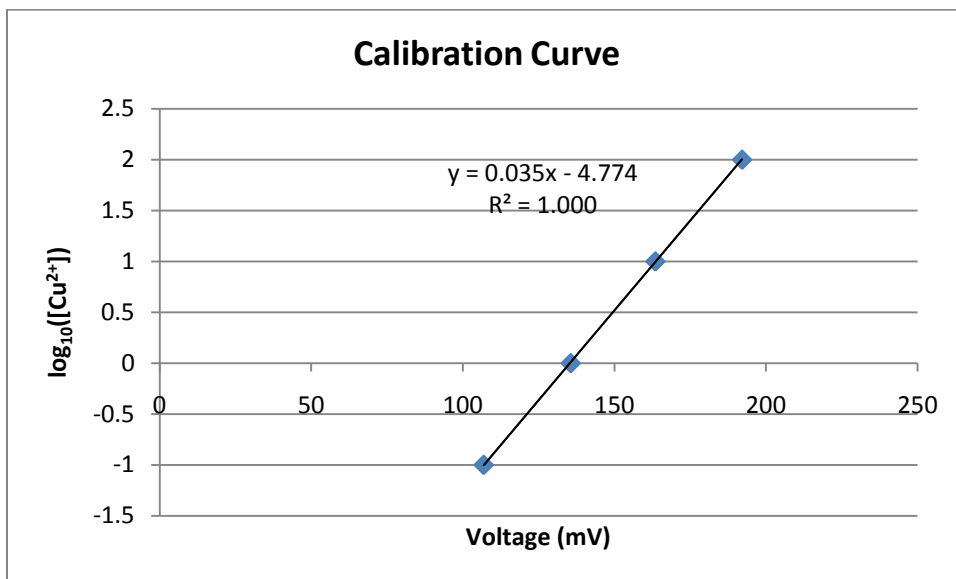


Figure 22: Calibration curve for glucosamine-salicylaldehyde Schiff's base titration.

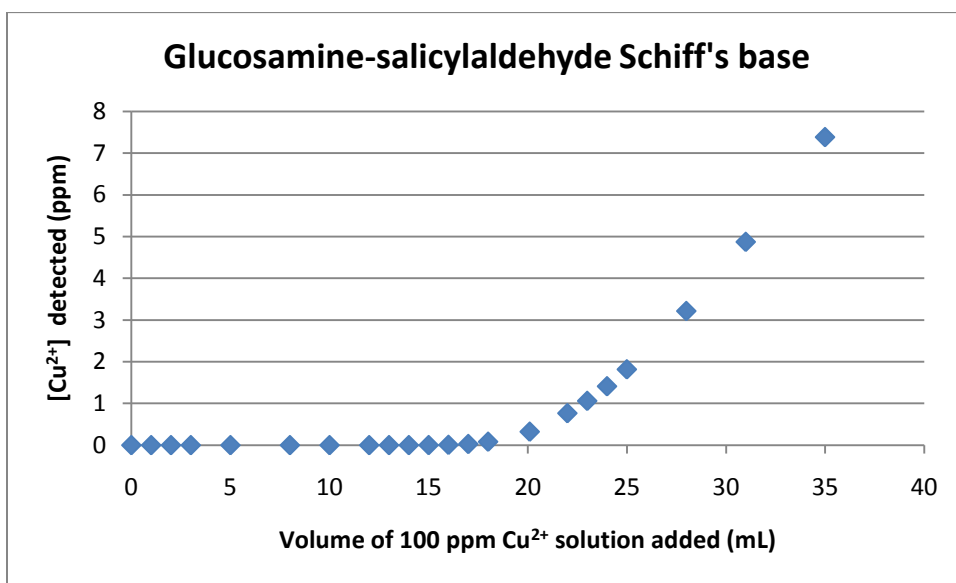


Figure 23: Plot of the volume of copper ion solution added (mL) vs. the concentration of copper ion detected (ppm) for the glucosamine-salicylaldehyde Schiff's base titration.

The “knee” or bend of the graph where the data begins to deviate from the baseline indicates that the solution is at equilibrium (at 18 mL on Figure 23). Thus, using the data from this point and the general equation

where $[M_xL_y]$ is the concentration of the metal-ligand complex and $[M]$ and $[L]$ are the concentrations of the metal ion and ligand respectively. The concentration of the free metal ion is measured directly by the ion-selective electrode. The complex is calculated from the difference between metal ion added and metal ion detected and the ligand concentration is calculated from the difference between the original amount of ligand and the amount of chelate formed.

Adam and Hall discuss their metal-chelates as having a 2:1 ligand to metal ratio⁸⁷; an example is shown in Figure 24. However, in the current work the equivalence point occurred at 18 mL of added copper solution which means that only 0.029 mmols of copper ion were used to reach equilibrium with 0.101 mmols of ligand, so a 3:1 ratio could also have been plausible. Hence, calculations were completed for both scenarios.

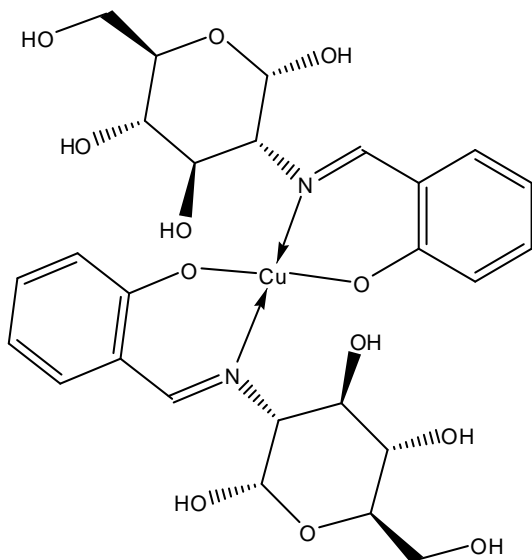


Figure 24: Adam and Hall's metal-ligand chelate structure.

Assuming a 2:1 ratio, the calculation is as follows:

with a concentration of 0.244mM total Cu^{2+} added and 0.00132mM Cu^{2+} detected
this gives:

where the amount of free ligand remaining is the difference between the original concentration of ligand used (adjusted for dilution) and the concentration of ligand that is chelated (which in this scenario is 2 mols of ligand for every 1 mol of metal-ligand chelate)

Similarly, the equation can be solved for a 3:1 ligand to metal ratio

The other ligand to perform reasonably well was the glucosamine-pyridoxal Schiff's base, as can be seen in Figure 25.

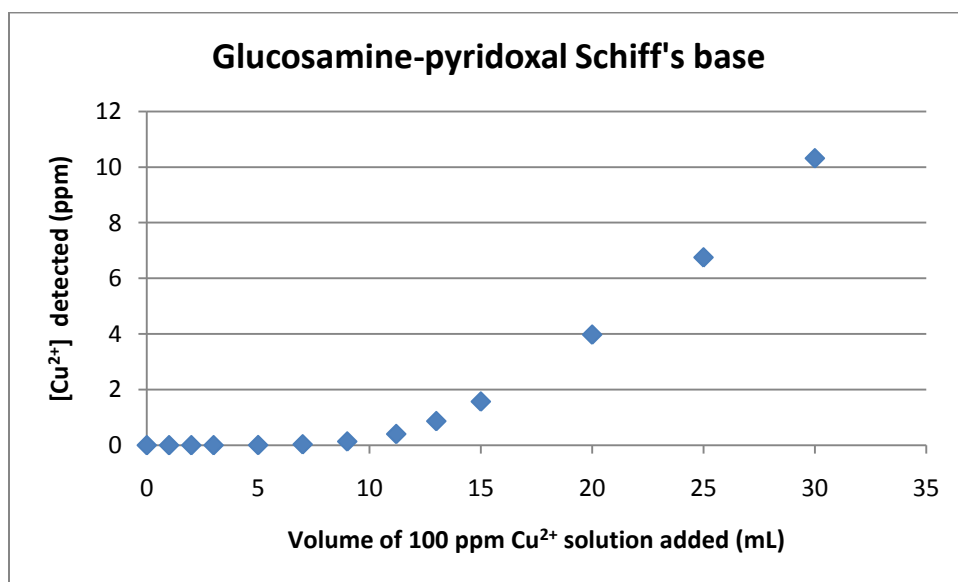


Figure 25: Plot of the volume of copper ion solution added (mL) vs. the concentration of copper ion detected (ppm) for the glucosamine-pyridoxal Schiff's base titration.

As with the previous titration, the equilibrium constant for the glucosamine-pyridoxal Schiff's base can be determined for the chelate as both a 2:1 and 3:1 ratio using the "knee" of the titration graph which was observed to occur at 9 mL of Cu^{2+} solution added.

For a 3:1 ligand to metal ratio the equation is

Unfortunately the Schiff's bases formed from tetraacetylglucosamine did not complex any copper ions as can be seen when comparing their graphs (Figures 26 and 27) to a graph of the addition of the copper (II) ion solution to deionized water (Figure 28).

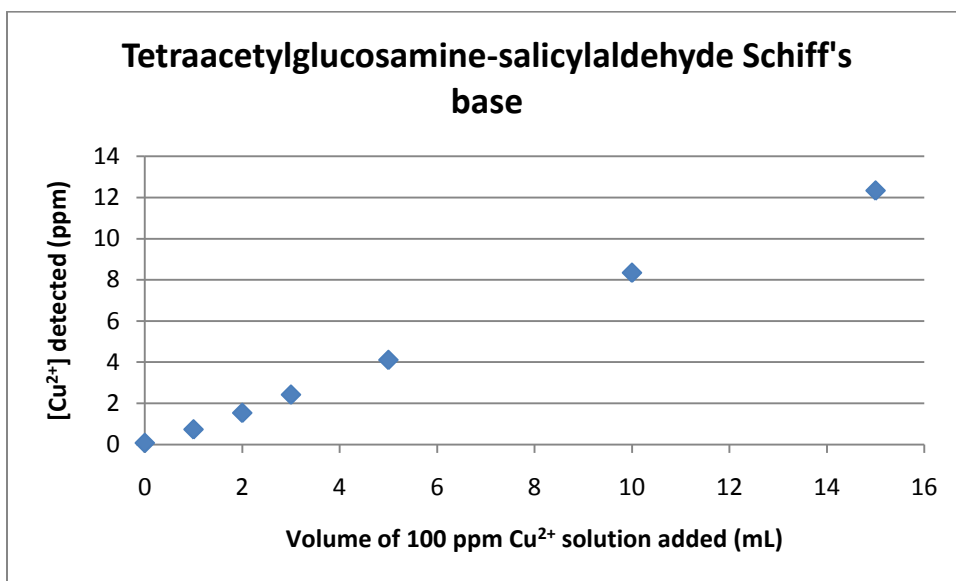


Figure 26: Plot of the volume of copper ion solution added (mL) vs. the concentration of copper ion detected (ppm) for the tetraacetylglucosamine-salicylaldehyde Schiff's base titration.

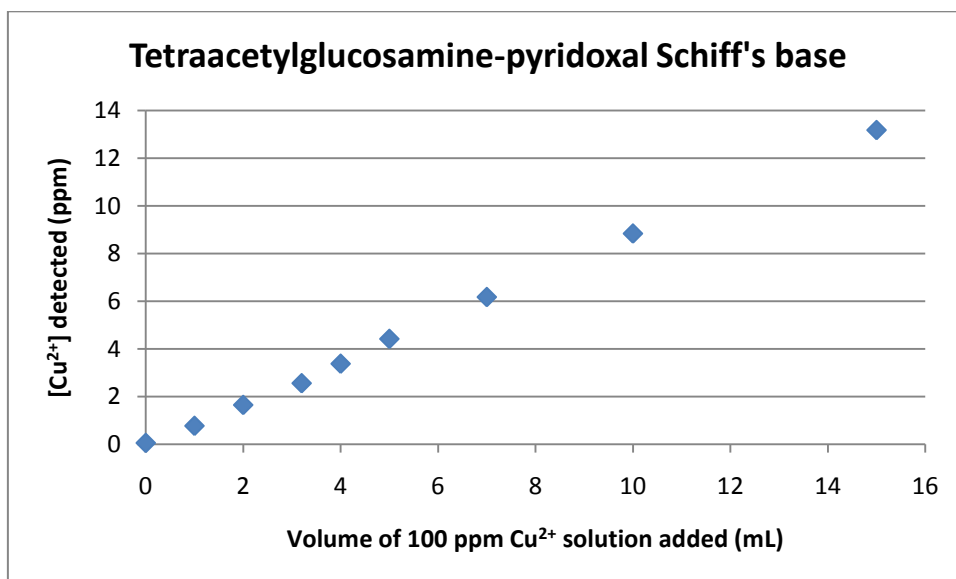


Figure 27: Plot of the volume of copper ion solution added (mL) vs. the concentration of copper ion detected (ppm) for the tetraacetylglucosamine-pyridoxal Schiff's base titration.

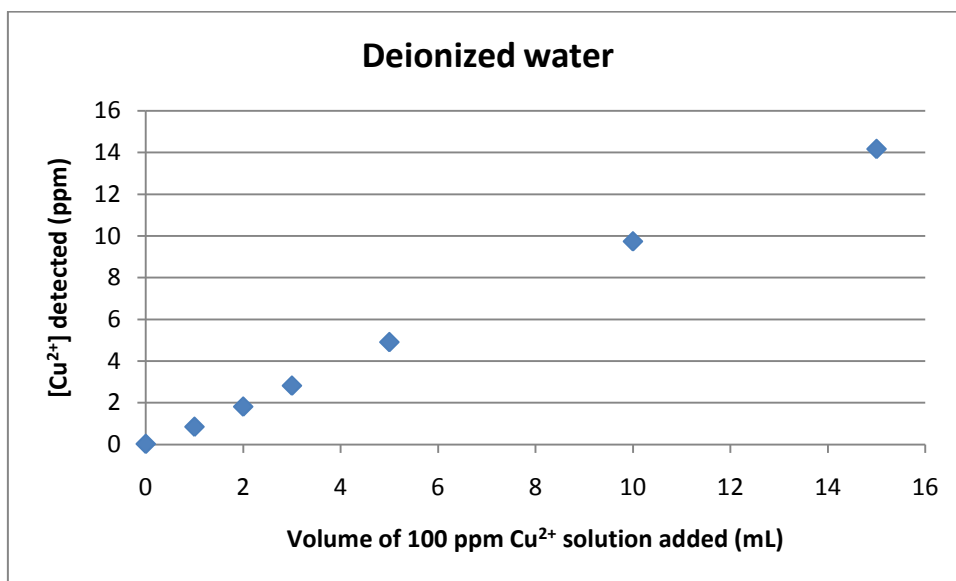


Figure 28: Plot of the volume of copper ion solution added (mL) vs. the concentration of copper ion detected (ppm) for deionized water.

5.6 Conclusion

The observed inability to chelate may be due to the limited solubility of the tetraacetyl compounds. Acylation of glucosamine makes for a larger molecule with a reduced number of OH groups, both factors which would diminish aqueous solubility. Additionally, acylation results in a bulkier ligand which may, sterically, find it difficult to chelate to a metal. Another possibility is that these ligands are fully protonated at a pH of 6. If the hydroxyl functionality of the aldehyde moiety remains protonated, the ligand may be entirely unable to chelate. Alternatively, in the case of **6** and **7**, the ligand may still chelate to the metal, but it may just be via donation from the nitrogen lone pair as opposed to the expected bidentate chelation. This may result in a weaker affinity for the metal. Unfortunately, the

ion-selective electrode used was designed for use only in aqueous media in a pH range of 2-7, thus we cannot attempt to use other solvents or a more basic environment.

The Schiff's base ligand with the strongest stability constant was glucosamine-salicylaldehyde Schiff's Base **6** with a pK_{eq} of 9.126 for a 2:1 ligand to metal ratio. Unfortunately, this is many orders of magnitude lower than the pK_{eq} of copper (II) and EDTA which has been reported as 18.8.⁹³ Thus, these Schiff's bases would make unlikely choices as commercial ligand unless the application required a mitigation of the strength of chelation.

5.7 Experimental

5.7.1 Equipment and analysis

Masses were measured using an *OHAUS* Adventurer Pro AV412C balance. The rotary evaporator used to isolate moisture stable compounds was a *BUCHI* Rotovapor R-210. NMR spectra were obtained on a *Bruker Avance* 500 MHz spectrophotometer. IR spectra were recorded using a *Bruker Vertex* 70 infrared spectrometer as potassium bromide pellets. Elemental analyses were obtained on a *Perkin Elmer 2400 Series II* CHN analyzer. Binding studies were completed using an ELIT 8227 Cupric Ion-Selective Electrode, ELIT 003N Double Junction Reference Electrode, ELIT 201 Dual Electrode Head and Fisher-Scientific Accumet Model 20 pH/Conductivity Meter.

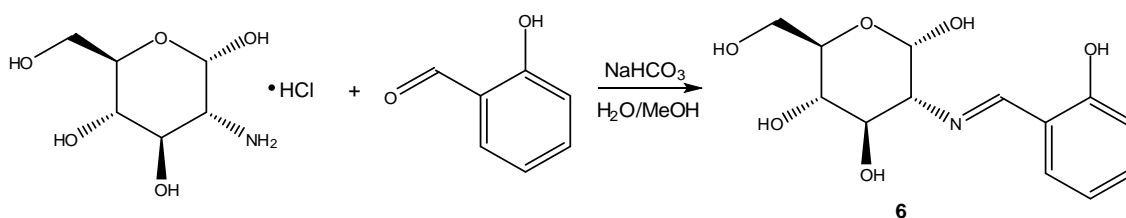
The NMR data was collected by Dr. Michael Lumsden of the Atlantic Region Magnetic Resonance Centre. ^1H spectral shifts were reported in relation to either known residual solvent peaks or TMS, when available. Elemental analysis data was collected by Jessica McClintick using the equipment in the Centre for Environmental Analysis and Remediation (CEAR) at Saint Mary's University. Crystal structures were solved by Arthur Hendsbee and Dr. Katherine Robertson at Saint Mary's University.

5.7.2 Preparation of ligands

Glucosamine-salicylaldehyde Schiff's base (6)

Glucosamine-D-hydrochloride (1.00 g) was weighed out and added to a 50 mL beaker containing a magnetic stir bar. The solid was dissolved in ~15 mL of 50% by volume aqueous methanol. Sodium bicarbonate (0.39 g) was then added to free the glucosamine. Next, salicylaldehyde (0.56 g) was added along with another ~10 mL of solvent. The solution became yellow. The beaker was then covered with a watch glass and the solution was stirred for two hours. At this point the stirring was stopped and the watch glass was removed. The solution was left to evaporate overnight. By the next day, yellow crystals had formed. The product was filtered and dried under reduced pressure. These crystals were then characterized as **6** using infrared spectroscopy, NMR

spectroscopy, elemental analysis and crystallographic data. As the compound is sugar-based it would char, not melt, and thus no melting point was determined.

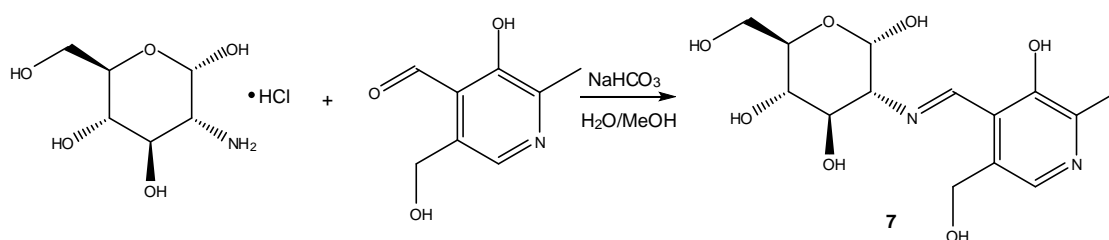


Scheme 15: Synthesis of glucosamine-salicylaldehyde Schiff's base **6**. Product **6** was collected as a yellow solid. Yield = 1.25g, 95%. ^1H NMR (500 MHz, D_2O) δ (ppm): 9.82 (s, Ar-CH), 8.36 (d, Ar-H), 7.33 (m, Ar-H), 6.83 (m, Ar-H), 6.72 (m, Ar-H), 5.28 (d, OH), 4.92 (d, OH), 4.70 (s, OH), 3.84 (m, CH), 3.72 (m, CH_2), 3.44 (m, CH), 3.04 (m, CH). See Appendix A (p. 27-28). IR: See Appendix B (p. 10). E.A. $\text{C}_{13}\text{H}_{17}\text{NO}_6$: Calculated C 55.12, H 6.05, N 4.94. Found C 51.91, H 5.64, N 4.69.

Glucosamine-pyridoxal Schiff's base (7)

Glucosamine-D-hydrochloride (1.00 g) was weighed out and added to a 50 mL beaker containing a magnetic stir bar. The solid was dissolved in ~15 mL of 50% by volume aqueous methanol. Sodium bicarbonate (0.39 g) was then added to free up the glucosamine. Next, pyridoxal hydrochloride (0.94 g) was added along with another ~10 mL of solvent. The solution became yellow. More

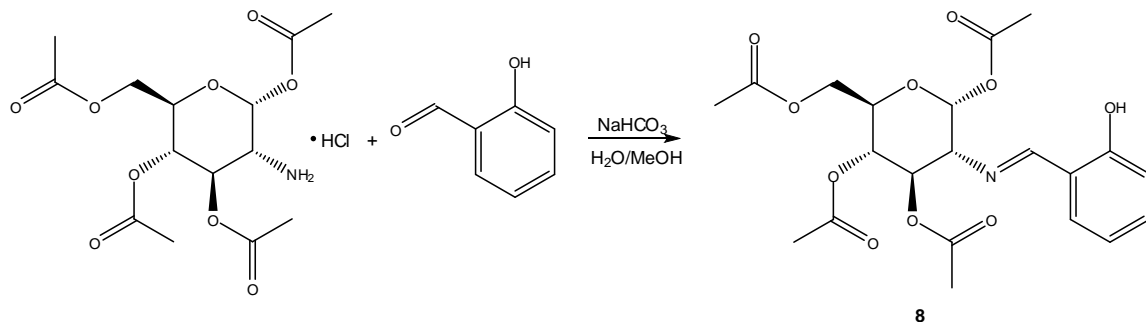
sodium bicarbonate (0.39 g) was added to react with the hydrochloride and free the pyridoxal. This resulted in vigorous bubbling of the solution. The beaker was then covered with a watch glass and the solution was stirred for two hours. At this point the stirring was stopped and the watch glass was removed. The solution was left to evaporate overnight. By the next day, a yellow solid had formed. The product was filtered and dried under reduced pressure. This compound was then characterized as **7** using infrared spectroscopy, NMR spectroscopy and elemental analysis data. As the compound is sugar-based it would char, not melt, and thus no melting point was determined.



Scheme 16: Synthesis of glucosamine-pyridoxal Schiff's base **7**. Product **7** was collected as a yellow solid. Yield = 1.39g, 91%. ^1H NMR (500 MHz, D_2O) δ (ppm): 8.80 (d, Ar-H), 7.45 (s, Ar-CH), 6.44 (d, CH), 5.30 (d, OH), 5.17 (d, OH), 5.12 (d, OH), 5.00 (d, OH), 4.93 (d, OH), 4.51 (d, OH), 3.6 (m, CH, CH_2), 2.34 (s, CH_3). See Appendix A (p. 29). IR: See Appendix B (p. 11). E.A. $\text{C}_{14}\text{H}_{20}\text{N}_2\text{O}_7$: Calculated C 51.22, H 6.14, N 8.53. Found C 55.36, H 5.47, N 8.12.

Tetraacetylglucosamine-salicylaldehyde (8)

1,3,4,6-Tetra-O-acetyl-2-amino-2-deoxy- β -D-glucopyranose hydrochloride (0.50 g) was weighed out and added to a 50 mL beaker containing a magnetic stir bar. The compound was dissolved in ~15 mL of 50% by volume aqueous methanol. Sodium bicarbonate (0.12 g) was then added to free the glucosamine. Next, salicylaldehyde (0.16 g) was added along with another ~10 mL of solvent. The solution became yellow. The beaker was then covered with a watch glass and the solution was stirred for two hours. At this point the stirring was stopped and the watch glass was removed. The solution was left to evaporate overnight. By the next day, a yellow solid had formed. The product was filtered and dried under reduced pressure. This compound was then characterized as **8** using infrared spectroscopy, NMR spectroscopy and elemental analysis. As the compound is sugar-based it would char, not melt, and thus no melting point was determined.

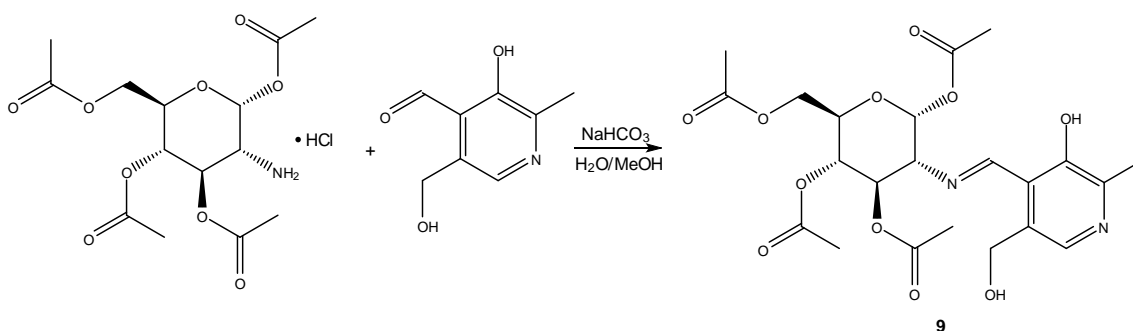


Scheme 17: Synthesis of tetraacetylglucosamine-salicylaldehyde Schiff's base **8**. Product **8** was collected as a yellow solid. Yield = 0.51g, 87%. ¹H NMR (500 MHz, C₃D₆O) δ (ppm): 12.26 (s, 1H, Ar-OH), 8.62 (s, 1H, CH), 7.49 (d,d, J = 1.6Hz, 7.7Hz, 1H, Ar-H), 7.39 (d,t, J = 1.7Hz, 7.9Hz, 1H, Ar-H), 6.94 (d,t, J = 0.8Hz, 7.8Hz, 1H, Ar-H), 6.90 (d, J = 8.3Hz, 1H, Ar-H), 6.16 (d, J = 8.3 Hz, 1H, CH), 5.62 (t, J = 9.7Hz, 1H, CH), 5.13 (t, J = 9.8Hz, 1H, CH), 4.35 (d,d, J = 4.7Hz, 12.4Hz, 1H, CH), 4.27 (d,d,d, J = 2.2Hz, 4.7Hz, 10.0Hz, 1H, CH), 4.14 (d,d, J = 2.2Hz, 12.3Hz, 1H, CH), 3.60 (d,d, J = 8.4Hz, 9.8Hz, 1H, CH), 2.04 (s, 3H, CH₃), 2.03 (s, 6H, CH₃), 1.90 (s, 3H, CH₃). See Appendix A (p. 30-31). IR: See Appendix B (p. 12). E.A. C₂₁H₂₅NO₁₀: Calculated C 55.87, H 5.58, N 3.10. Found C 55.38, H 5.54, N 3.09.

Tetraacetylglucosamine-pyridoxal (**9**)

1,3,4,6-Tetra-O-acetyl-2-amino-2-deoxy-β-D-glucopyranose hydrochloride (0.50 g) was weighed out and added to a 50 mL beaker containing a magnetic stir bar. The compound was dissolved in ~15 mL of 50% by volume aqueous methanol. Sodium bicarbonate (0.12 g) was then added to free up the glucosamine. Next, pyridoxal hydrochloride (0.27 g) was added along with

another ~10 mL of solvent. The solution became yellow. More sodium bicarbonate (0.12 g) was added to react with the hydrochloride and free the pyridoxal. This resulted in vigorous bubbling of the solution. The beaker was then covered with a watch glass and the solution was stirred for two hours. At this point the stirring was stopped and the watch glass was removed. The solution was left to evaporate overnight. By the next day, a yellow solid had formed. The product was filtered and dried under reduced pressure. This compound was then characterized as **9** using infrared spectroscopy, NMR spectroscopy and elemental analysis data. As the compound is sugar-based it would char, not melt, and thus no melting point was determined.



Scheme 18: Synthesis of tetraacetylglucosamine-pyridoxal Schiff's base **9**. Product **9** was collected as a yellow solid. Yield = 0.49g, 76%. ¹H NMR (500 MHz, C₃D₆O) δ (ppm): 9.11 (s, 1H, Ar-*H*), 7.97 (s, 1H, Ar-*CH*), 6.25 (d, J = 8.3Hz, 1H, *CH*), 5.68 (t, J = 9.6Hz, 1H, *OH*), 5.15 (t, J = 9.8Hz, 1H, *OH*), 4.85 (q, J = 12.7Hz, 2H, *CH*₂), 4.35 (d,d, J = 4.7Hz, 12.3Hz, *OH*), 4.28 (d,d,d, J = 2.2Hz, 10.0Hz, 4.7Hz, 1H, *CH*), 4.15 (d,d, J = 2.2Hz, 12.3Hz, 1H, *CH*), 3.76 (d,d, J = 8.4Hz, 9.8Hz, 1H, *CH*), 2.44 (s, 3H, *CH*₃), 2.04 (m, 9H, *CH*₃), 1.92 (s, 3H, *CH*₃). See Appendix A (p. 32-33). IR: See Appendix B (p. 13).

5.7.3 Preparation of solutions for the binding study

A 5 M NaNO₃ ionic strength adjustment buffer (ISAB) was prepared by dissolving 21.25 g NaNO₃ in ~35 mL of warm water in a 50 mL beaker. This solution was diluted to a final volume of 50.00 mL using a volumetric flask.

Calibration solutions of 100 ppm, 10 ppm, 1 ppm and 0.1 ppm Cu²⁺ were prepared. From a bottle containing a solution of 1000 ppm Cu²⁺, 10.00 mL was transferred to a 100.00 mL volumetric flask via volumetric pipette. To this, 2.00 mL of ISAB was added, and the solution was then diluted with deionized water to the final volume. From this 100 ppm Cu²⁺ solution, 10.00 mL was transferred to a 100.00 mL volumetric flask via volumetric pipette. To this, 1.80 mL of ISAB was added, and the solution was then diluted with deionized water to the appropriate volume. This step was repeated using the new 10 ppm solution to prepare a 1 ppm solution. It was then repeated again using the 1 ppm solution to prepare the 0.1 ppm solution.

The 100 ppm Cu²⁺ titrant was prepared by scaling up the above procedure. Solutions of the Schiff's base ligands were prepared by weighing approximately 1 mmol (0.0286 g of product **6**, 0.0335 g of product **7**) of each ligand and adding it to a 100.00 mL volumetric flask. ISAB (2 mL) was then added and the solution was diluted to the final volume. The same procedure was followed for products **8** and **9** (0.0456 g of product **8** and 0.0491 g of product **9**) except they were first dissolved in 150 mL beakers each containing ~50 mL of warm water.

5.7.4 Binding study

For the binding study, the cupric ion-selective electrode and double junction reference electrode were secured to the dual electrode head which was connected to the conductivity meter.

The electrodes were partially immersed into a 250 mL beaker containing a calibration solution and a magnetic stir bar stirring at a speed of approximately 100 rpm. Once the voltage display remained stable for ten seconds, the value was recorded. With a reading from each calibration solution, a calibration curve was plotted.

The same procedure was followed when testing samples, with a reading taken after each addition of titrant. Generally, titrant was added in 1-2 mL increments.

Between ligands, the calibration was always checked using one of the known standards. No significant drift was noted.

6. Conclusion

The projects described in this work were met with varying amounts of success. The generation of a radical through the reaction of an ionic liquid with lithium was very successful in that it may shed new light on reactions of electron rich olefins. The ionic liquid dispersants were also very successful as some of the tested samples dispersed oil half as well as the industry leader. This is quite impressive for a biodegradable alternative.

The methylation of carbonyl stabilized ylides was a sound idea and though methylation did occur, it was unfortunately not at the desired site. The chelating abilities of amino-sugar based Schiff bases were also worth investigating, however they are not nearly as effective as current industrial solutions.

Regardless of the progress made in decreasing the environmental impact of industrial processes, there will always be room for improvement. It is our firm belief that chemical solutions, such as those attempted in this body of work, are essential in resolving these issues.

References

- ¹ Weingartner, H. *Angew. Chem. Int. Ed.* **2008**, *47*, 654-670.
- ² Zein El Abedin, S.; Endres, F. *Acct. Chem. Res.* **2007**, *40*, 1106-1113.
- ³ Hough, W.L.; Smiglak, M.; Rodriguez, H.; Swatloski, R.P.; Spear, S.K.; Daly, D.T.; Pernak, J.; Grisel, J.E.; Carliss, R.D.; Soutullo, M.D.; Davis Jr., J.H.; Rogers, R.D. *New J. Chem.* **2007**, *31*, 1429-1436.
- ⁴ Boardman, N.K.; Palmer, A.R.; Heymann, E. *Trans. Faraday Soc.* **1955**, *51*, 277-286.
- ⁵ Lipsztajn, M.; Osteryoung, R.A. *Inorg. Chem.* **1985**, *24*, 3492-3494.
- ⁶ Laus, G.; Bentivoglio, G.; Schottenberger, H.; Kahlenberg, V.; Kopacka, H.; Roeder, H.; Roeder, T.; Sixta, H. *Lenz. Ber.* **2005**, *84*, 71-85.
- ⁷ Plechkova, N.V.; Seddon, K.R. *Chem. Soc. Rev.* **2008**, *37*, 123-150.
- ⁸ Ni, B.; Zhang, Q.; Headley, A.D. *Tet. Letts.* **2008**, *49*, 1249-1252.
- ⁹ Harjani, J.R.; Farrell, J.; Garcia, M.T.; Singer, R.D.; Scammells, P.J. *Green Chem.* **2009**, *11*, 821-829.
- ¹⁰ Scammells, P.J.; Scott, J.L.; Singer, R.D. *Aust. J. Chem.* **2005**, *58*, 155-169.
- ¹¹ Anastas, P.T.; Warner, J.C. *Green Chemistry: Theory and Practice*, Oxford University Press: New York, 1998.
- ¹² Sowmiah, S.; Srinivasadesikan, V.; Tseng, M.; Chu, Y. *Molecules.* **2009**, *14*, 3780-3813.
- ¹³ Kirmse, W. *Angew. Chem. Int. Ed.* **2010**, DOI: 10.1002/anie.201001658.

-
- ¹⁴ Dove, A.P.; Pratt, R.C.; Lohmeijer, B.G.G.; Li, H.; Hagberg, E.C.; Waymouth, R. M.; Hedrick, J.L. N-Heterocyclic Carbenes as Organic Catalysts. In *N-Heterocyclic Carbenes in Synthesis*; Nolan, S.P., Ed.; Wiley: New York, 2006; p. 275.
- ¹⁵ Canal, J.P.; Ramnial, T.; Dickie, D.A.; Clyburne, J.A.C. *Chem. Comm.* **2006**, 1809-1818.
- ¹⁶ Cowan, J.A.; Clyburne, J.A.C.; Davidson, M.G.; Harris, R.L.W.; Howard, J.A.K.; Küpper, P.; Leech, M.A.; Richards, S.P. *Angew. Chem. Int. Ed. Engl.* **2002**, *41*, 1432-1434.
- ¹⁷ Wanzlick, H.W.; Buchler, J.W. *Chem. Ber.* **1964**, *97*, 2447-2452.
- ¹⁸ Arduengo, III, A.J.; Harlow, R.L.; Kline, M.J. *J. Am. Chem. Soc.* **1991**, *113*, 361-363; Arduengo, III, A.J. *Acc. Chem. Res.* **1999**, *32*, 913-921.
- ¹⁹ Arduengo, III, A.J.; Goerlich, J.R.; Marshall, W.J. *Liebigs. Ann.* **1997**, 365-374; Liu, Y.; Lindner, P.E.; Lemal, D.M. *J. Am. Chem. Soc.* **1999**, *121*, 10626-10627; Böhm, V.P.; Herrmann, W.A. *Angew. Chem. Int. Ed.* **2000**, *39*, 4036-4038; Hahn, F.E.; Wittenbecher, L.; Le Van, D.; Fröhlich, R. *Angew. Chem. Int. Ed.* **2000**, *39*, 541-544;
- ²⁰ Alder, R.W.; Blake, M.E.; Chaker, L.; Harvery, J.N.; Paolini, F.; Schütz, J. *Angew. Chem. Int. Ed.* **2004**, *43*, 5896-5911.
- ²¹ Berthon, L.; Nikitenki, S.I.; Bisel, I.; Berthon, C.; Faucon, M.; Saucerotte, B.; Zorz, N.; Moisy, Ph. *Dalton Trans.* **2006**, 2526-2534.

-
- ²² Wishart, J.F.; Shkrob, I.A. In *Ionic Liquids: From Knowledge to Application*; Plechkova, N.V.; Rogers, R.D.; Seddon, K.R., Eds.; ACS Symposium Series 1030; American Chemical Society, Washington, DC, 2009, pp. 119-134.
- ²³ Shkrob, I.A.; Wishart, J.F. *J. Phys. Chem. B.* **2009**, *113*, 5582-5592.
- ²⁴ Shkrob, I.A.; Chemerisov, S.D.; Wishart, J.F. *J. Phys. Chem. B.*, **2007**, *111*, 11786-11793.
- ²⁵ Goodenough, J.B.; Kim, Y. *Chem. Mat.* **2010**, *22*, 587-603.
- ²⁶ Seki, S.; Kobayashi, Y.; Miyashiro, H.; Ohno, Y.; Usami, A.; Mita, Y.; Kihira, N.; Watanabe, M.; Terada, N. *J. Phys Chem. B.* **2006**, *110*, 10228-10230.
- ²⁷ Choi, H.; Baik, C.; Kang, S.O.; Ko, J.; Kang, M.; Nazeeruddin, Md.K.; Grätzel, M. *Angew. Chem. Int. Ed.* **2008**, *47*, 327-330.
- ²⁸ Kuang, D.; Uchida, S.; Humphrey-Baker, R.; Zakeeruddin, S.M.; Grätzel, M. *Angew. Chem. Int. Ed.* **2008**, *47*, 1923-1927.
- ²⁹ Pearce, A.J. Honour's Thesis. St. Catherine's College, Oxford. 1979.
- ³⁰ Graham, D.C.; Cavell, K.J.; Yates, B.F. *J. Phys. Org. Chem.* **2005**, *18*, 298-309.
- ³¹ Le Rouzo, G.; Lamoureux, C.; Dauvois, V.; Dannoux, A.; Legand, S.; Durand, D.; Moisy, P.; Moutiers, G. *Dalton Trans.* **2009**, 6175-6184.
- ³² Shkrob, I.A. *J. Phys. Chem. B.* **2010**, *114*, 368-375.
- ³³ *Spartan '06*, Wavefunction Inc., Irvine, CA, **2006**.
- ³⁴ Stoll, S.; Schweiger, A. *J. Magn. Reson.* **2006**, *178*, 42-55.

³⁵ M. J. T. Frisch, G. W.; Schlegel, H. B.; Scuseria, G. E.; Robb, M. A.; Cheeseman, J. R.; Montgomery, Jr., J. A.; Vreven, T.; Kudin, K. N.; Burant, J. C.; Millam, J. M.; Iyengar, S. S.; Tomasi, J.; Barone, V.; Mennucci, B.; Cossi, M.; Scalmani, G.; Rega, N.; Petersson, G. A.; Nakatsuji, H.; Hada, M.; Ehara, M.; Toyota, K.; Fukuda, R.; Hasegawa, J.; Ishida, M.; Nakajima, T.; Honda, Y.; Kitao, O.; Nakai, H.; Klene, M.; Li, X.; Knox, J. E.; Hratchian, H. P.; Cross, J. B.; Bakken, V.; Adamo, C.; Jaramillo, J.; Gomperts, R.; Stratmann, R. E.; Yazyev, O.; Austin, A. J.; Cammi, R.; Pomelli, C.; Ochterski, J. W.; Ayala, P. Y.; Morokuma, K.; Voth, G. A.; Salvador, P.; Dannenberg, J. J.; Zakrzewski, V. G.; Dapprich, S.; Daniels, A. D.; Strain, M. C.; Farkas, O.; Malick, D. K.; Rabuck, A. D.; Raghavachari, K.; Foresman, J. B.; Ortiz, J. V.; Cui, Q.; Baboul, A. G.; Clifford, S.; Cioslowski, J.; Stefanov, B. B.; Liu, G.; Liashenko, A.; Piskorz, P.; Komaromi, I.; Martin, R. L.; Fox, D. J.; Keith, T.; Al-Laham, M. A.; Peng, C. Y.; Nanayakkara, A.; Challacombe, M.; Gill, P. M. W.; Johnson, B.; Chen, W.; Wong, M. W.; Gonzalez, C.; and Pople, J. A., *Gaussian 09, Revision A.02*, Gaussian, Inc., Wallingford, CT, **2009**.

³⁶ Becke, A.D. *J. Chem. Phys.* **1993**, *98*, 5648-5652. a) Stephens, P.J.; Devlin, F.J.;

Chabalowski, C.F.; Frisch, M.J. *J. Phys. Chem.* **1994**, *98*, 11623-11627.

³⁷ Barone, V. In *In Recent Advances in Density Functional Methods* Chong, D.P., Ed.; World Scientific, Singapore, **1995**, p. 155-159.

³⁸ Bertani, R.; Casarin, M.; Pandolfo, L. *Coord. Chem. Rev.* **2003**, *236*, 15-33.

-
- ³⁹ Wittig, G.; Geissler, G. *Liebigs Ann. Chem.* **1953**, *580*, 44-57.
- ⁴⁰ Press Release: The 1979 Nobel Prize in Chemistry.
http://nobelprize.org/nobel_prizes/chemistry/laureates/1979/press.html (accessed September 2010).
- ⁴¹ Leung, S.H.; Angel, S. A. *J. Chem. Ed.* **2004**, *81*, 1492-1493.
- ⁴² Nguyen, K.C.; Weizman, H. *J. Chem. Ed.* **2007**, *84*, 119-121.
- ⁴³ Bestmann, H.J. *Angew. Chem. Int. Ed. Engl.* **1977**, *16*, 349-364.
- ⁴⁴ Schobert, R.; Hölzel, C. *Topics in Heterocyclic Chemistry.* **2008**, *12*, 193-218.
- ⁴⁵ Daly, J.J.; Wheatley, P.J. *J. Chem. Soc. Sect. A.* **1966**, 1703-1706.
- ⁴⁶ Bertani, R.; Casarin, M.; Ganis, P.; Maccato, C.; Pandolfo, L.; Venzo, A.; Vittadini, A.; Zanotto, L. *Organometallics.* **2000**, *19*, 1373-1383.
- ⁴⁷ Matthews, C.N.; Birum, G.H. *Tet. Letts.* **1966**, *46*, 5707-5710.
- ⁴⁸ Bestmann, H.J.; Schmid, G.; Sandmaier, D. *Chem. Ber.* **1980**, *113*, 912-918.
- ⁴⁹ Sabounchei, S. J.; Nemattalab, H.; Salehzadeh, S.; Khani, S.; Bayat, M.; Adams, H.; Ward, M.D. *Inorganica Chimica Acta.* **2009**, *362*, 105-112.
- ⁵⁰ Geometry optimization was performed at the B3LYP/6-31+G* level using Spartan '06 Windows from Wavefunction, Inc.
- ⁵¹ Tonner, R.; Frenking, G. *Chem. Eur. J.* **2008**, *14*, 3260-3272.
- ⁵² El-Saeed, S.M.; Farag, R.K.; Abdul-Raouf, M.E.; Abdel-Azim, A.A. *Int. J. Poly. Mat.* **2008**, *57*, 860-77.
- ⁵³ Fiocco, R.J.; Lewis, A. *Pure Appl. Chem.* **1999**, *71*, 1, 27-42.

-
- ⁵⁴ Shi, H.; Zhu, W.; Li, H.; Liu, H.; Zhang, M.; Yan, Y.; Wang, Z. *Catalysis Commun.* **2010**, *11*, 588-91.
- ⁵⁵ Liu, L.; Zhi, H.; Luo, J.; Lu, C. *Hanneng Cailiao*, **2009**, *17*, 717-21.
- ⁵⁶ Lee, E.; Ahn, J.; Dharman, M. M.; Park, D.; Park, S.; Kim, I. *Catalysis Today*. **2008**, *131*, 130-4.
- ⁵⁷ Zech, O.; Thomaler, S.; Bauduin, P.; Rück, T.; Touraud, D.; Kunz, W. *J. Phys Chem.* **2009**, *113*, 465-73.
- ⁵⁸ Singh, K.; Marangoni, D.G.; Quinn, J.G.; Singer, R.D. *J. Col. Int. Sci.* **2009**, *335*, 105-11.
- ⁵⁹ Safavi, A.; Maleki, N.; Farjami, F. *Physicochem. Eng. Aspects.* **2010**, *355*, 61-6.
- ⁶⁰ Merrigan, T.L.; Bates, E.D.; Dorman, S.C.; Davis Jr., J.H. *Chem Commun.* **2000**, 2051-2.
- ⁶¹ Boukherissa, M.; Mutelet, F.; Modarressi, A.; Dicko, A.; Dafri, D.; Rogalski, M. *Energy & Fuels.* **2009**, *23*, 2557-64.
- ⁶² Corexit is a registered trademark of Nalco Energy Services, L.P.
- ⁶³ *EPA Response to the BP Spill in the Gulf of Mexico*;
<http://www.epa.gov/bpspill/dispersants-qanda.html#list> (accessed 07/21/10).
- ⁶⁴ Howard, P.; Boethling, R.; Stiteler, W.; Meylan, W.; Beaman, J. *Sci. Tot. Env.* **1991**, *109-10*, 635-41.
- ⁶⁵ Wells, A.S.; Coombe, V.T. *Organic Process Research & Development.* **2006**, *10*, 794-8.

-
- ⁶⁶ Gathergood, N.; Scammells, P.J.; Garcia, M.T. *Green Chem*, **2006**, 8, 156-60.
- ⁶⁷ Erhan, S.M.; Kleiman, R. *J. Am. Oil Chem.Soc.* **1997**, 74, 5, 605-7.
- ⁶⁸ Lalman, J.A.; Bagley, D.M. *Wat. Res.* **2000**, 34, 17, 4220-8.
- ⁶⁹ Aluyor, E.O.; Obahiagbon, K.O.; Ori-jesu, M. *Scientific Research and Essay*. **2009**, 4, 6, 543-8.
- ⁷⁰ Zeisel, S.H.; Da Costa, K.; Franklin, P.D.; Alexander, E.A.; Lamont, J.T.; Sheard, N.F.; Beiser, A. *The FASED Journal*. **1991**, 5, 7, 2093-8.
- ⁷¹ Phadtare, S.B.; Shankarling, G.S. *Green Chem*. **2010**, 12, 458-62.
- ⁷² Murray, S. M.; O'Brien, R. A.; Mattson, K. M.; Ceccarelli, C.; Sykora, R. E.; West, K. N.; Davis, J. H. *Angew. Chem. Int. Ed.* **2010**, 49, 2755-2758.
- ⁷³ Parmar, Y.I.; Sparks, D.L.; Frohlich, J.; Cullis, P.R.; Pritchard, P.H. *J. Lip. Res.* **1989**, 30, 765-71.
- ⁷⁴ Forato, L.A.; Yushmanov, V.E.; Colnago, L.A. *Biochemistry*. **2004**, 43, 7121-6.
- ⁷⁵ Awasthi, N.P.; Singh, R.P. *Eur. J. Lipid. Sci. Technol.* **2009**, 111, 202-6.
- ⁷⁶ Kaku, V.J.; Boufadel, M.C.; Venosa, A.D.; *J. Env. Eng.* **2006**, 132, 93-101.
- ⁷⁷ Cole, M.G., King, T.L. and Lee, K. *Can. Tech. Rep. Fish. Aquat. Sci.* **2007**, 2733 vi + 12p.
- ⁷⁸ Oviedo, C.; Rodríguez, J. *Quim. Nova*. **2003**, 26, 901-905.
- ⁷⁹ Flora, S. J.; Pachauri, V. *Int. J. Env. Res. Pub. Hea.* **2010**, 7, 2745-88.
- ⁸⁰ Williams, D.; *Chem. Br.* **1998**, 1, 48-52.
- ⁸¹ Martell, A. E.; Smith, R. M. *Critical stability constants*. Plenum Press: New York, 1974.

-
- ⁸² Lanigan, R. S.; Yamarik, T. A. *Int. J. Tox.* **2002**, *21*, 95-142.
- ⁸³ Friedly, J. C.; Kent, D. B.; Davis, J. A. *Env. Sci. Technol.* **2002**, *36*, 355-63.
- ⁸⁴ Hakem, N.; Allen, P.; Sylwester, E.; *Radioanal. Nucl. Chem.* **2001**, *250*, 47-53.
- ⁸⁵ Saifullah; Meers, E.; Qadir, M.; de Caritat, P.; Tack, F. M.; Du Laing, G.; Zia, M. H. *Chemosphere.* **2009**, *74*, 1279-91.
- ⁸⁶ Irvine, J.C.; Earl, J.C. *J. Chem. Soc.* **1922**, *121*, 2376.
- ⁸⁷ Adam, M. J.; Hall, L. D. *Can. J. Chem.* **1982**, *60*, 2229-37.
- ⁸⁸ Saghatforoush, L. A.; Aminkhani, A.; Ershad, S.; Karimnezhad, G.; Ghamammy, S.; Kabiri, R. *Molecules.* **2008**, *13*, 804-811.
- ⁸⁹ Costamagna, J.; Barroso, N.; Matsuhira, B.; M *Inorg. Chim. Acta.* **1998**, *20*, 191-195.
- ⁹⁰ Ringbom, A. *Complexation in Analytical Chemistry: A Guide for the Critical Selection of Analytical Methods Based on Complexation Reactions*; Chemical Analysis, Vol. 16, Elving, P.J.; Kolthoff, I.M., Eds.; Robert E. Krieger: New York, 1963.
- ⁹¹ Eriks, J. C.; Gaisser, H. D.; Van Der Goot, H.; Timmerman, H. *Pharm. Week. Sci. Ed.* **1983**, *5*, 319-24.
- ⁹² Radic, N.; Komljenovic, J. *J. Chem. Ed.* **1993**, *70*, 509.
- ⁹³ Smith, R.M.; Martell, A.E. NIST Critically Selected Stability Constants of Metal Complexes Database Version 8.0 for Windows. College Station, Texas. **2004**.

Appendix A:

^1H , ^{13}C and ^{31}P NMR spectra for selected compounds

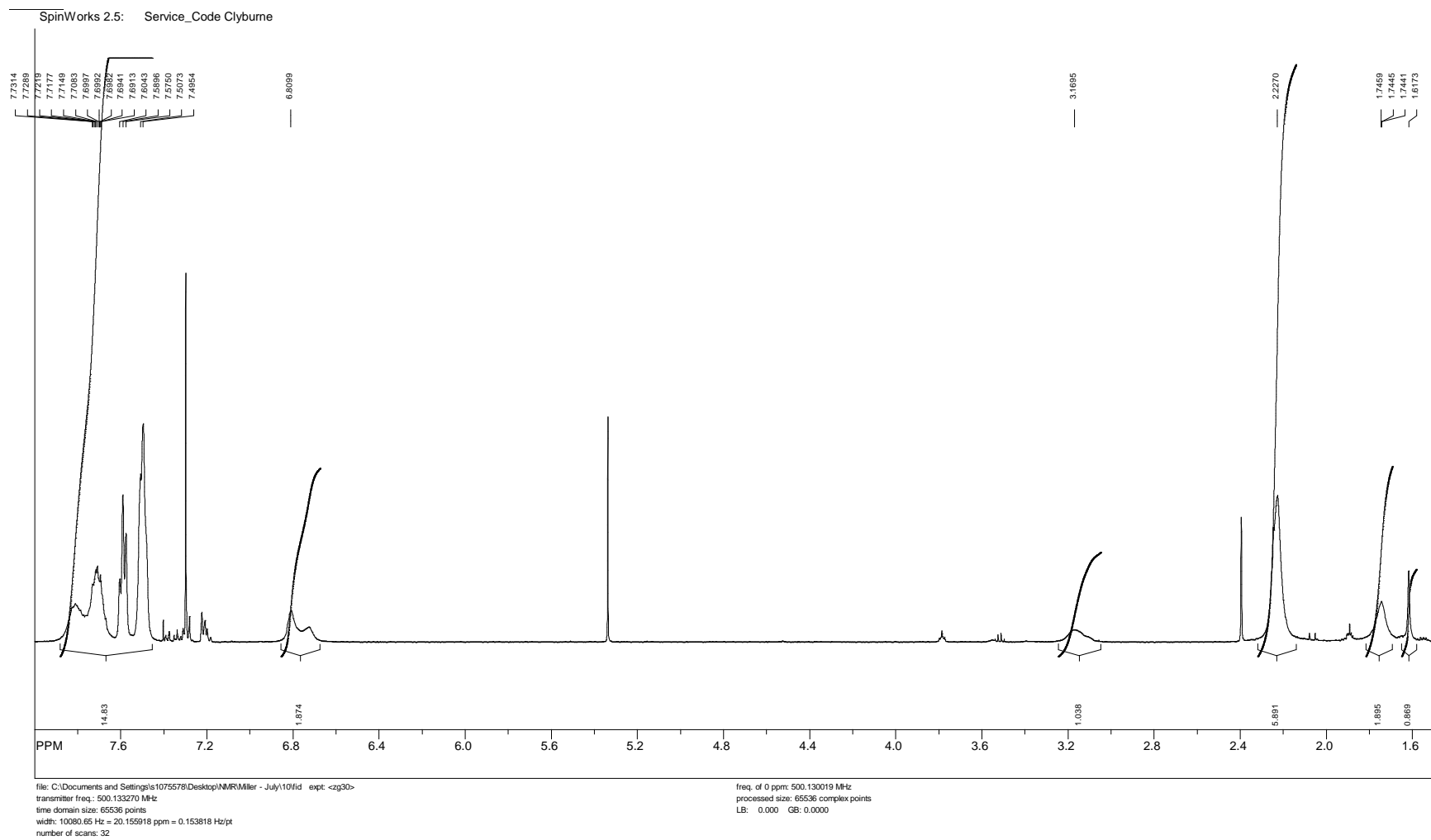
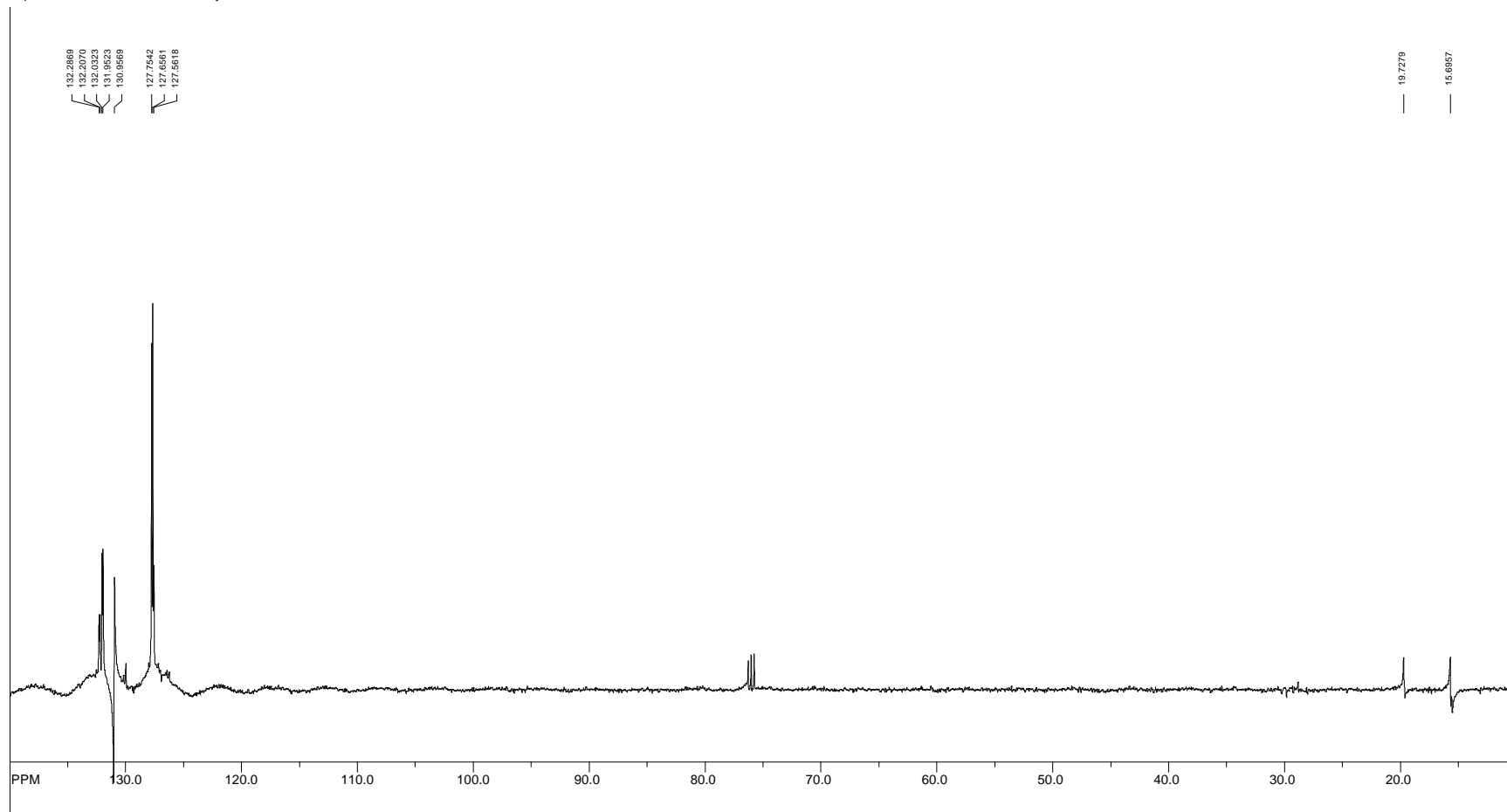


Figure A1: Trimethylphenol substituted carbon stabilized ylide (**2**) ^1H NMR.

SpinWorks 2.5: Service_Code Clyburne

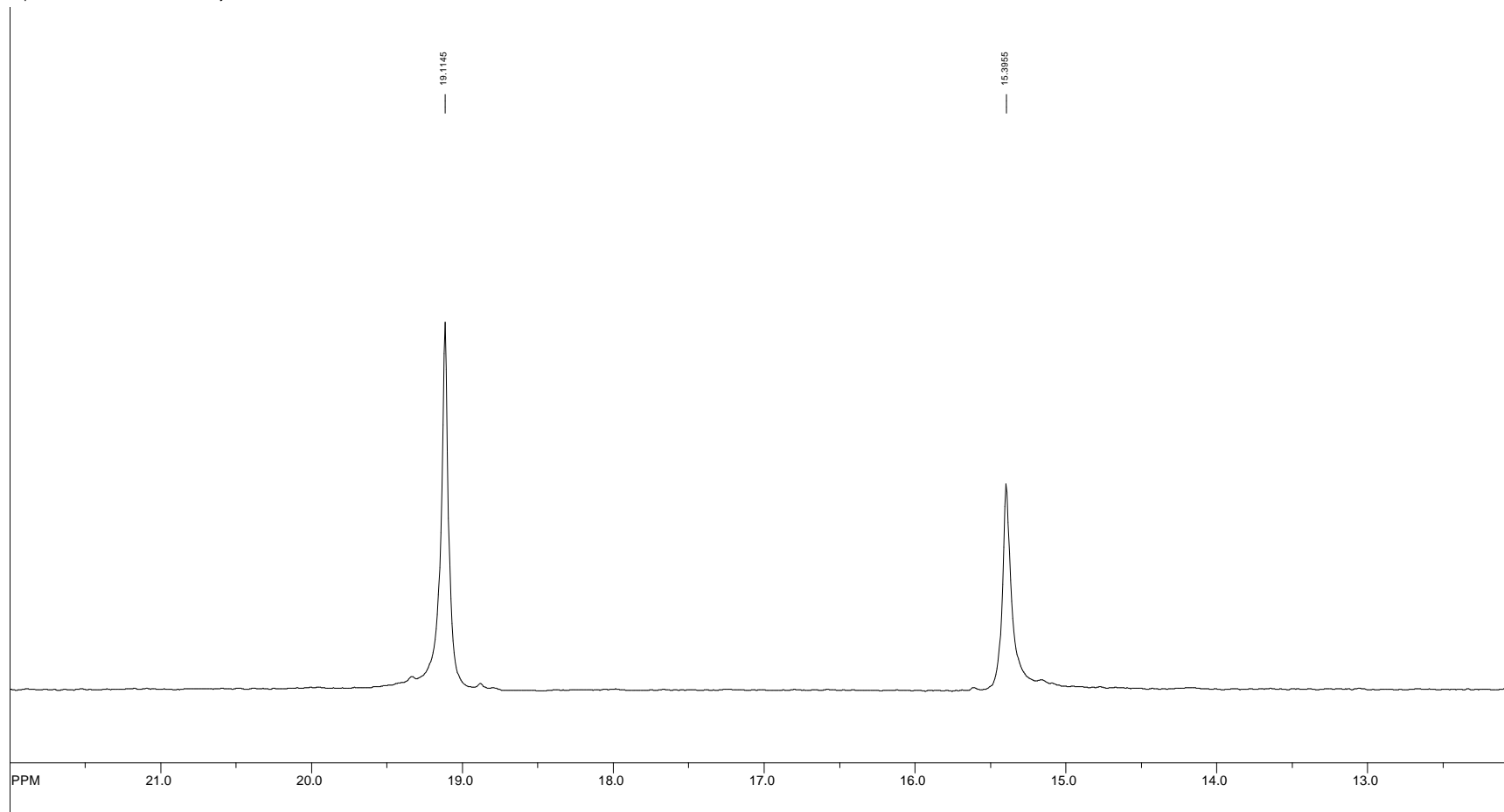


file: C:\Documents and Settings\1075578\Desktop\NMR\April 9 2010\CS060\221fid -expt -<deplqsp.dmc>
transmitter freq.: 125.771627 MHz
time domain size: 50670 points
width: 33783.78 Hz = 268.612123 ppm = 0.666741 Hz/pt
number of scans: 512

freq. of 0 ppm: 125.757928 MHz
processed size: 65536 complex points
LB: 0.000 GB: 0.0000

Figure A2: Trimethylphenol substituted carbon stabilized ylide (**2**) ^{13}C NMR.

SpinWorks 2.5: Service_Code Clyburne

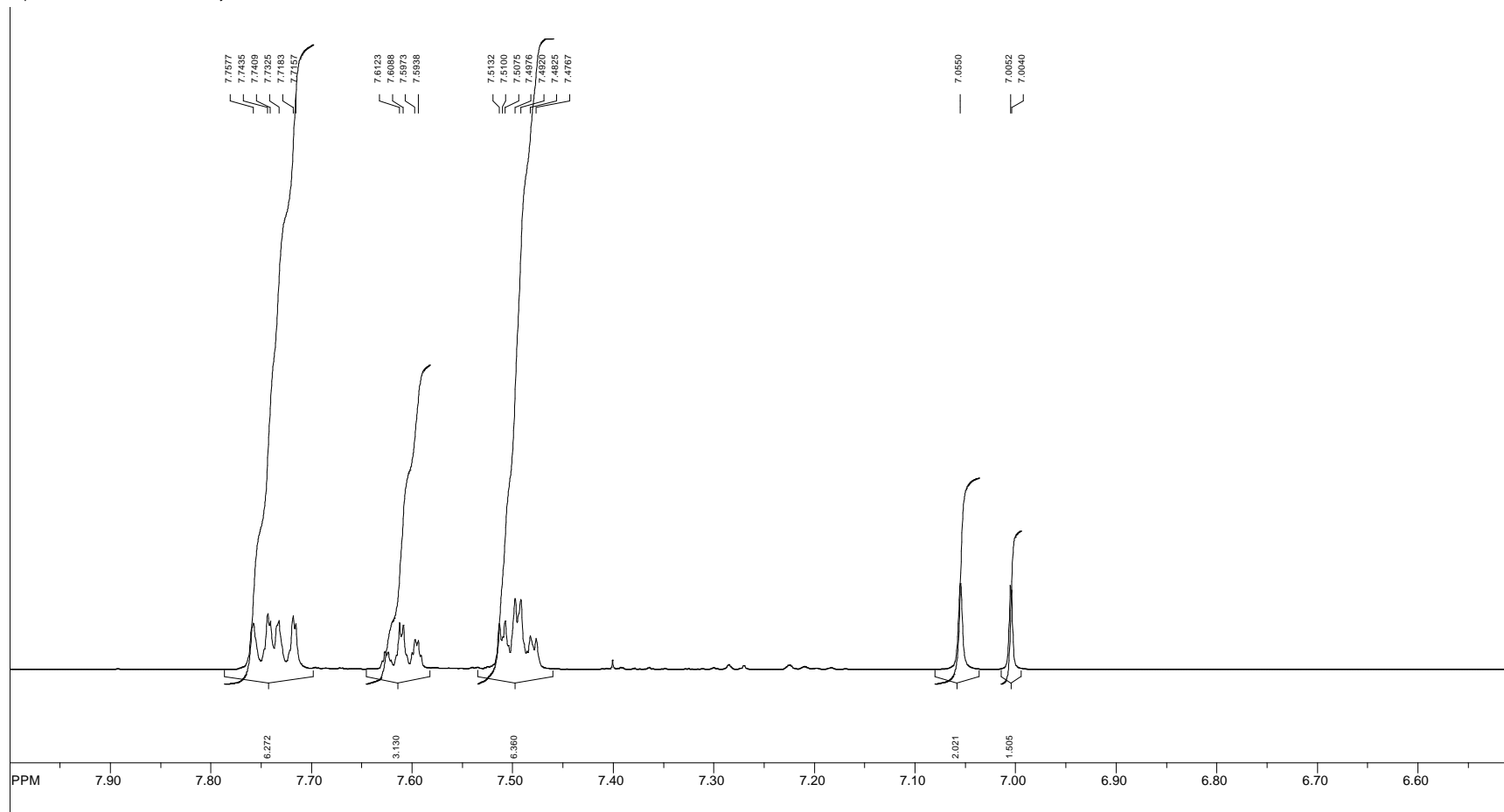


file: C:\Documents and Settings\1075578\Desktop\NMR\April 9 2010\CS060121\fid -expt -<zggg30>
transmitter freq.: 202.466466 MHz
time domain size: 65536 points
width: 98039.22 Hz = 484.224463 ppm = 1.495960 Hz/pt
number of scans: 128

freq. of 0 ppm: 202.456343 MHz
processed size: 65536 complex points
LB: 0.000 GB: 0.0000

Figure A3: Trimethylphenol substituted carbon stabilized ylide (**2**) ^{31}P NMR.

SpinWorks 2.5: Service_Code Clyburne

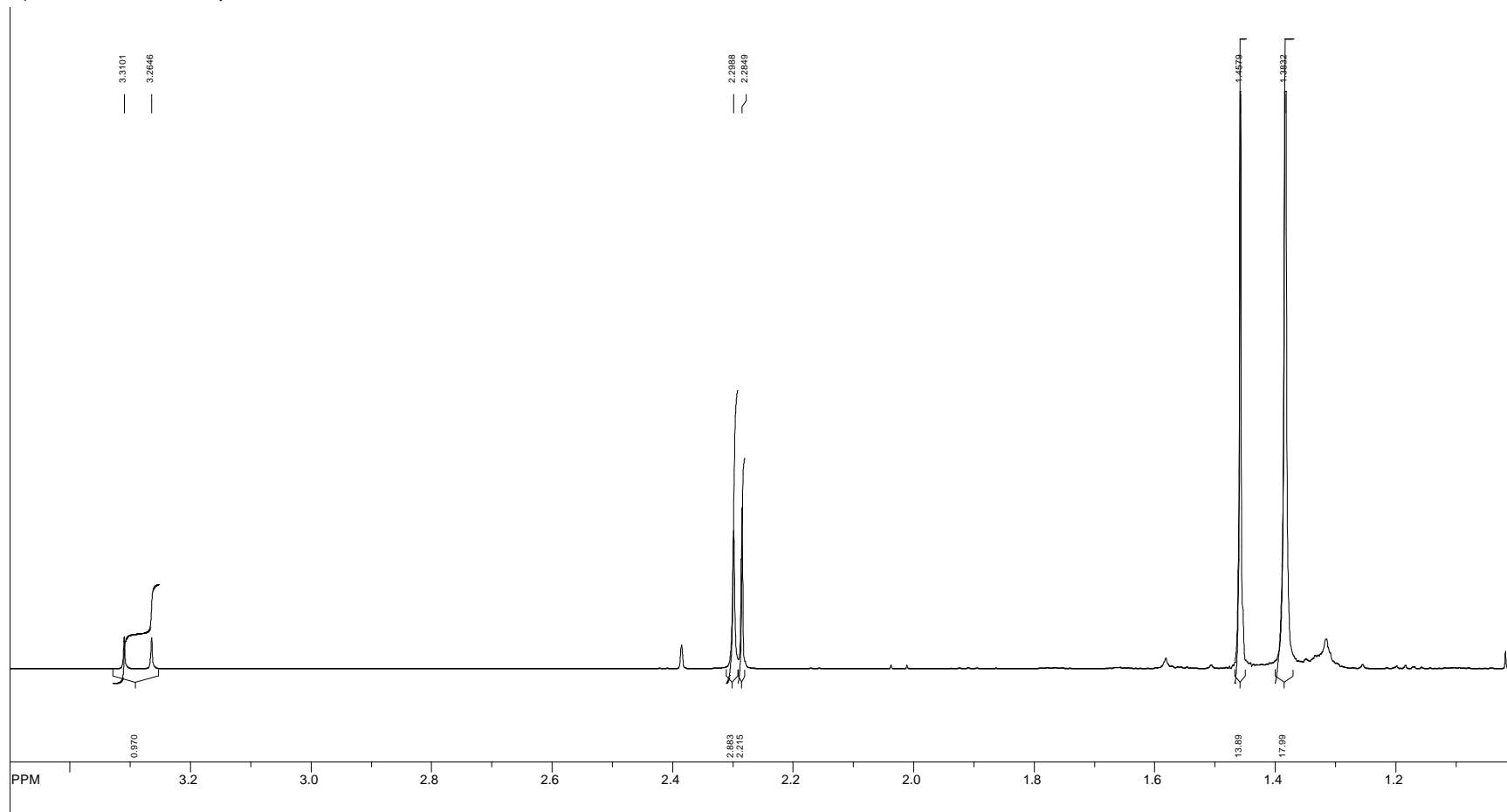


file: C:\Documents and Settings\1075578\Desktop\NMR\December\CL014\10\fid exp: <2330>
transmitter freq.: 500.133270 MHz
time domain size: 65536 points
width: 10080.65 Hz = 20.155918 ppm = 0.153818 Hz/pt
number of scans: 32

freq. of 0 ppm: 500.130019 MHz
processed size: 65536 complex points
LB: 0.000 GB: 0.0000

Figure A4: Tert-butylhydroxytoluene substituted carbon stabilized ylide (**3**) ^1H NMR.

SpinWorks 2.5: Service_Code Clyburne

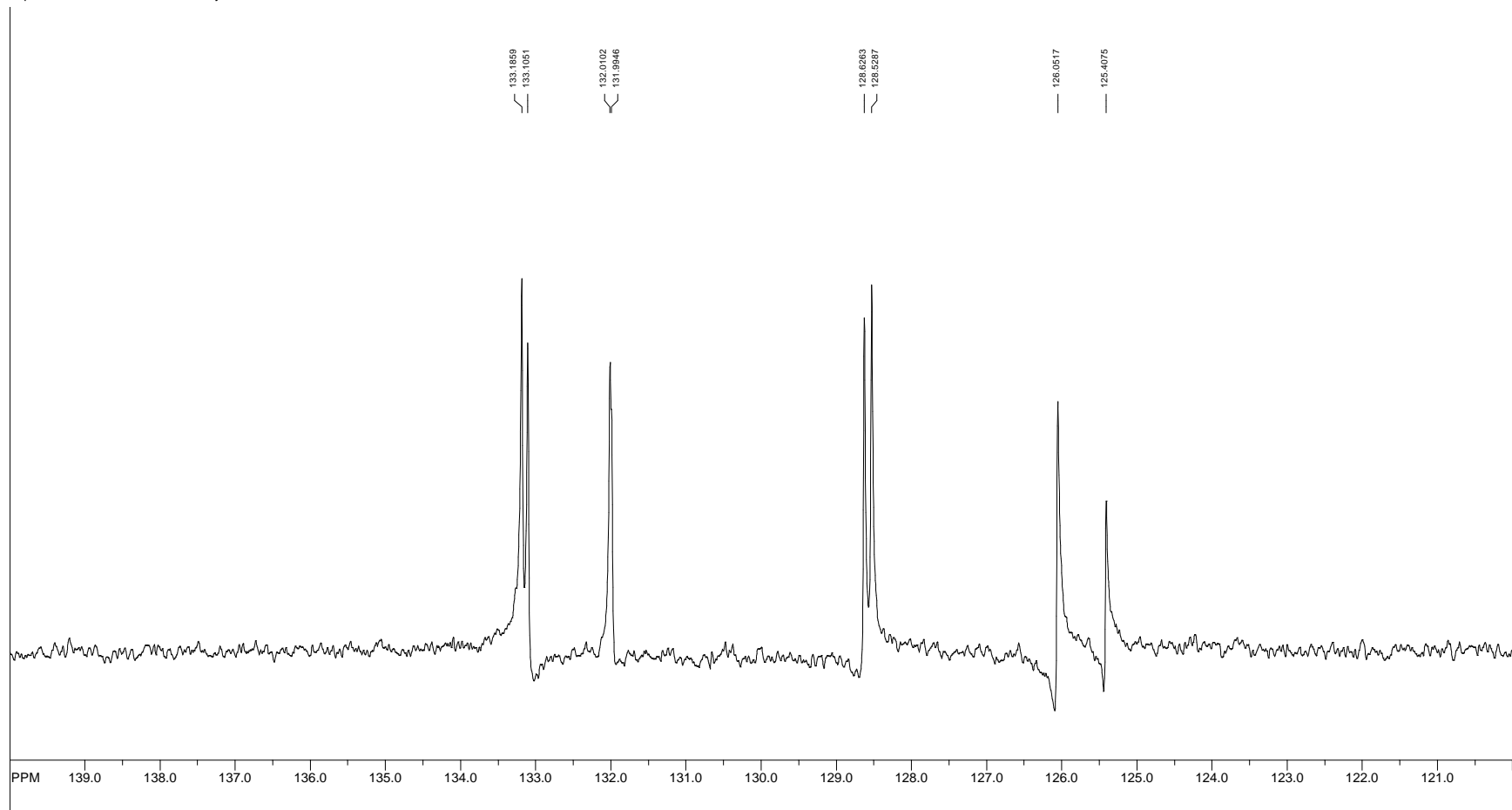


file: C:\Documents and Settings\1075578\Desktop\NMR\December\CL014110\fid exp: <2330>
transmitter freq.: 500.133270 MHz
time domain size: 65536 points
width: 10080.65 Hz = 20.155918 ppm = 0.153818 Hz/pt
number of scans: 32

freq. of 0 ppm: 500.130019 MHz
processed size: 65536 complex points
LB: 0.000 GB: 0.0000

Figure A5: Tert-butylhydroxytoluene substituted carbon stabilized ylide (**3**) ^1H NMR.

SpinWorks 2.5: Service_Code Clyburne

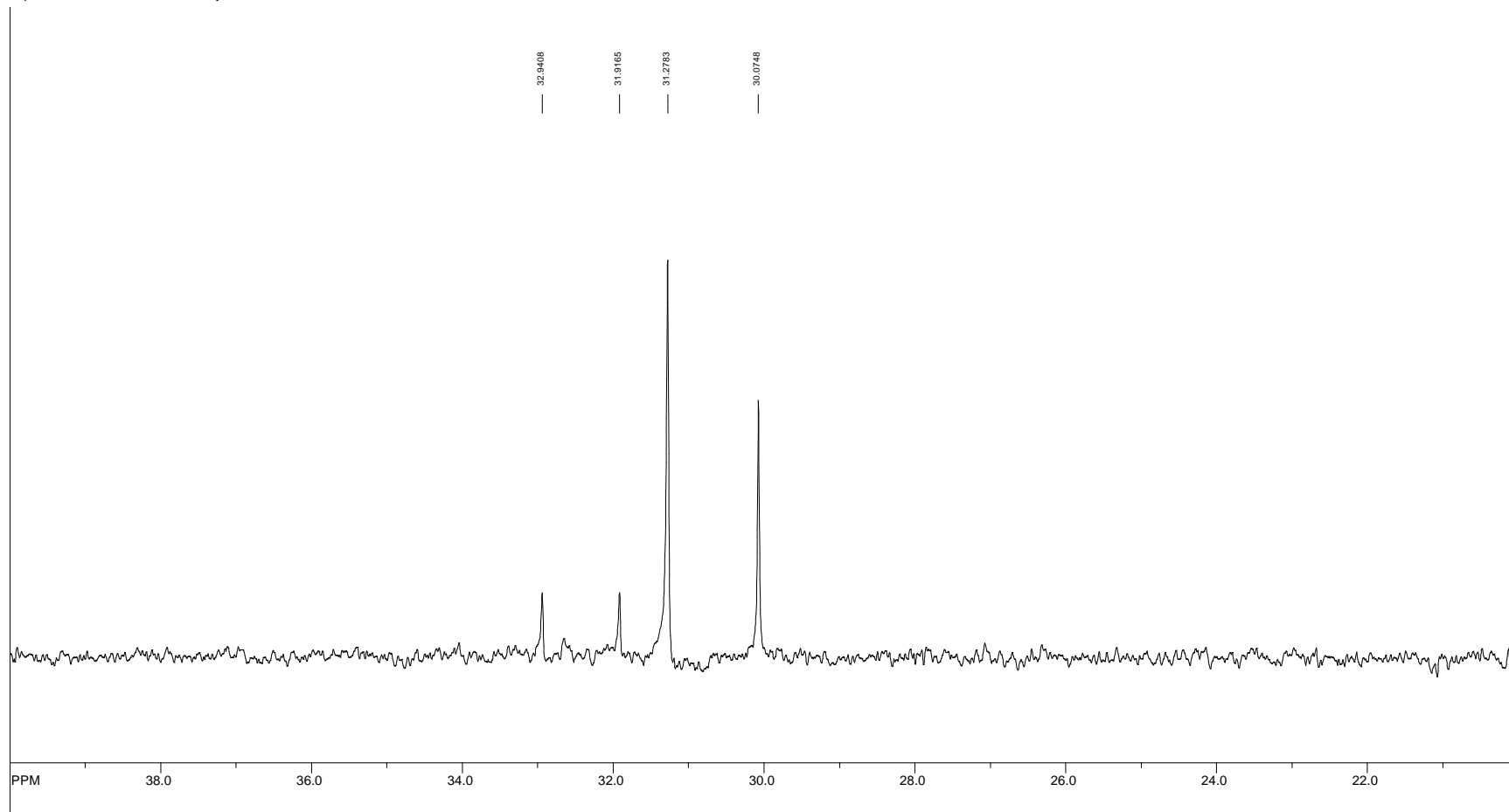


file: C:\Documents and Settings\1075578\Desktop\NMR\December\CL014\12fid exp: <deftsp13>
transmitter freq.: 125.771627 MHz
time domain size: 32768 points
width: 33783.78 Hz = 268.612123 ppm = 1.030999 Hz/pt
number of scans: 775

freq. of 0 ppm: 125.757793 MHz
processed size: 65536 complex points
LB: 0.000 GB: 0.0000

Figure A6: Tert-butylhydroxytoluene substituted carbon stabilized ylide (**3**) ^{13}C NMR.

SpinWorks 2.5: Service_Code Clyburne

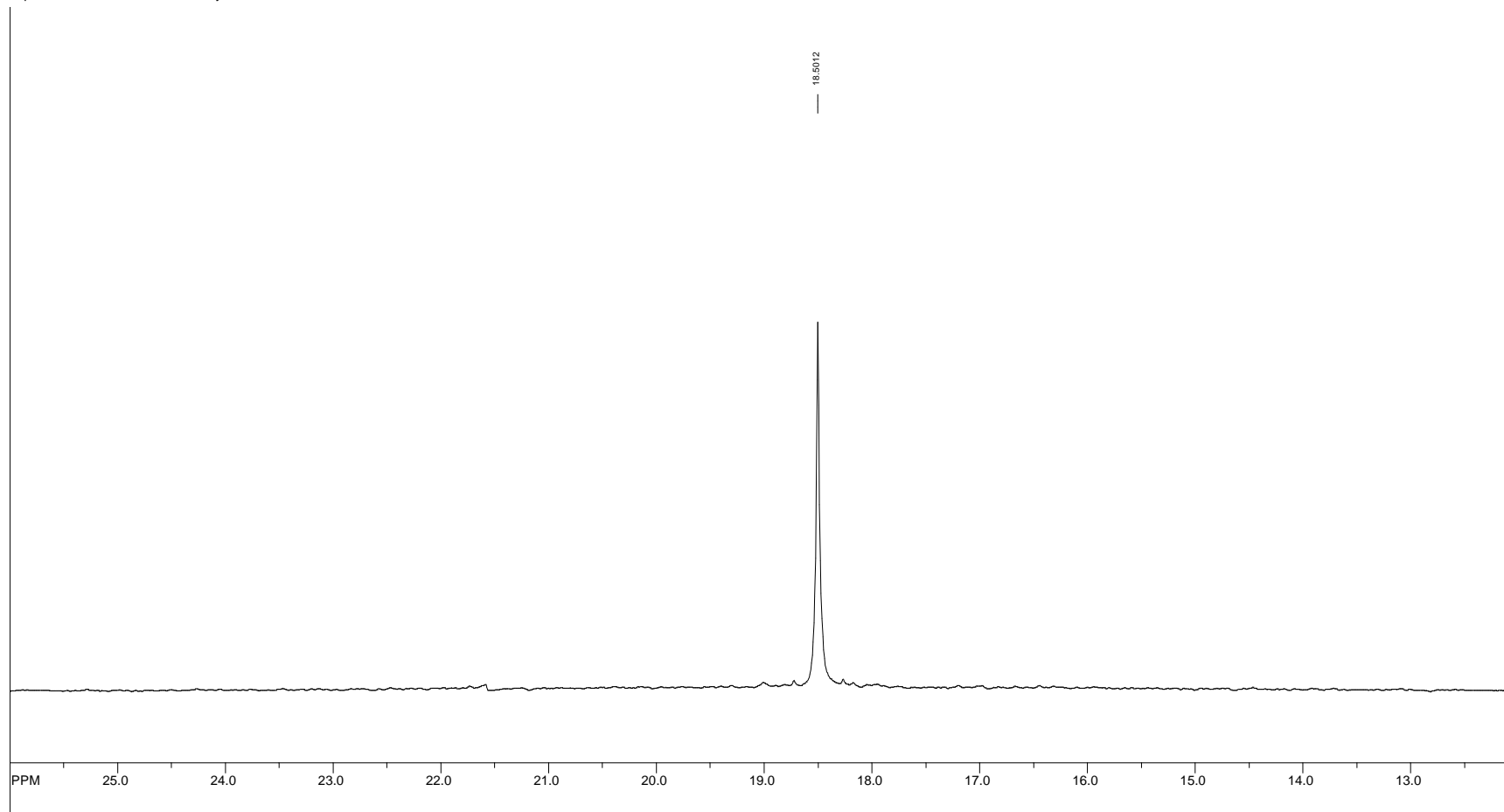


file: C:\Documents and Settings\1075578\Desktop\NMR\December\CL014112\fid exp: <deftsp135>
transmitter freq.: 125.771627 MHz
time domain size: 32768 points
width: 33783.78 Hz = 268.612123 ppm = 1.030999 Hz/pt
number of scans: 775

freq. of 0 ppm: 125.757793 MHz
processed size: 65536 complex points
LB: 0.000 GB: 0.0000

Figure A7: Tert-butylhydroxytoluene substituted carbon stabilized ylide (**3**) ^{13}C NMR.

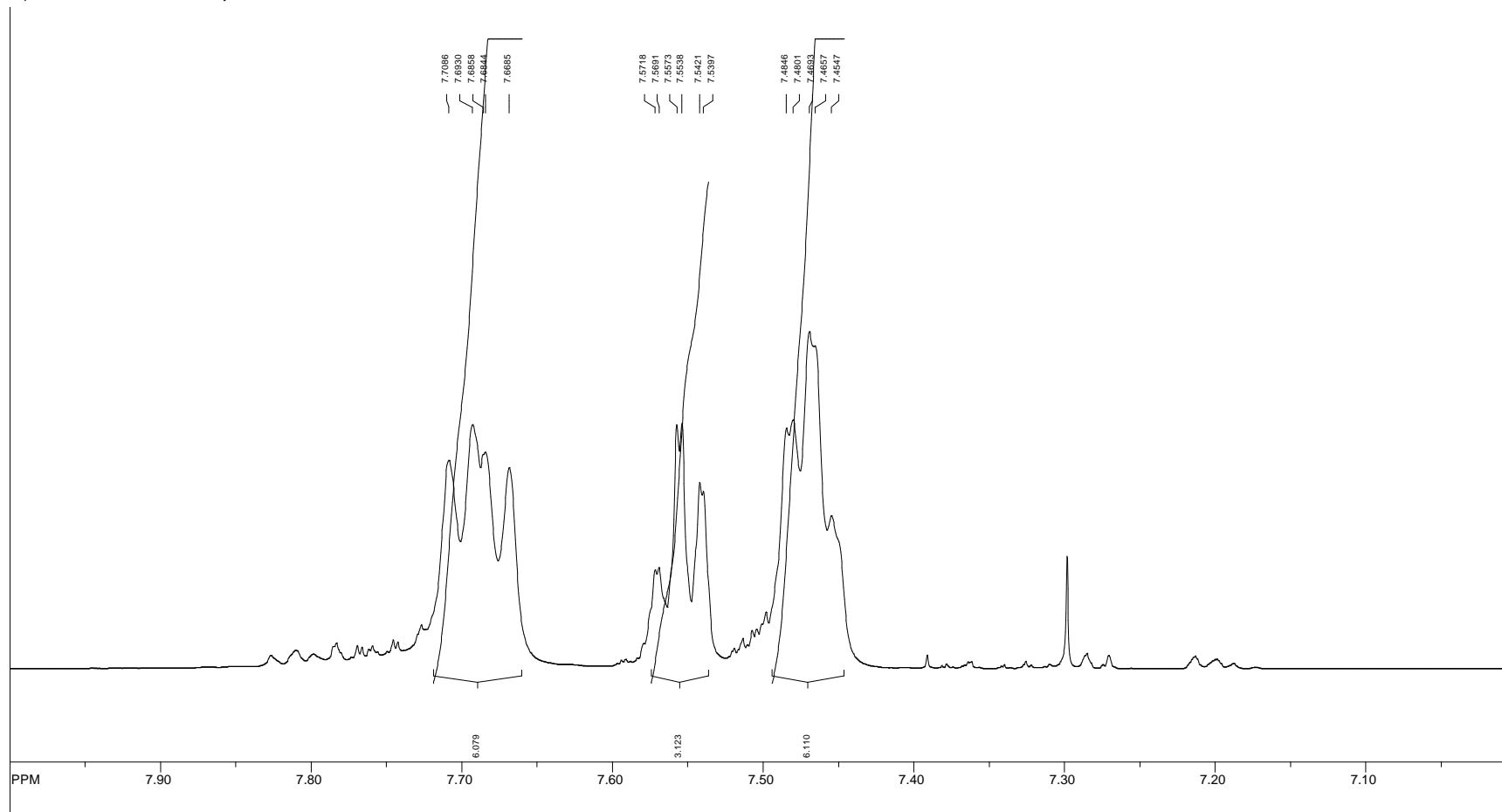
SpinWorks 2.5: Service_Code Clyburne



file: C:\Documents and Settings\1075578\Desktop\NMR\December\CL014111\fid exp: <zgpg30>
transmitter freq.: 202.466466 MHz
time domain size: 65536 points
width: 98039.22 Hz = 484.224463 ppm = 1.495960 Hz/pt
number of scans: 128

freq. of 0 ppm: 202.456343 MHz
processed size: 65536 complex points
LB: 0.000 GB: 0.0000

Figure A8: Tert-butylhydroxytoluene substituted carbon stabilized ylide (**3**) ^{31}P NMR.

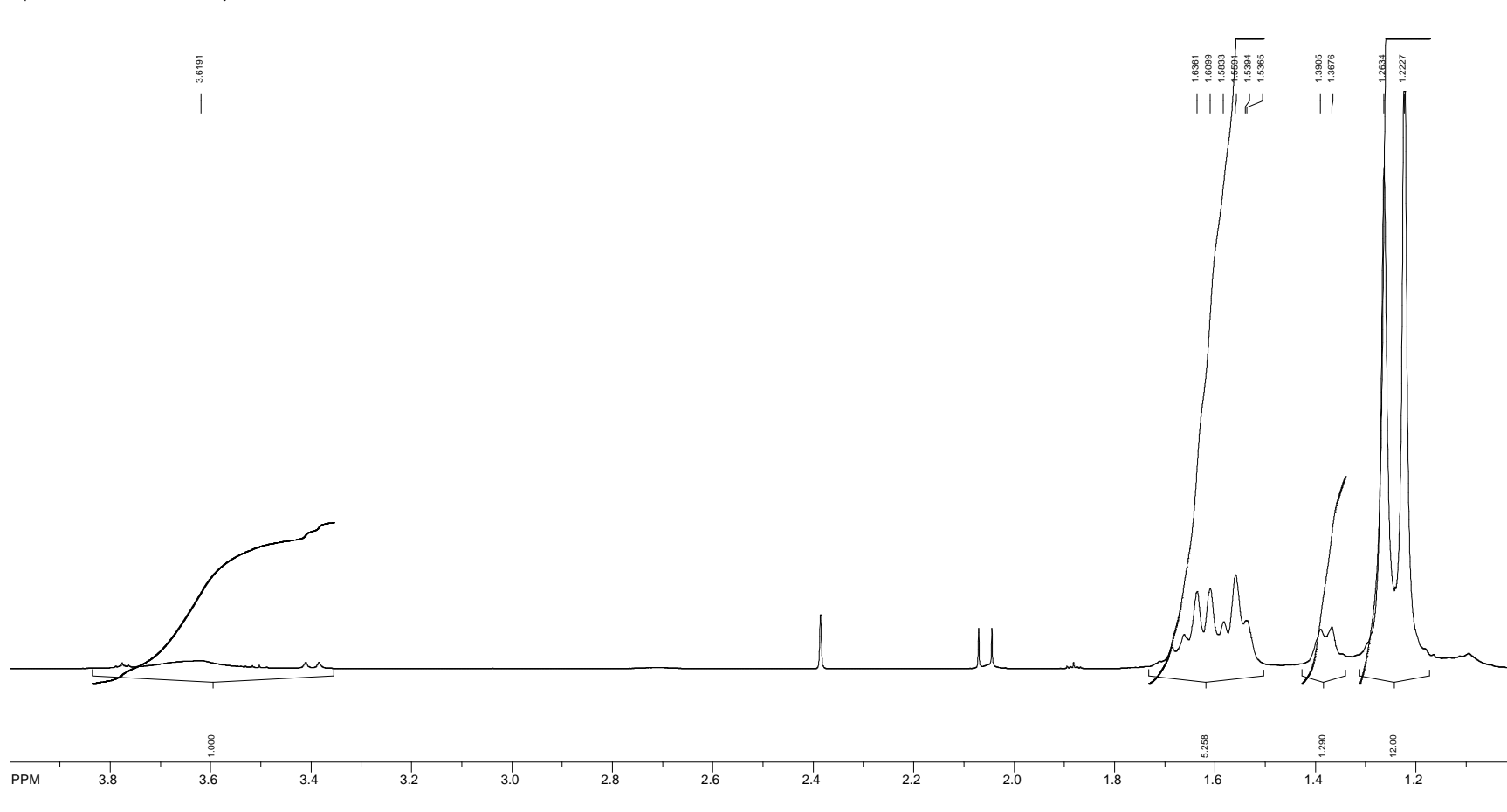


file: C:\Documents and Settings\1075578\Desktop\NMRMiller - TEMPO Aug 10\Aug09-service\10\fid -expt <zg30>
transmitter freq.: 500.133270 MHz
time domain size: 65536 points
width: 10080.65 Hz = 20.155918 ppm = 0.153818 Hz/pt
number of scans: 32

freq. of 0 ppm: 500.130019 MHz
processed size: 65536 complex points
LB: 0.000 GB: 0.0000

Figure A9: 1-hydroxyl-2,2,6,6-tetramethyl-piperidine substituted carbon stabilized ylide (**4**) ¹H NMR.

SpinWorks 2.5: Service_Code Clyburne



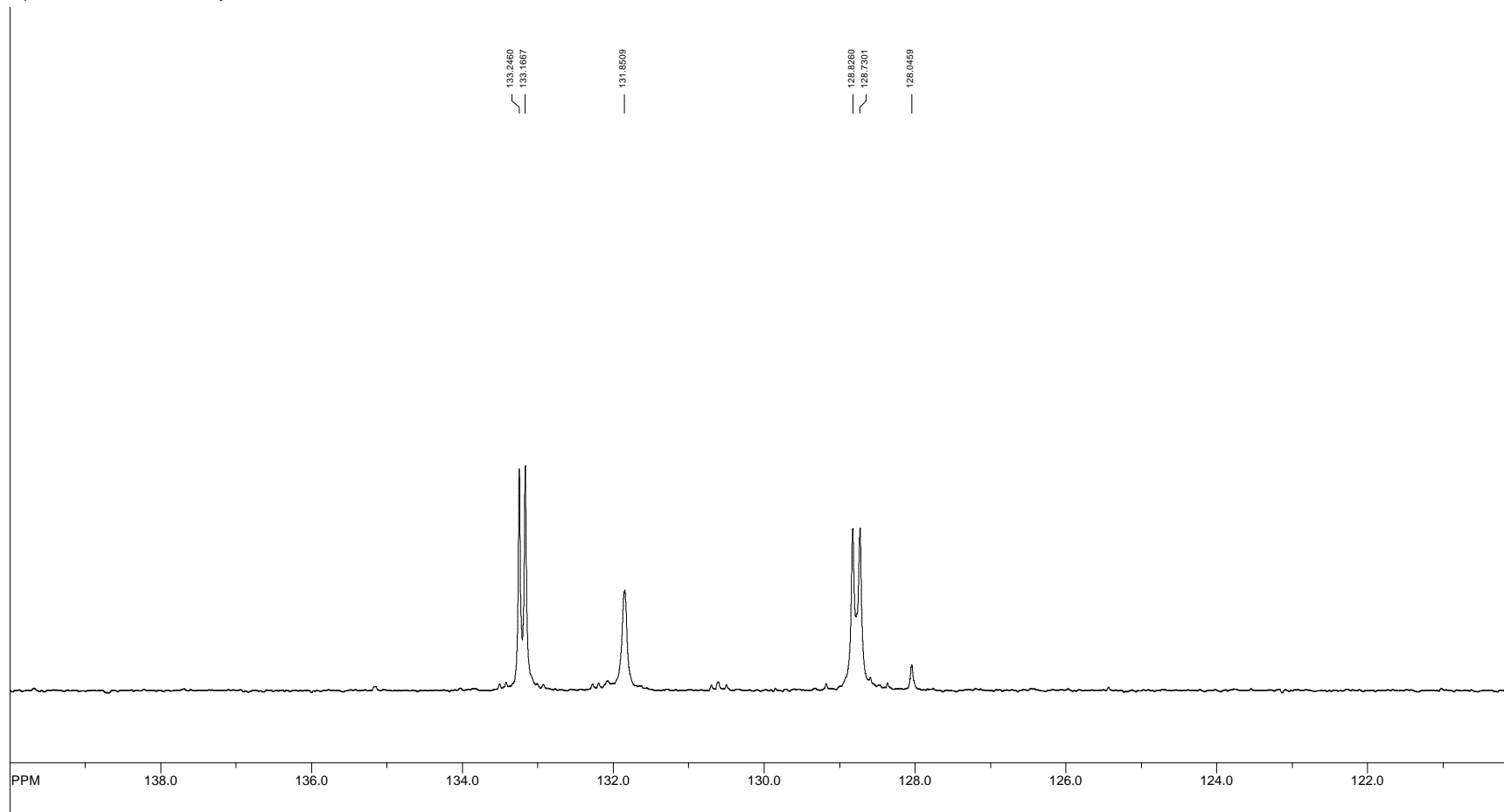
file: C:\Documents and Settings\1075578\Desktop\NMRMiller - TEMPO Aug 10\Aug09-service\10\fid - expt -<zg30>

transmitter freq.: 500.133270 MHz
time domain size: 65536 points
width: 10080.65 Hz = 20.155918 ppm = 0.153818 Hz/pt
number of scans: 32

freq. of 0 ppm: 500.130019 MHz
processed size: 65536 complex points
LB: 0.000 GB: 0.0000

Figure A10: 1-hydroxyl-2,2,6,6-tetramethyl-piperidine substituted carbon stabilized ylide (**4**) ^1H NMR.

SpinWorks 2.5: Service_Code Clyburne

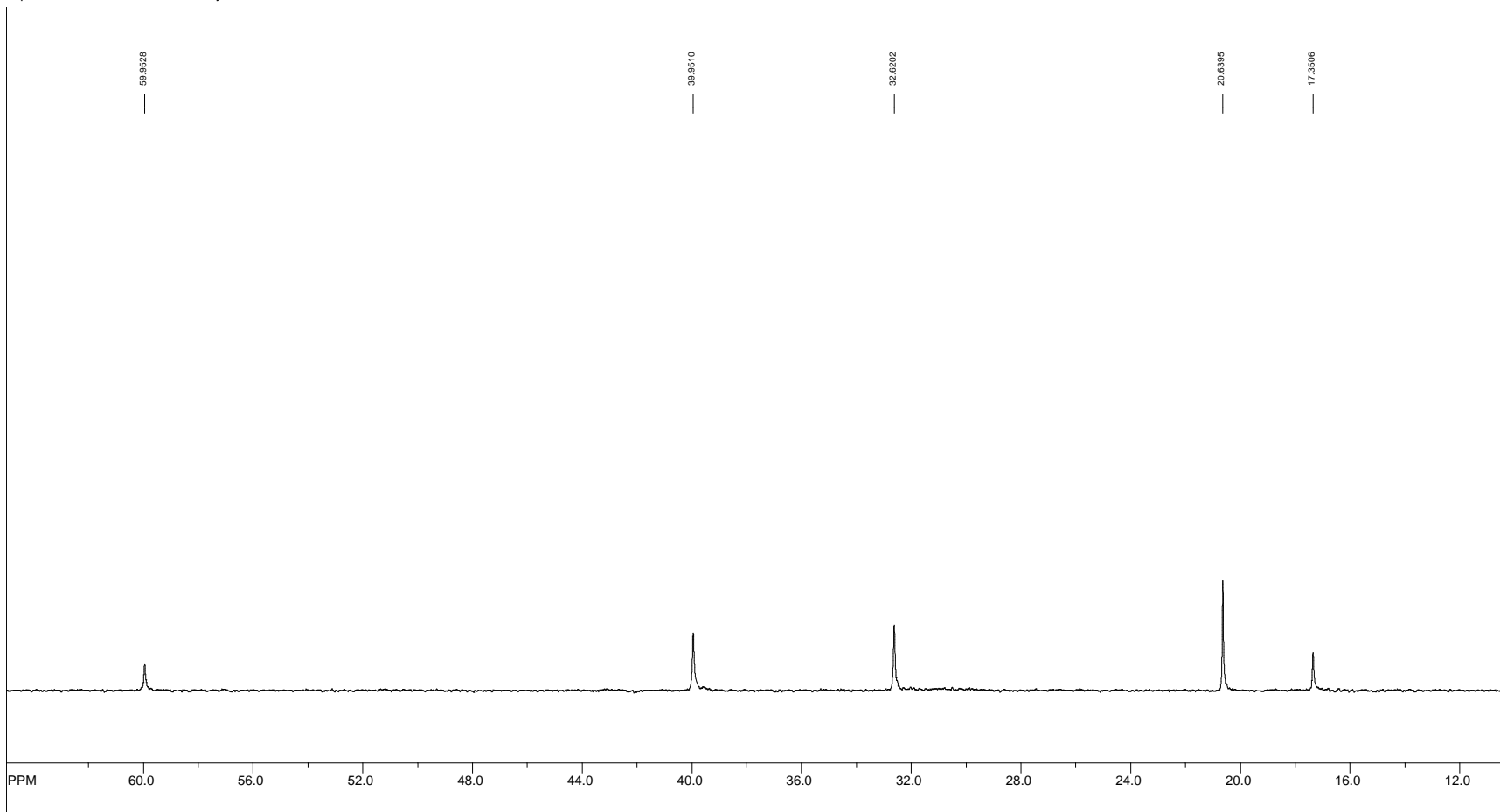


file: C:\Documents and Settings\1075578\Desktop\NMRMiller - TEMPO Aug 10\Aug09-service\11\fid - expt <undef>
transmitter freq.: 125.771627 MHz
time domain size: 23994 points
width: 33333.33 Hz = 265.030628 ppm = 1.389236 Hz/pt
number of scans: 180

freq. of 0 ppm: 125.757779 MHz
processed size: 262144 complex points
LB: 0.000 GB: 0.0000

Figure A11: 1-hydroxyl-2,2,6,6-tetramethyl-piperidine substituted carbon stabilized ylide (**4**) ^{13}C NMR.

SpinWorks 2.5: Service_Code Clyburne

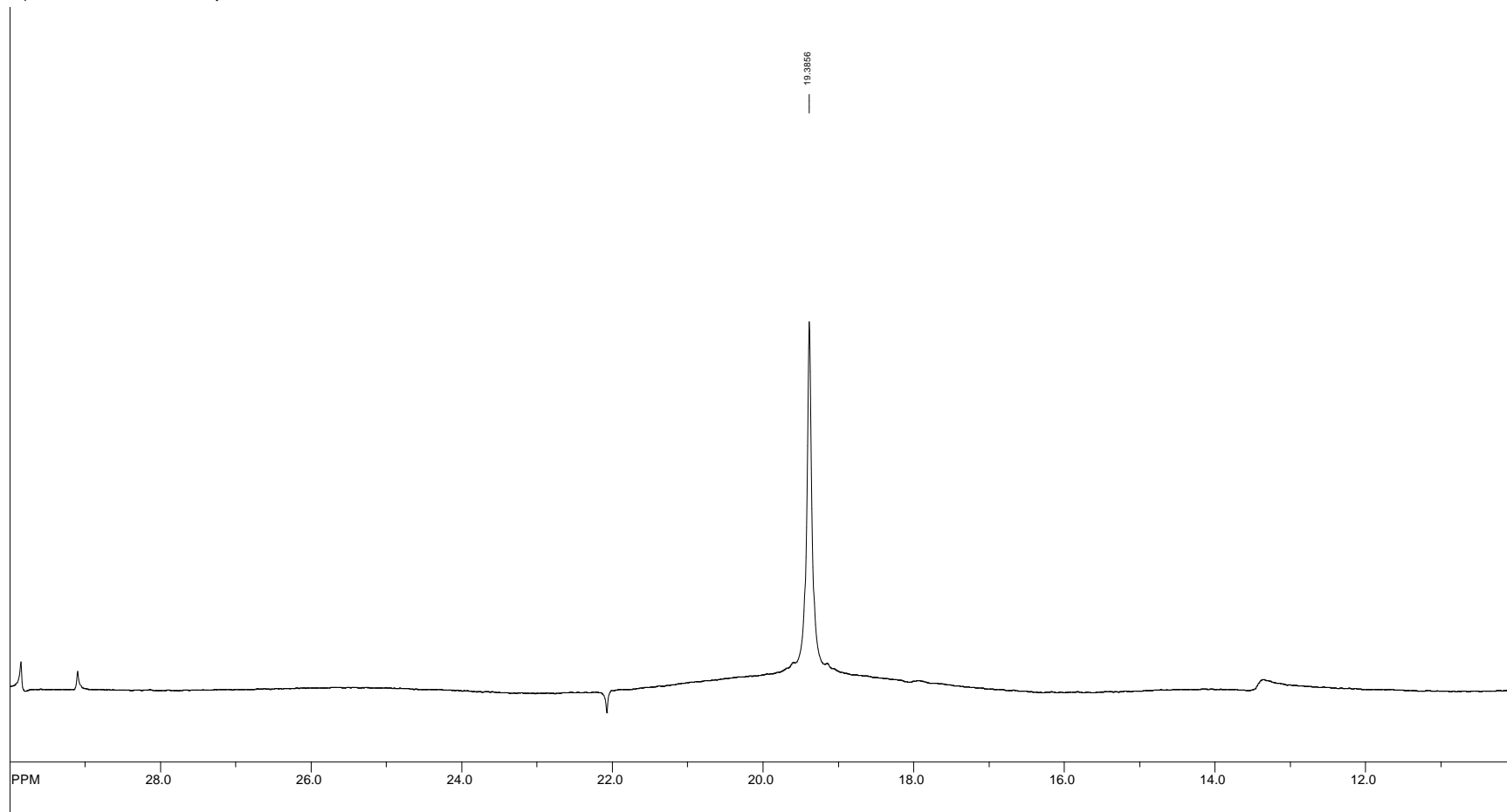


file: C:\Documents and Settings\1075578\Desktop\NMRMiller - TEMPO Aug 10\Aug09-service\11\fid - expt -<def>
transmitter freq.: 125.771627 MHz
time domain size: 23994 points
width: 33333.33 Hz = 265.030628 ppm = 1.389236 Hz/pt
number of scans: 180

freq. of 0 ppm: 125.757779 MHz
processed size: 262144 complex points
LB: 0.000 GB: 0.0000

Figure A12: 1-hydroxyl-2,2,6,6-tetramethyl-piperidine substituted carbon stabilized ylide (**4**) ^{13}C NMR.

SpinWorks 2.5: Service_Code Clyburne

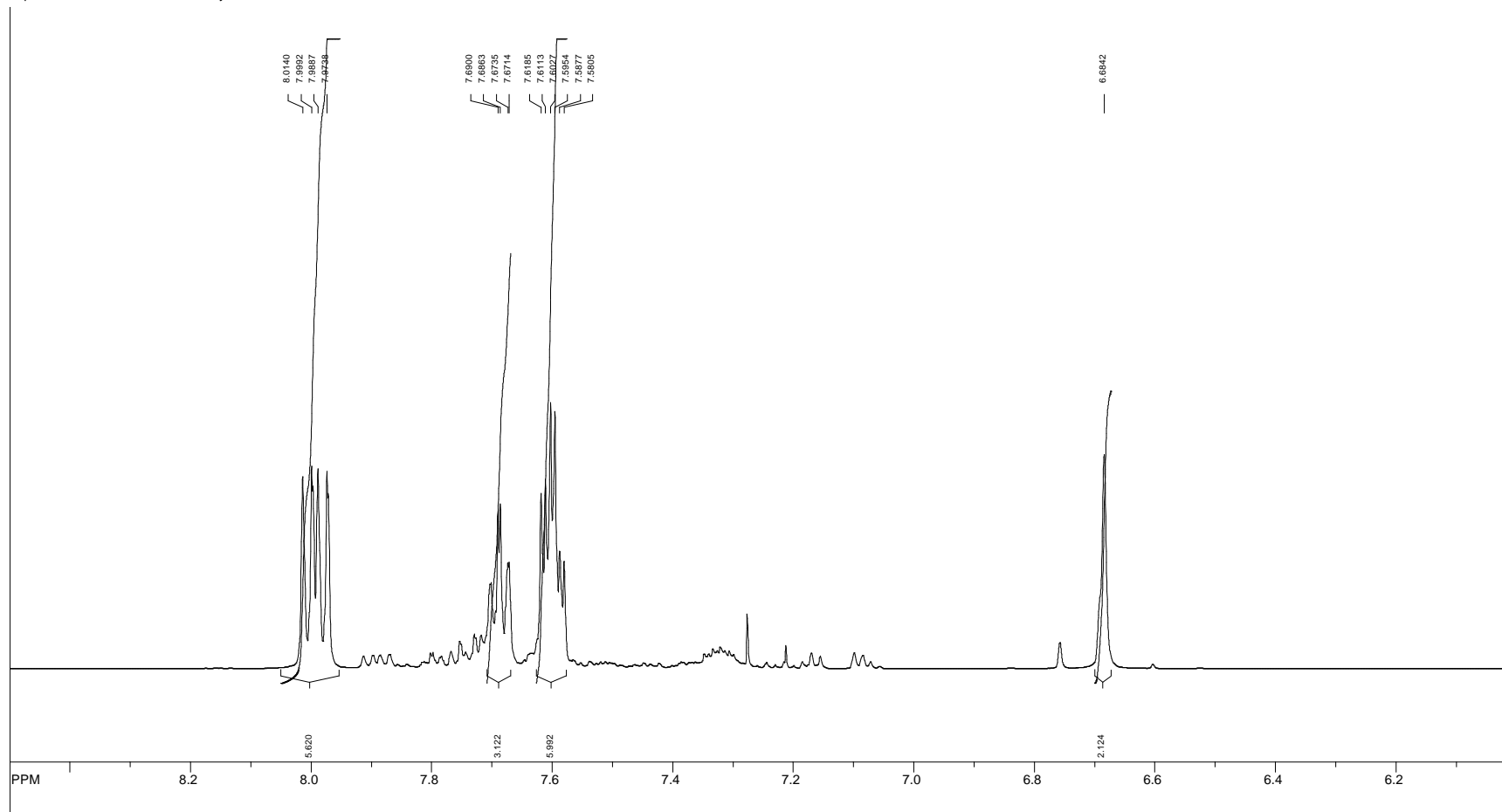


file: C:\Documents and Settings\1075578\Desktop\NMRMiller - TEMPO Aug 10\Aug09-service\131\fid - expt -<zggg30>
transmitter freq.: 202.466466 MHz
time domain size: 65536 points
width: 98039.22 Hz = 484.224463 ppm = 1.495960 Hz/pt
number of scans: 256

freq. of 0 ppm: 202.456343 MHz
processed size: 65536 complex points
LB: 0.000 GB: 0.0000

Figure A13: 1-hydroxyl-2,2,6,6-tetramethyl-piperidine substituted carbon stabilized ylide (**4**) ^{31}P NMR.

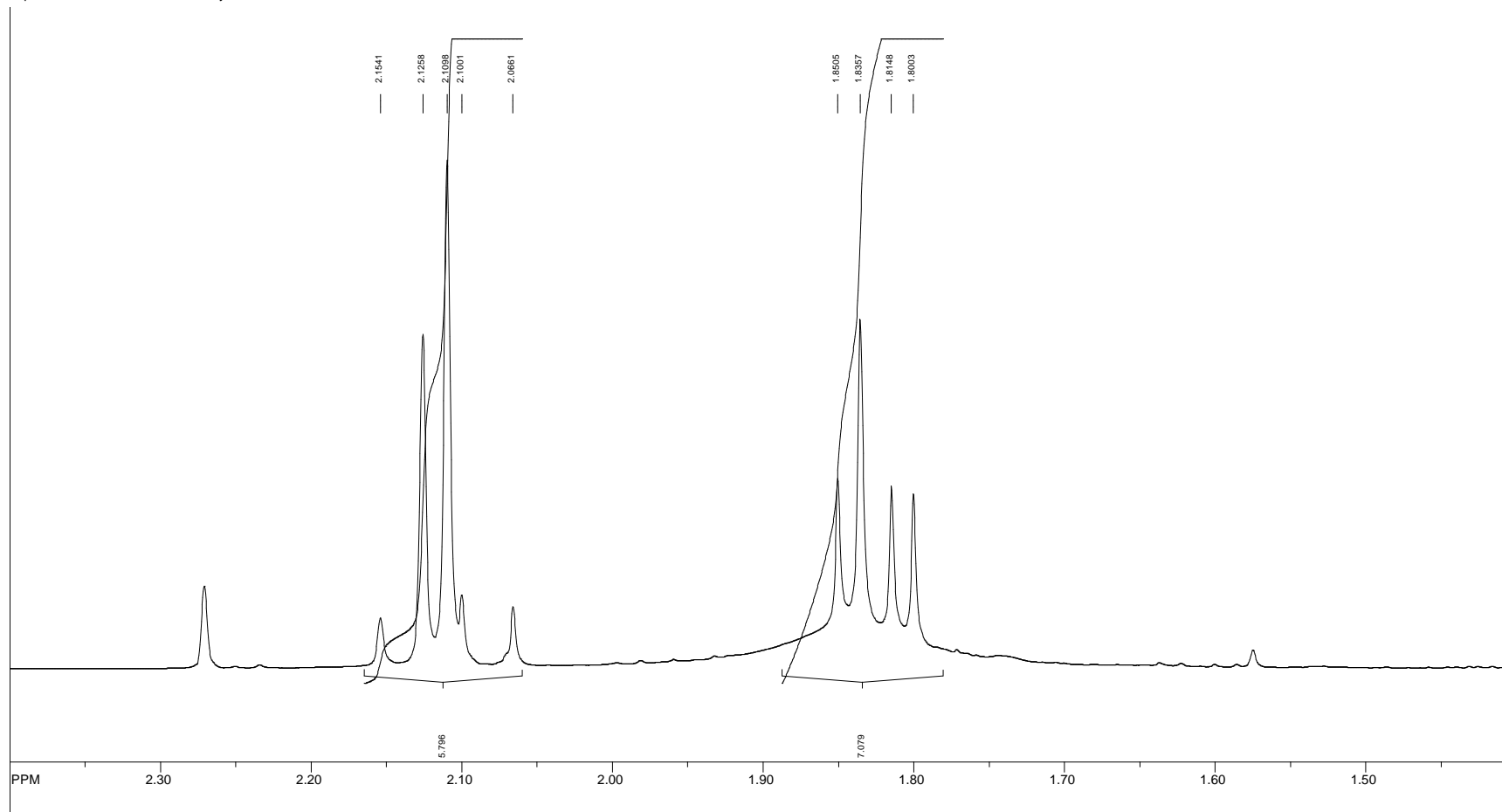
SpinWorks 2.5: Service_Code Clyburne



file: C:\Documents and Settings\1075578\Desktop\NMR\April 9 2010\CS050810\spectrum.dcx exp: <zg30>
transmitter freq.: 500.133270 MHz
time domain size: 65536 points
width: 10080.65 Hz = 20.155918 ppm = 0.153818 Hz/pt
number of scans: 32

freq. of 0 ppm: 500.130063 MHz
processed size: 65536 complex points
LB: 0.000 GB: 0.0000

Figure A14: Methylated trimethylphenol substituted carbon stabilized ylide (**5**) ^1H NMR.

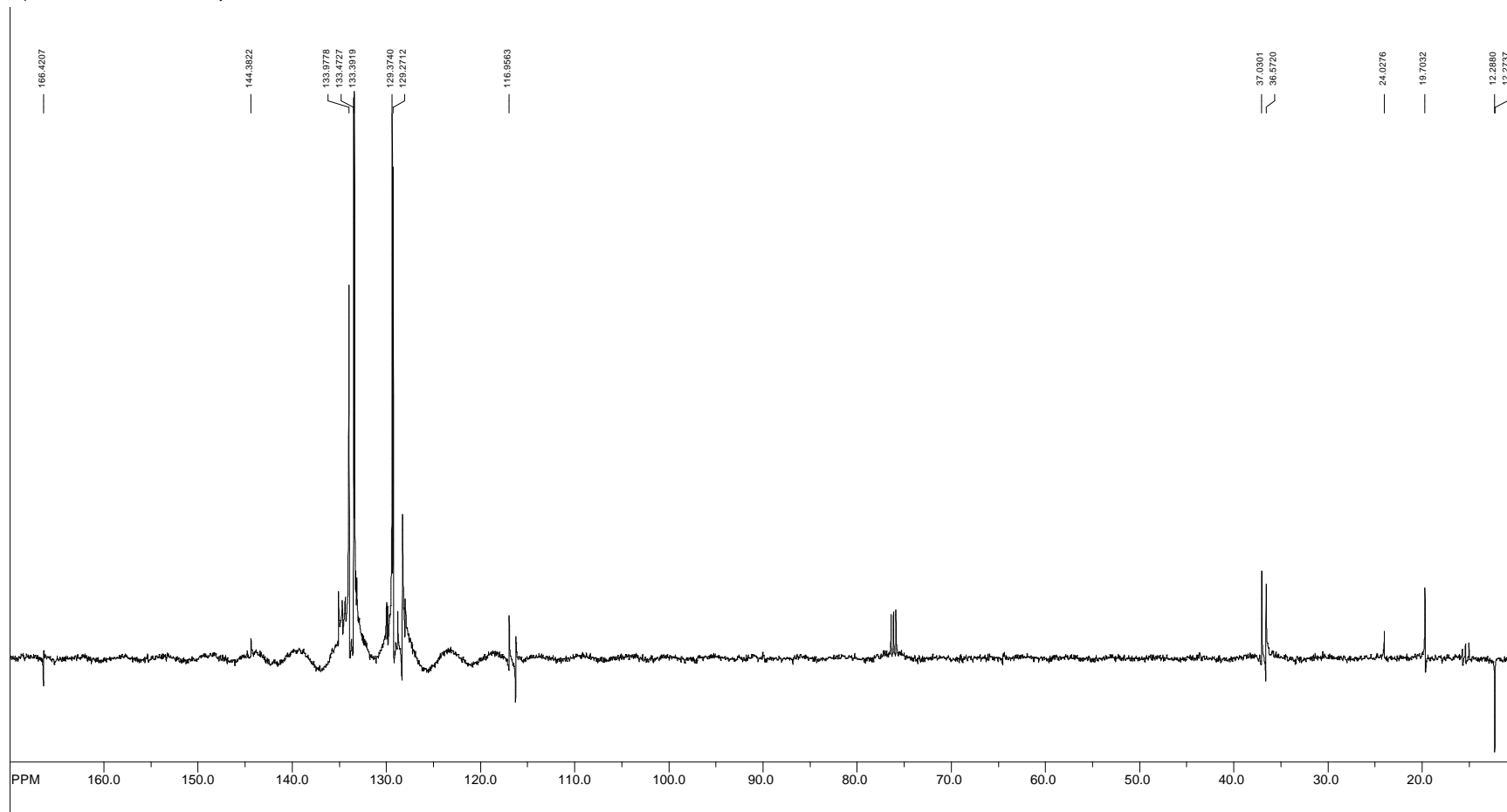


file: C:\Documents and Settings\1075578\Desktop\NMR\April 9 2010\CS05810\spectrum.dx exp: <zg30>
transmitter freq.: 500.133270 MHz
time domain size: 65536 points
width: 10080.65 Hz = 20.155918 ppm = 0.153818 Hz/pt
number of scans: 32

freq. of 0 ppm: 500.130063 MHz
processed size: 65536 complex points
LB: 0.000 GB: 0.0000

Figure A15: Methylated trimethylphenol substituted carbon stabilized ylide (**5**) ¹H NMR.

SpinWorks 2.5: Service_Code Clyburne

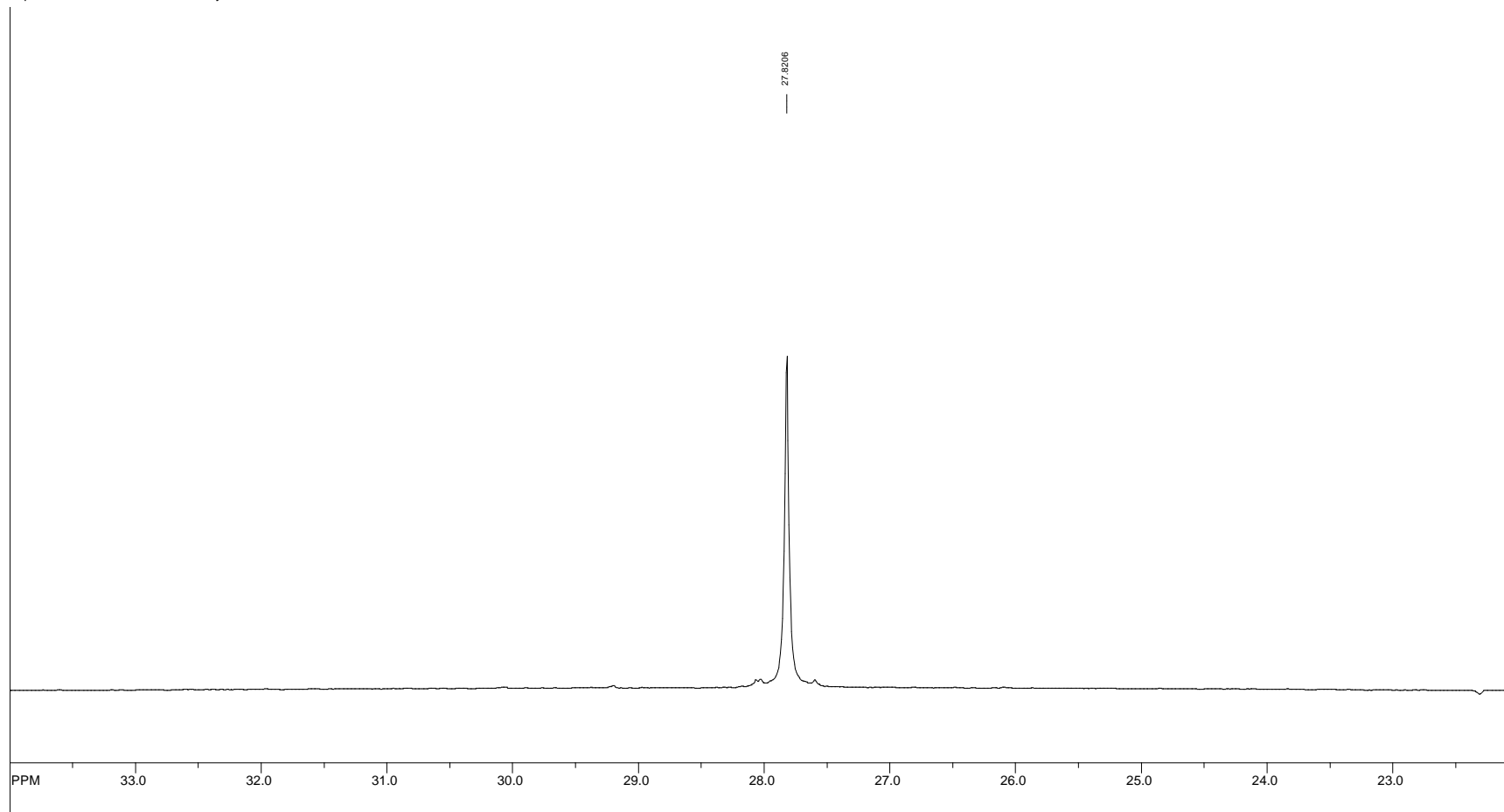


file: C:\Documents and Settings\1075578\Desktop\NMR\April 9 2010\CS05812\spectrum.dx exp: <deftqsp.dmo>
transmitter freq.: 125.771627 MHz
time domain size: 50670 points
width: 33783.78 Hz = 268.612123 ppm = 0.666741 Hz/pt
number of scans: 512

freq. of 0 ppm: 125.757922 MHz
processed size: 65536 complex points
LB: 0.000 GB: 0.0000

Figure A16: Methylated trimethylphenol substituted carbon stabilized ylide (5) ¹³C NMR.

SpinWorks 2.5: Service_Code Clyburne

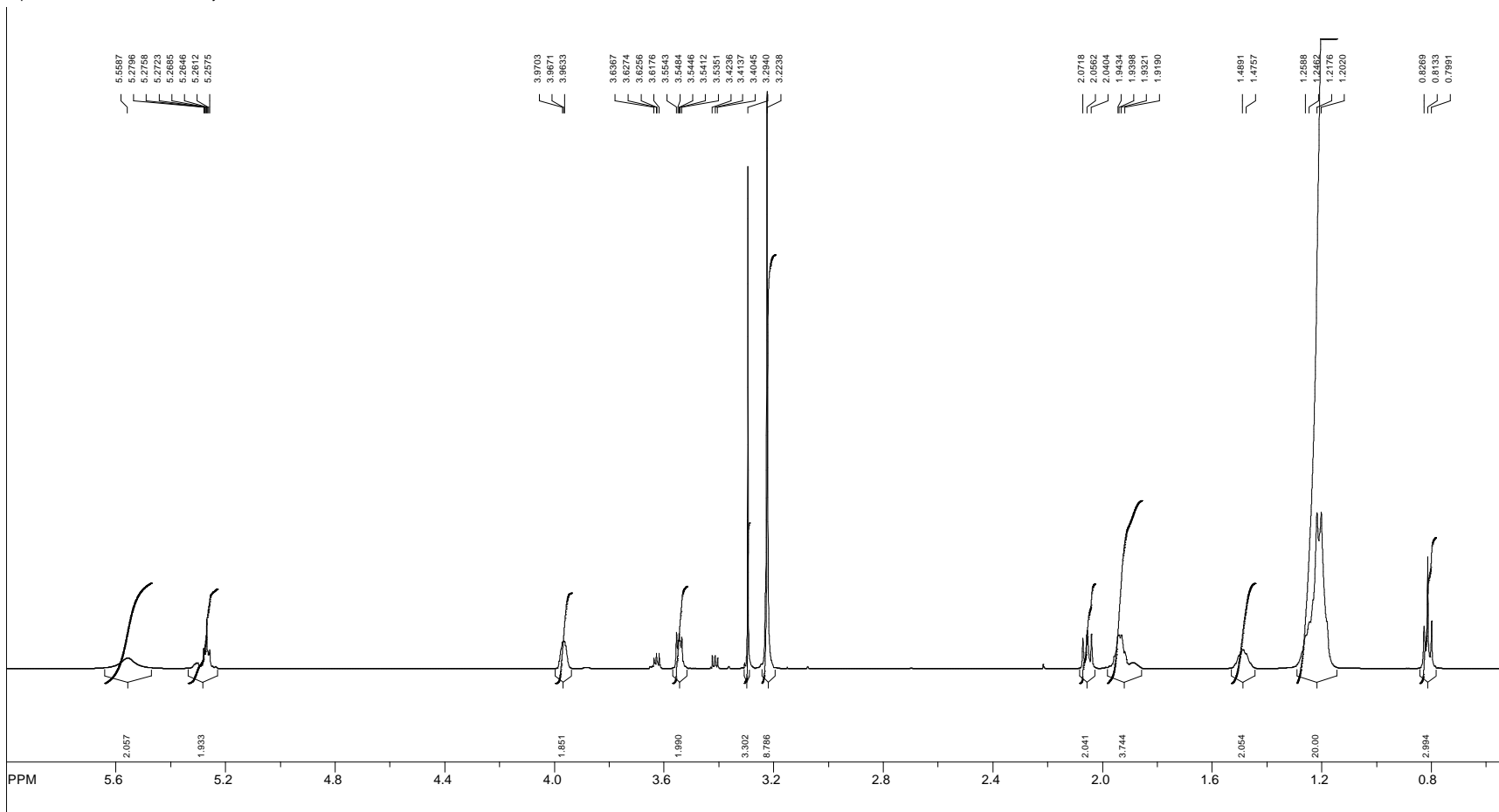


file: C:\Documents and Settings\1075578\Desktop\NMR\April 9 2010\CS058111\fid -expt -<zggg30>
transmitter freq.: 202.466466 MHz
time domain size: 65536 points
width: 98039.22 Hz = 484.224463 ppm = 1.495960 Hz/pt
number of scans: 128

freq. of 0 ppm: 202.456343 MHz
processed size: 65536 complex points
LB: 0.000 GB: 0.0000

Figure A17: Methylated trimethylphenol substituted carbon stabilized ylide (**5**) ^{31}P NMR.

SpinWorks 2.5: Service_Code Clyburne



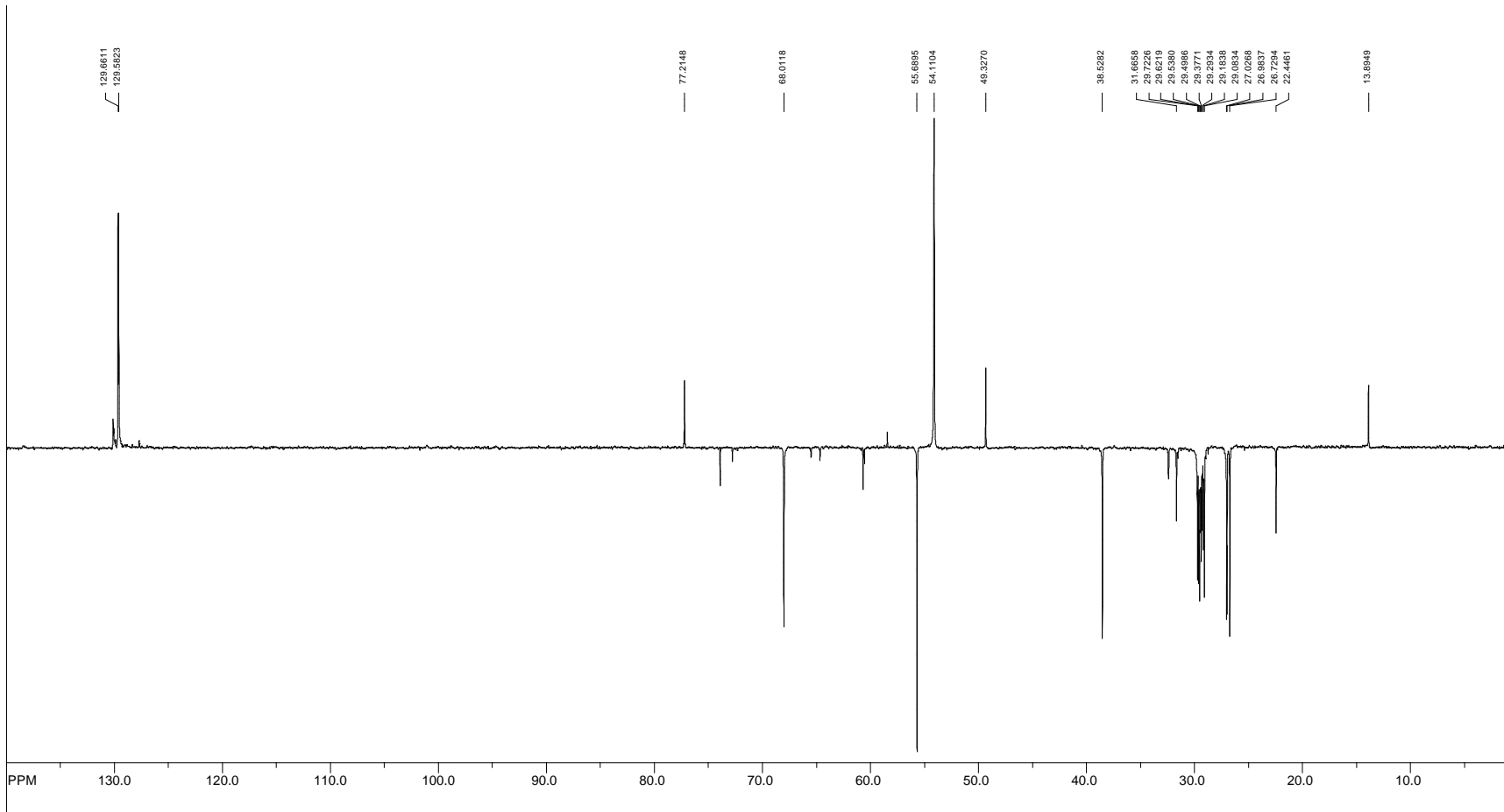
file: C:\Documents and Settings\1075578\Desktop\NMR oil\10\fid exp: <zg30>

transmitter freq.: 500.133270 MHz
time domain size: 65536 points
width: 10080.65 Hz = 20.155918 ppm = 0.153818 Hz/pt
number of scans: 32

freq. of 0 ppm: 500.130019 MHz
processed size: 65536 complex points
LB: 0.000 GB: 0.0000

Figure A18: Choline oleate ¹H NMR.

SpinWorks 2.5: Service_Code Clyburne

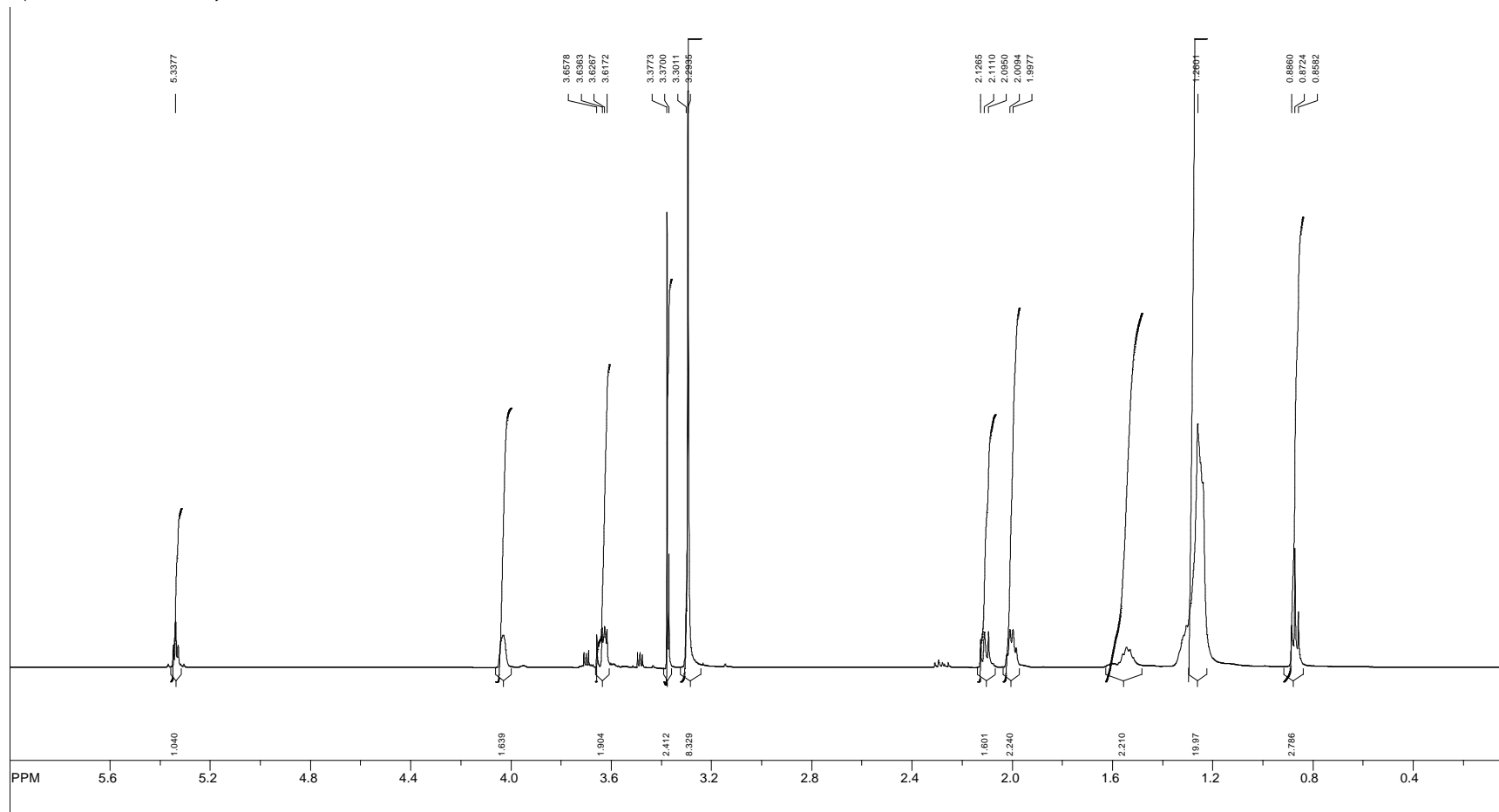


file: C:\Documents and Settings\1075578\Desktop\NMR oil\11\fid exp: <deplsp135>
transmitter freq.: 125.771627 MHz
time domain size: 32768 points
width: 33783.78 Hz = 268.612123 ppm = 1.030999 Hz/pt
number of scans: 256

freq. of 0 ppm: 125.757815 MHz
processed size: 65536 complex points
LB: 0.000 GB: 0.0000

Figure A19: Choline oleate ¹³C NMR.

SpinWorks 2.5: Service_Code Clyburne

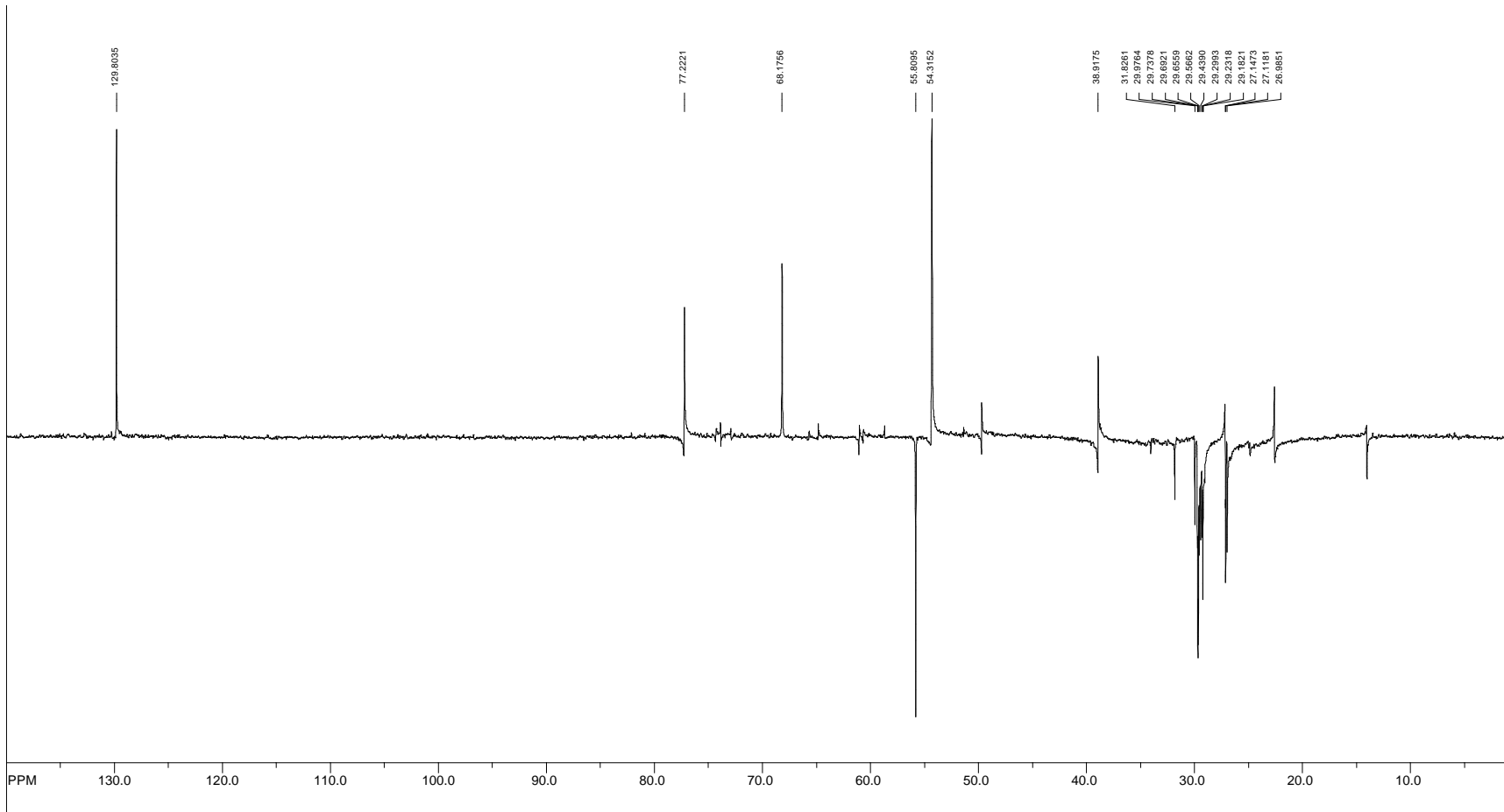


file: C:\Documents and Settings\1075578\Desktop\NMR oil\20\fid expt -zg30-
transmitter freq.: 500.133270 MHz
time domain size: 65536 points
width: 10080.65 Hz = 20.155918 ppm = 0.153818 Hz/pt
number of scans: 32

freq. of 0 ppm: 500.130019 MHz
processed size: 65536 complex points
LB: 0.000 GB: 0.0000

Figure A20: Choline erucate ¹H NMR.

SpinWorks 2.5: Service_Code Clyburne

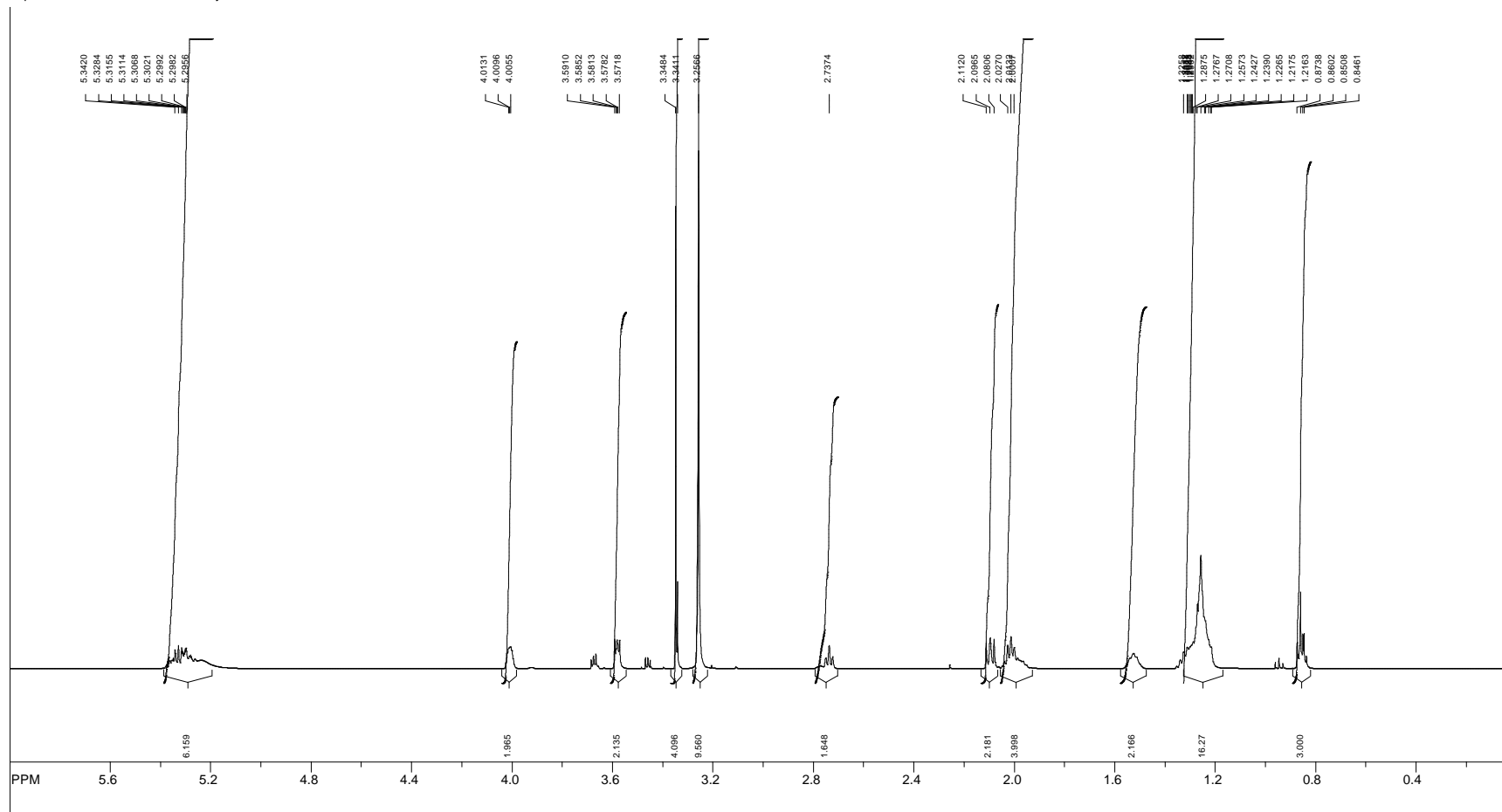


file: C:\Documents and Settings\1075578\Desktop\NMR oil\21\fid exp: <deftsp135>
transmitter freq.: 125.771627 MHz
time domain size: 32768 points
width: 33783.78 Hz = 268.612123 ppm = 1.030999 Hz/pt
number of scans: 640

freq. of 0 ppm: 125.757803 MHz
processed size: 65536 complex points
LB: 0.000 GB: 0.0000

Figure A21: Choline erucate ¹³C NMR.

SpinWorks 2.5: Service_Code Clyburne

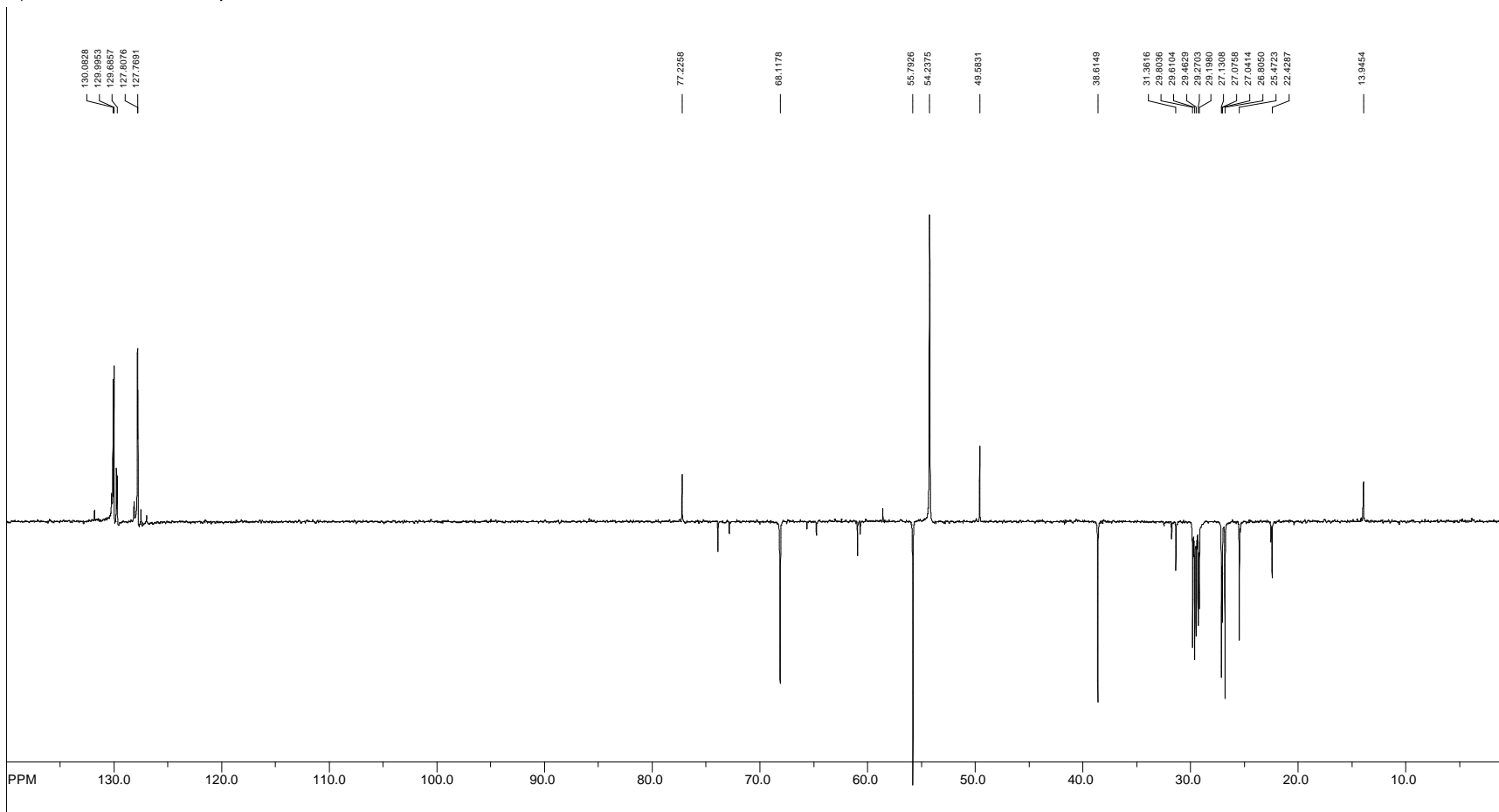


file: C:\Documents and Settings\1075578\Desktop\NMR oil\30\fid exp: <zg30>
transmitter freq.: 500.133270 MHz
time domain size: 65536 points
width: 10080.65 Hz = 20.155918 ppm = 0.153818 Hz/pt
number of scans: 32

freq. of 0 ppm: 500.130019 MHz
processed size: 65536 complex points
LB: 0.000 GB: 0.0000

Figure A22: Choline linoleate ¹H NMR.

SpinWorks 2.5: Service_Code Clyburne

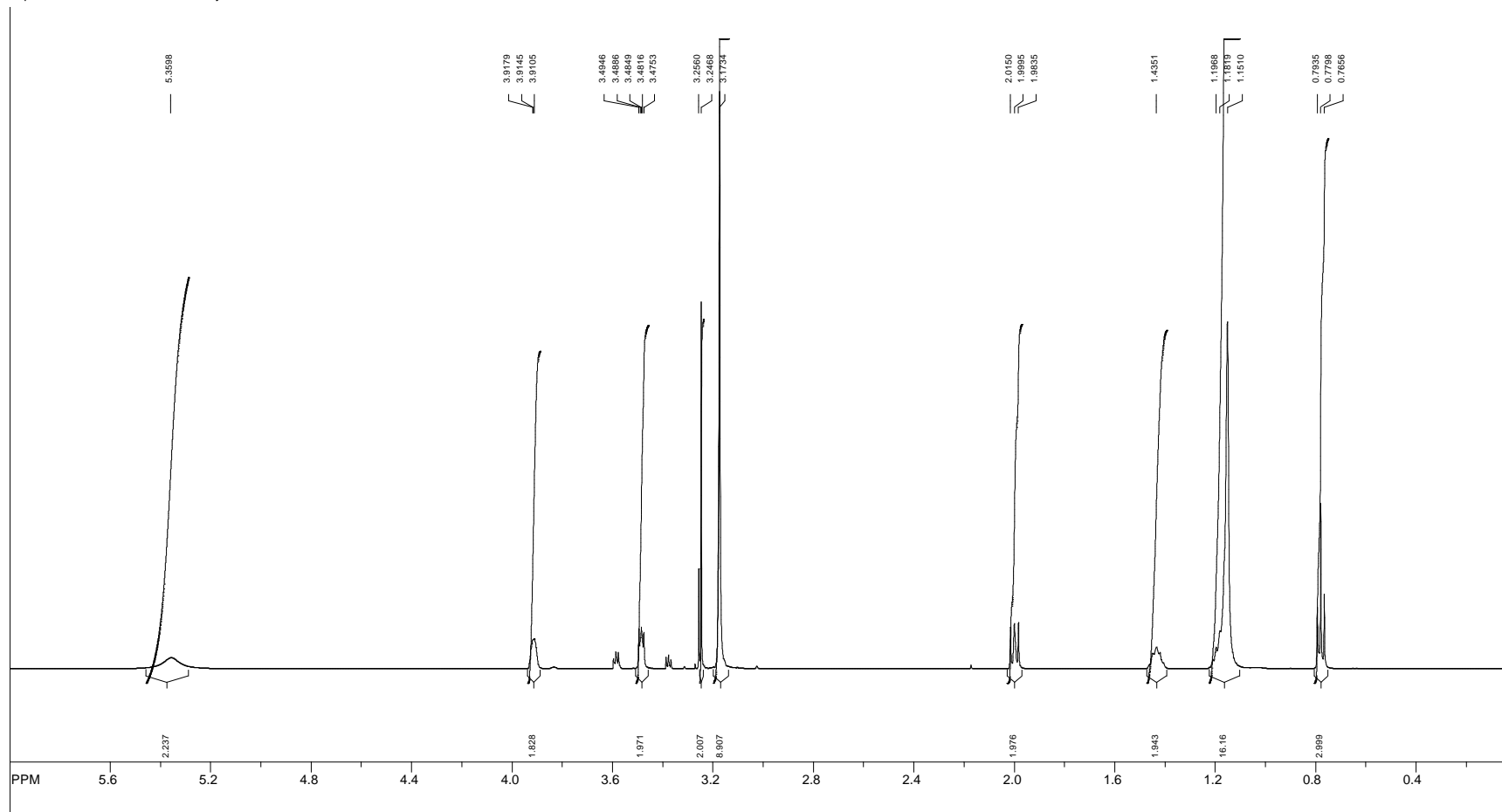


file: C:\Documents and Settings\1075578\Desktop\NMR oil\31\fid exp: <deftsp135>
transmitter freq.: 125.771627 MHz
time domain size: 32768 points
width: 33783.78 Hz = 268.612123 ppm = 1.030999 Hz/pt
number of scans: 384

freq. of 0 ppm: 125.757808 MHz
processed size: 65536 complex points
LB: 0.000 GB: 0.0000

Figure A23: Choline linoleate ¹³C NMR.

SpinWorks 2.5: Service_Code Clyburne



file: C:\Documents and Settings\1075578\Desktop\NMR oil\40\fid exp: <zg30>
transmitter freq.: 500.133270 MHz
time domain size: 65536 points
width: 10080.65 Hz = 20.155918 ppm = 0.153818 Hz/pt
number of scans: 32

freq. of 0 ppm: 500.130019 MHz
processed size: 65536 complex points
LB: 0.000 GB: 0.0000

Figure A24: Choline laurate ¹H NMR.

SpinWorks 2.5: Service_Code Clyburne

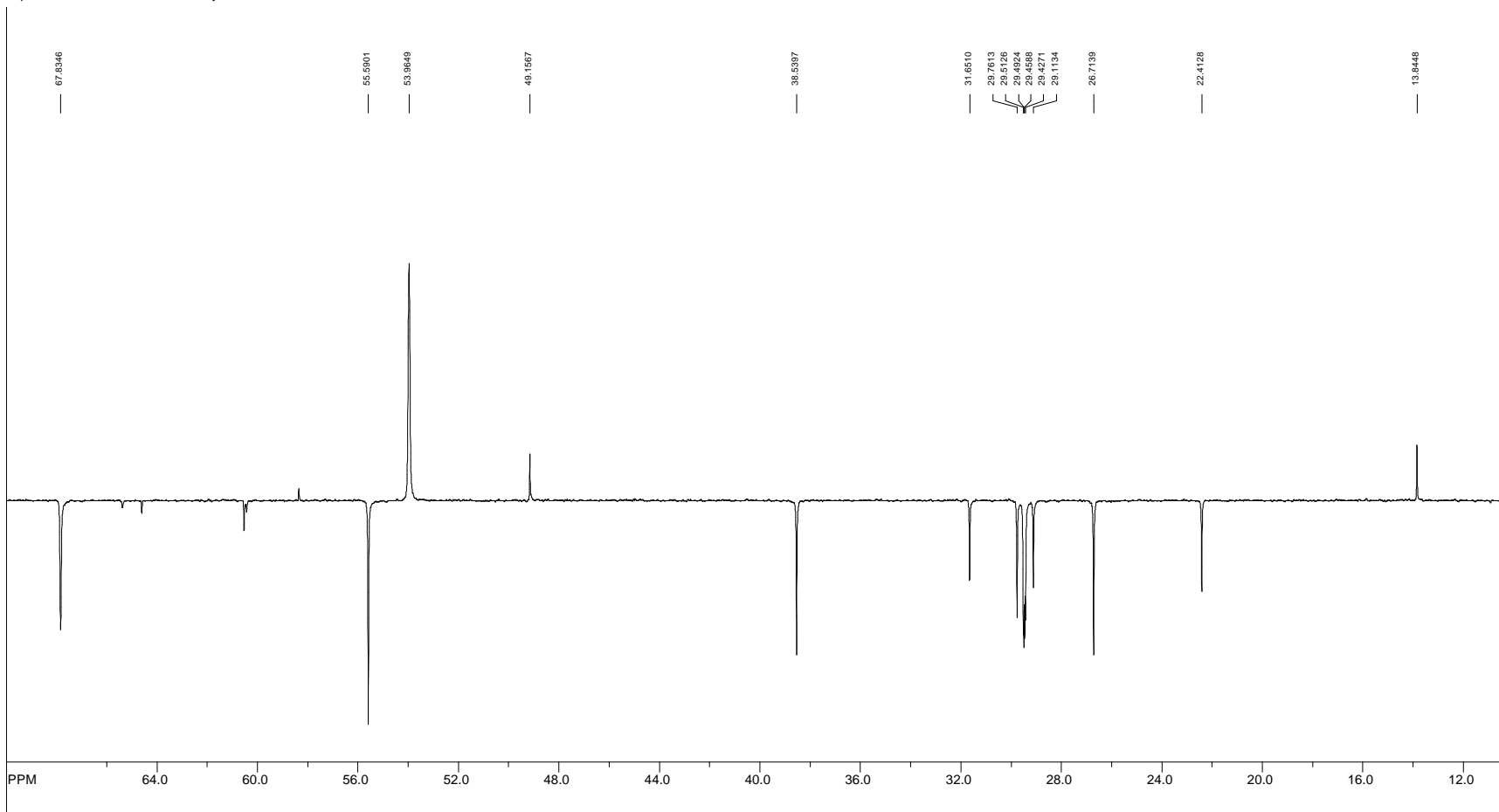
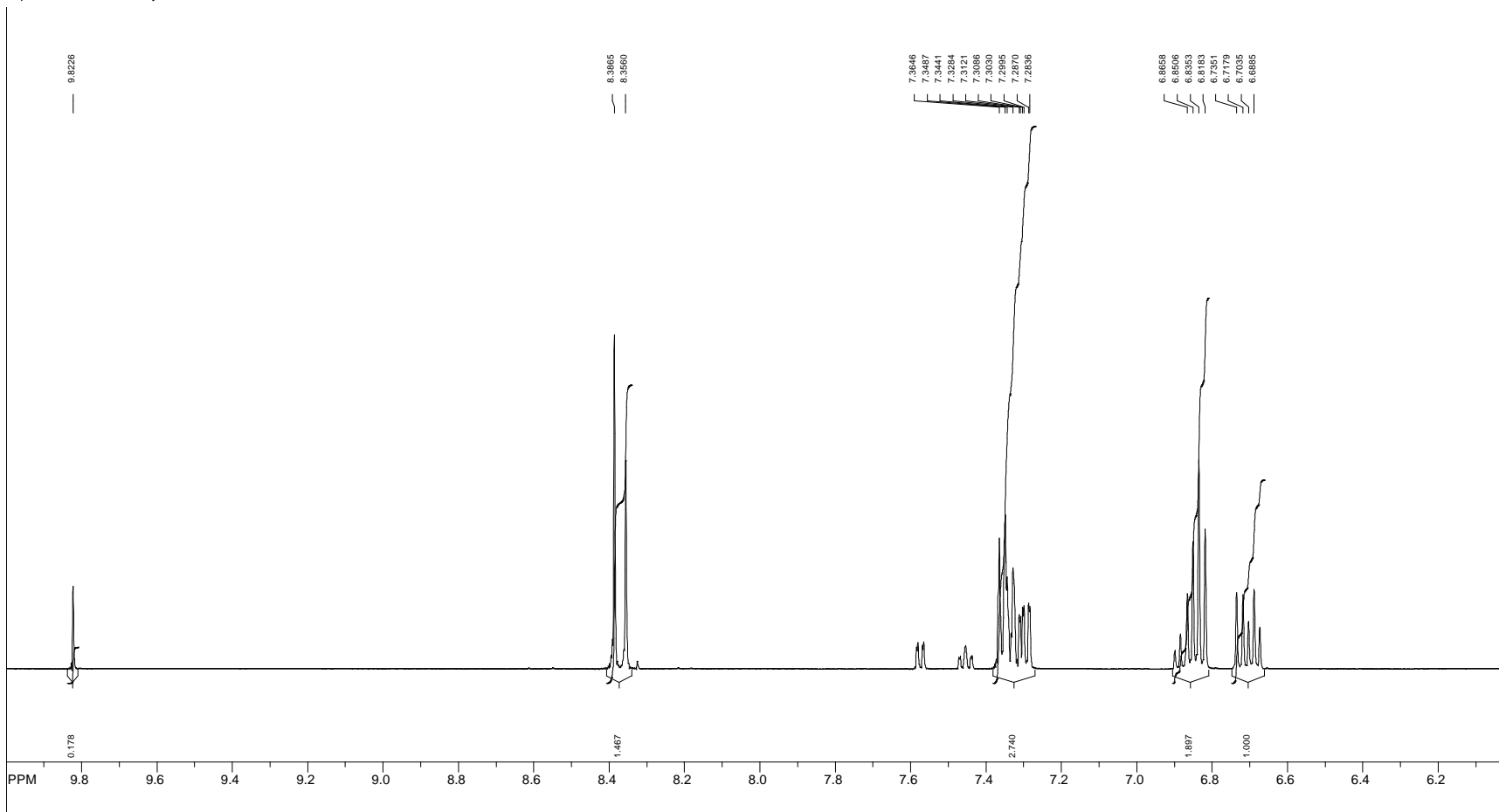


Figure A25: Choline laurate ^{13}C NMR.

SpinWorks 2.5: Bill Clyburne

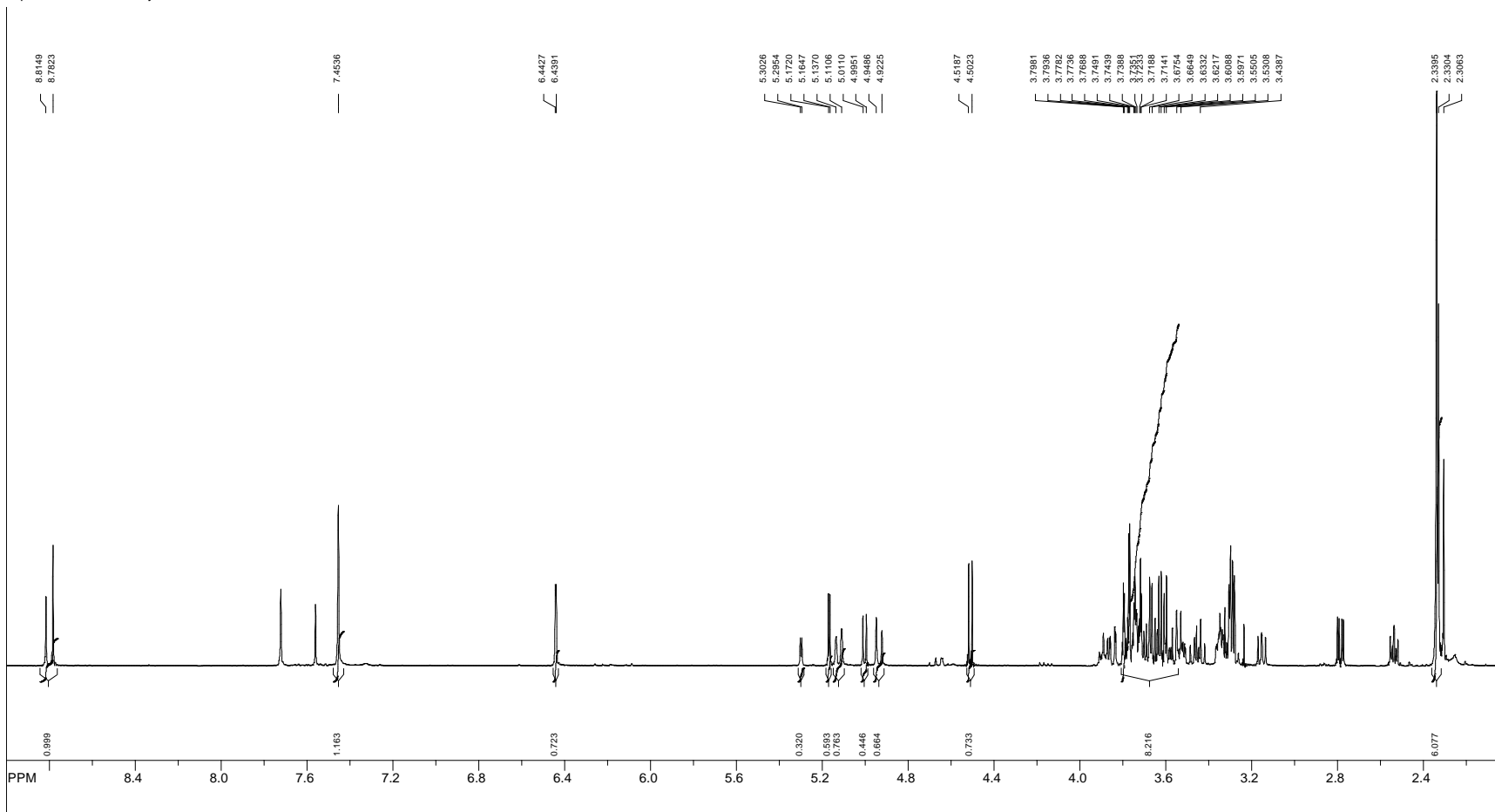


file: C:\Documents and Settings\1075578\Desktop\NMR\July 23 Schiff base\C1016B_Sept7_2010\11fid exp: <zgcpqpr>
transmitter freq.: 500.132369 MHz
time domain size: 8192 points
width: 7507.51 Hz = 15.011041 ppm = 0.916444 Hz/pt
number of scans: 64

freq. of 0 ppm: 500.130019 MHz
processed size: 32768 complex points
LB: 0.000 GB: 0.0000

Figure A26: Glucosamine-salicylaldehyde Schiff's base (**6**) ¹H NMR.

SpinWorks 2.5: Bill Clyburne



file: C:\Documents and Settings\1075578\Desktop\NMR\July 23 Schiff base\CJ017c_Sept14_2010\11\fid exp: <zqcpgr>

transmitter freq.: 500.132371 MHz

time domain size: 8192 points

width: 7507.51 Hz = 15.011041 ppm = 0.916444 Hz/pt

number of scans: 64

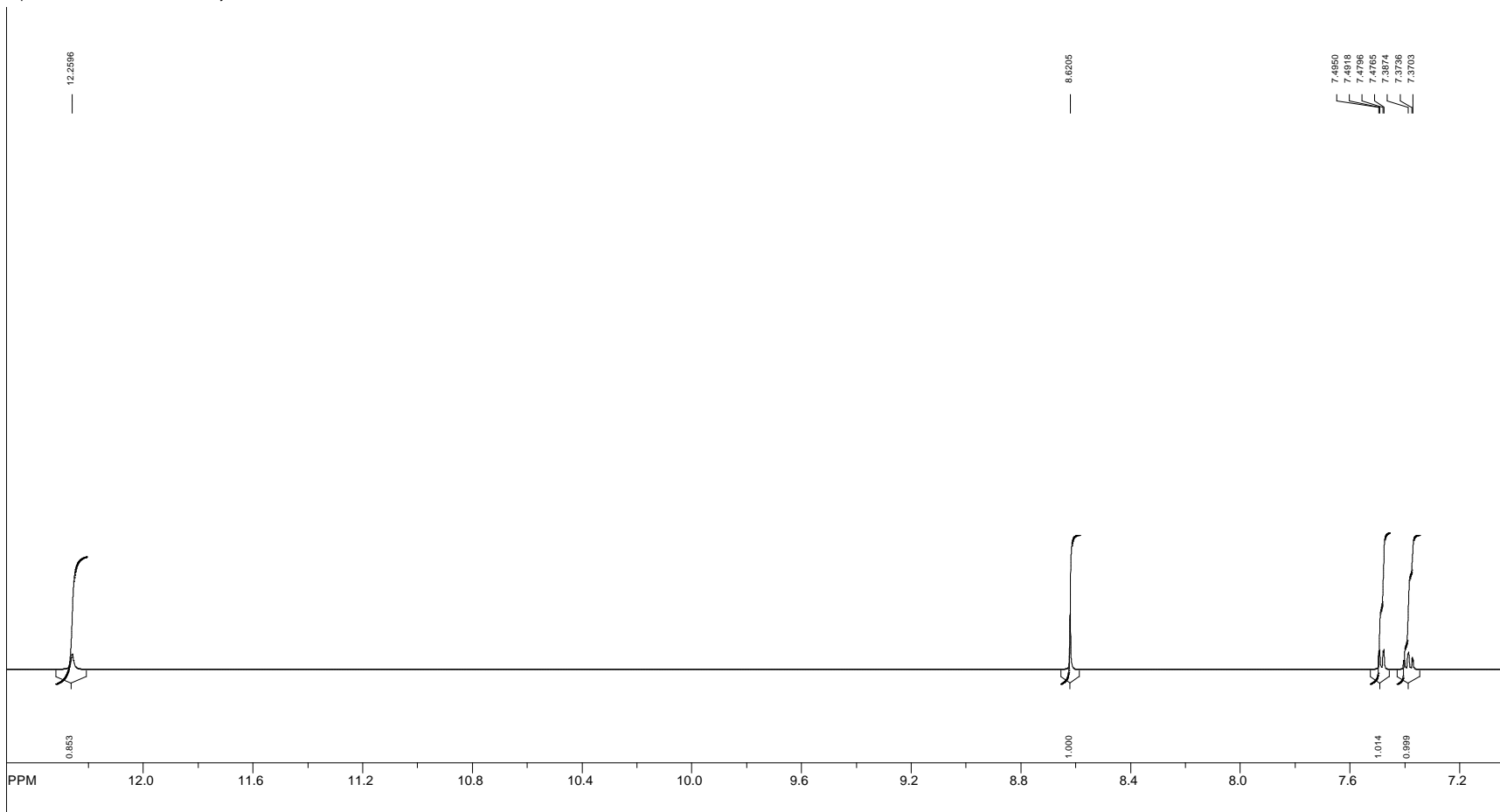
freq. of 0 ppm: 500.130019 MHz

processed size: 32768 complex points

LB: 0.000 GB: 0.0000

Figure A28: Glucosamine-pyridoxal Schiff's base (**7**) ¹H NMR.

SpinWorks 2.5: Service_Code Clyburne



file: C:\Documents and Settings\1075578\Desktop\NMR\July 23 Schiff base\Jul22-service\10fid exp1 -cg30-
transmitter freq.: 500.133270 MHz
time domain size: 65536 points
width: 10080.65 Hz = 20.155918 ppm = 0.153818 Hz/pt
number of scans: 32

freq. of 0 ppm: 500.130019 MHz
processed size: 65536 complex points
LB: 0.000 GB: 0.0000

Figure A29: Tetraacetylglucosamine-salicylaldehyde Schiff's base (**8**) ^1H NMR.

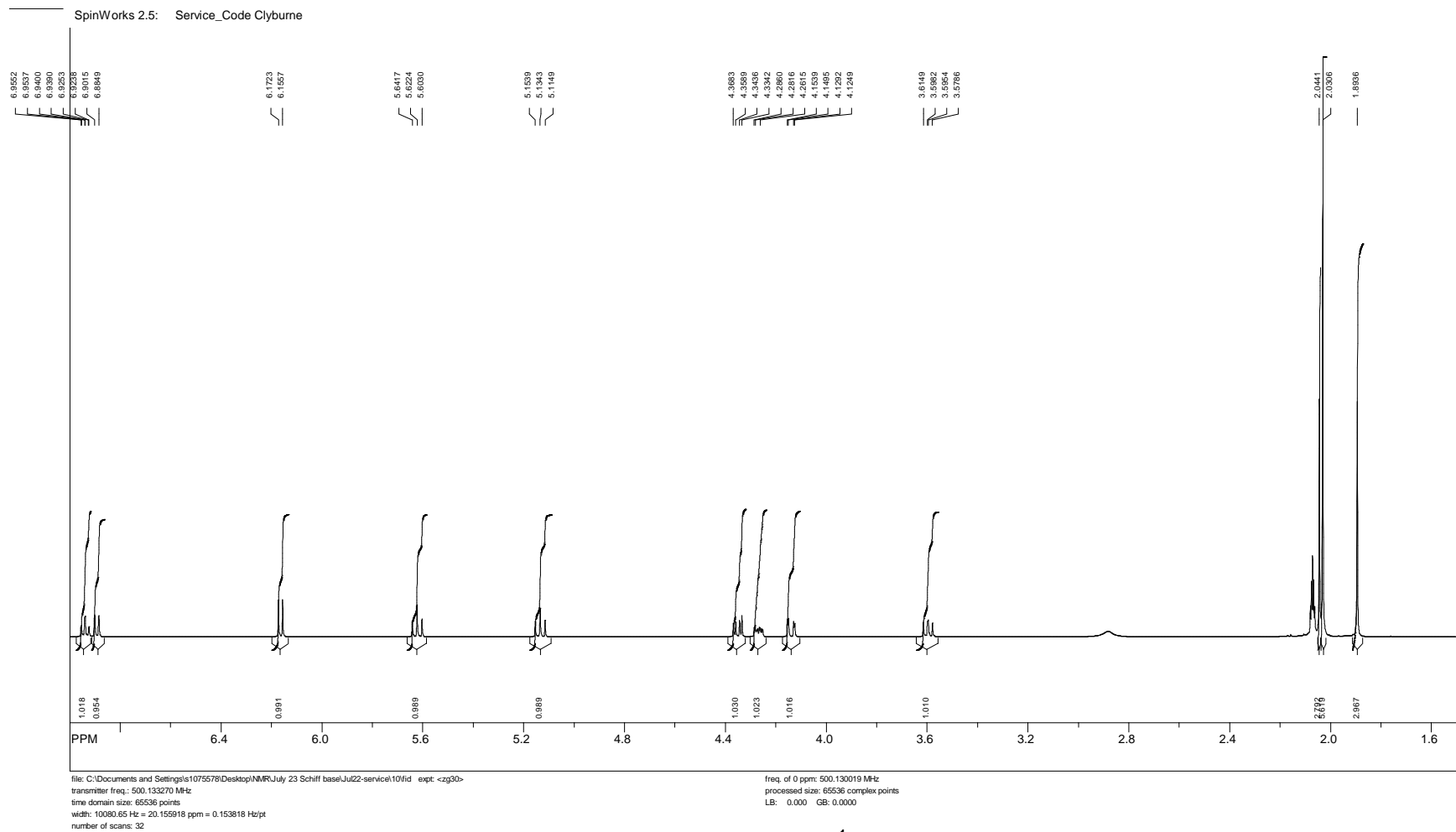
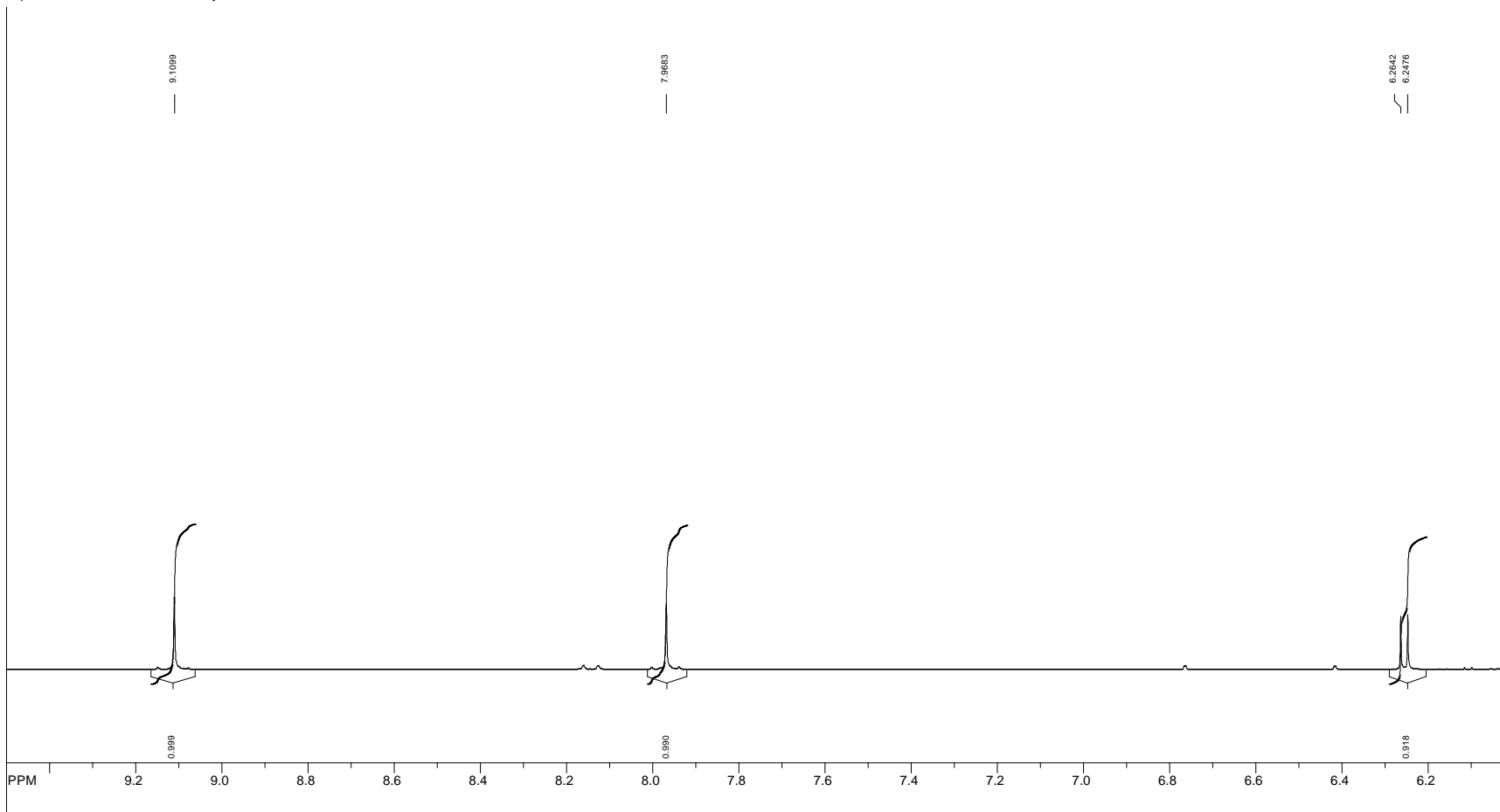


Figure A30: Tetracetylglucosamine-salicylaldehyde Schiff's base (**8**) ^1H NMR.

SpinWorks 2.5: Service_Code Clyburne

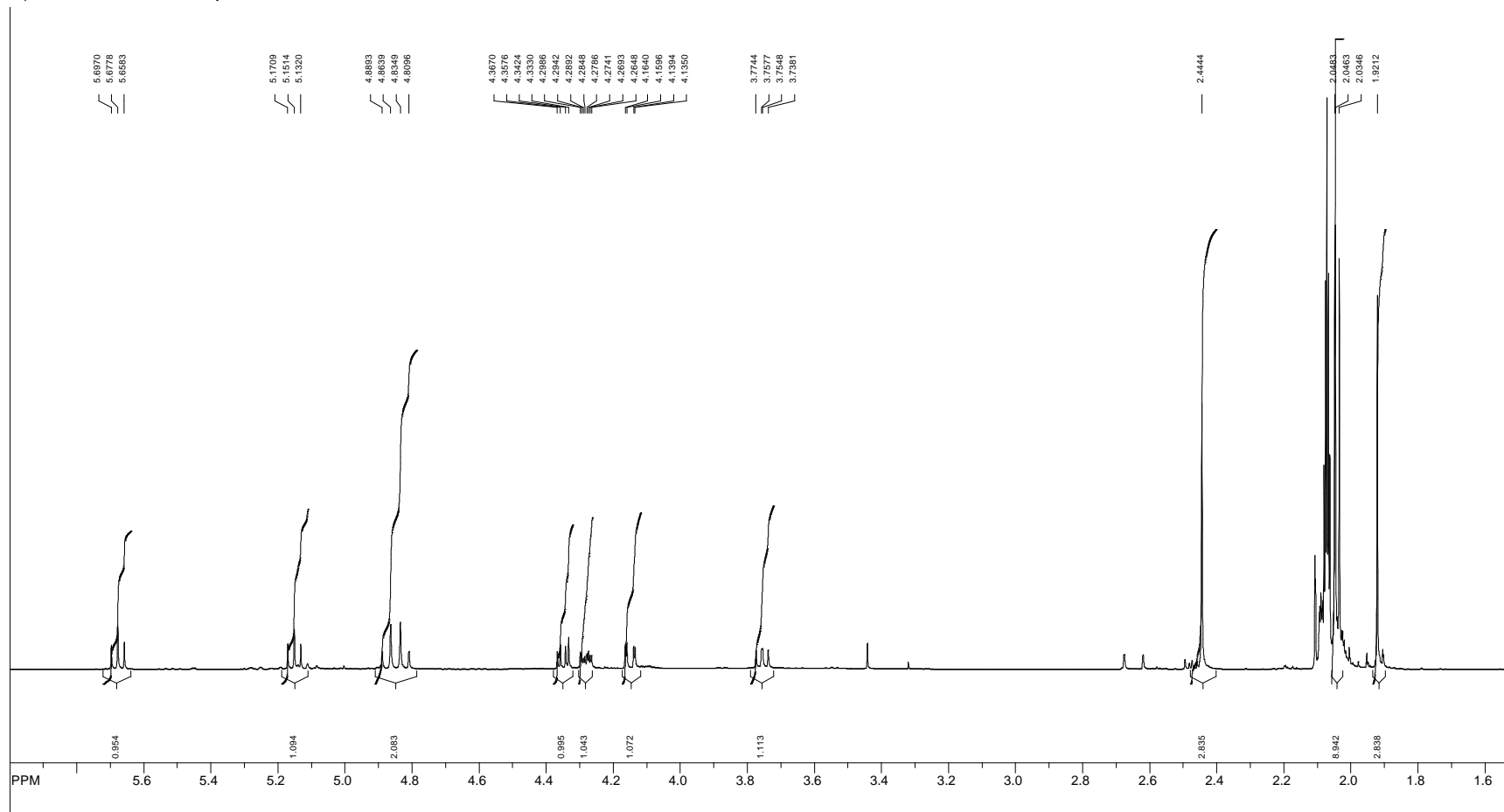


file: C:\Documents and Settings\1075578\Desktop\NMR\July 23 Schiff base\C1015B\10\fid exp: <zg30>
transmitter freq.: 500.133270 MHz
time domain size: 65536 points
width: 10080.65 Hz = 20.155918 ppm = 0.153818 Hz/pt
number of scans: 32

freq. of 0 ppm: 500.130019 MHz
processed size: 65536 complex points
LB: 0.000 GB: 0.0000

Figure A31: Tetracetylglucosamine-pyridoxal Schiff's base (9) ¹H NMR.

SpinWorks 2.5: Service_Code Clyburne



file: C:\Documents and Settings\1075578\Desktop\NMR\July 23 Schiff base\C1015B\10\fid exp: <zg30>
transmitter freq.: 500.133270 MHz
time domain size: 65536 points
width: 10080.65 Hz = 20.155918 ppm = 0.153818 Hz/pt
number of scans: 32

freq. of 0 ppm: 500.130019 MHz
processed size: 65536 complex points
LB: 0.000 GB: 0.0000

Figure A32: Tetracetylglucosamine-pyridoxal Schiff's base (**9**) ¹H NMR.

Appendix B:

Infrared spectra for selected compounds

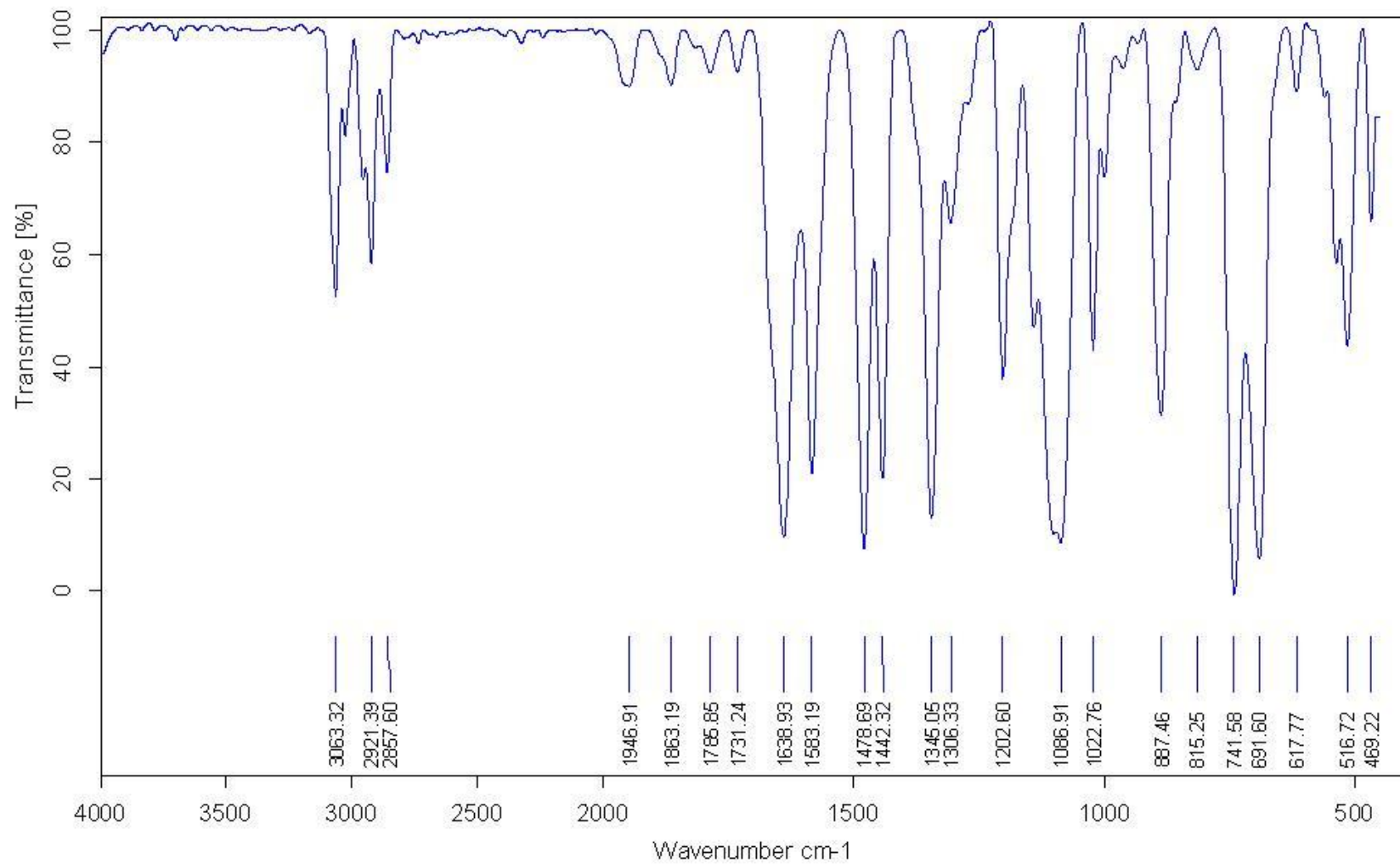


Figure B1: Trimethylphenol substituted carbon stabilized ylide (**2**) IR scan (CH₂Cl₂ solution)

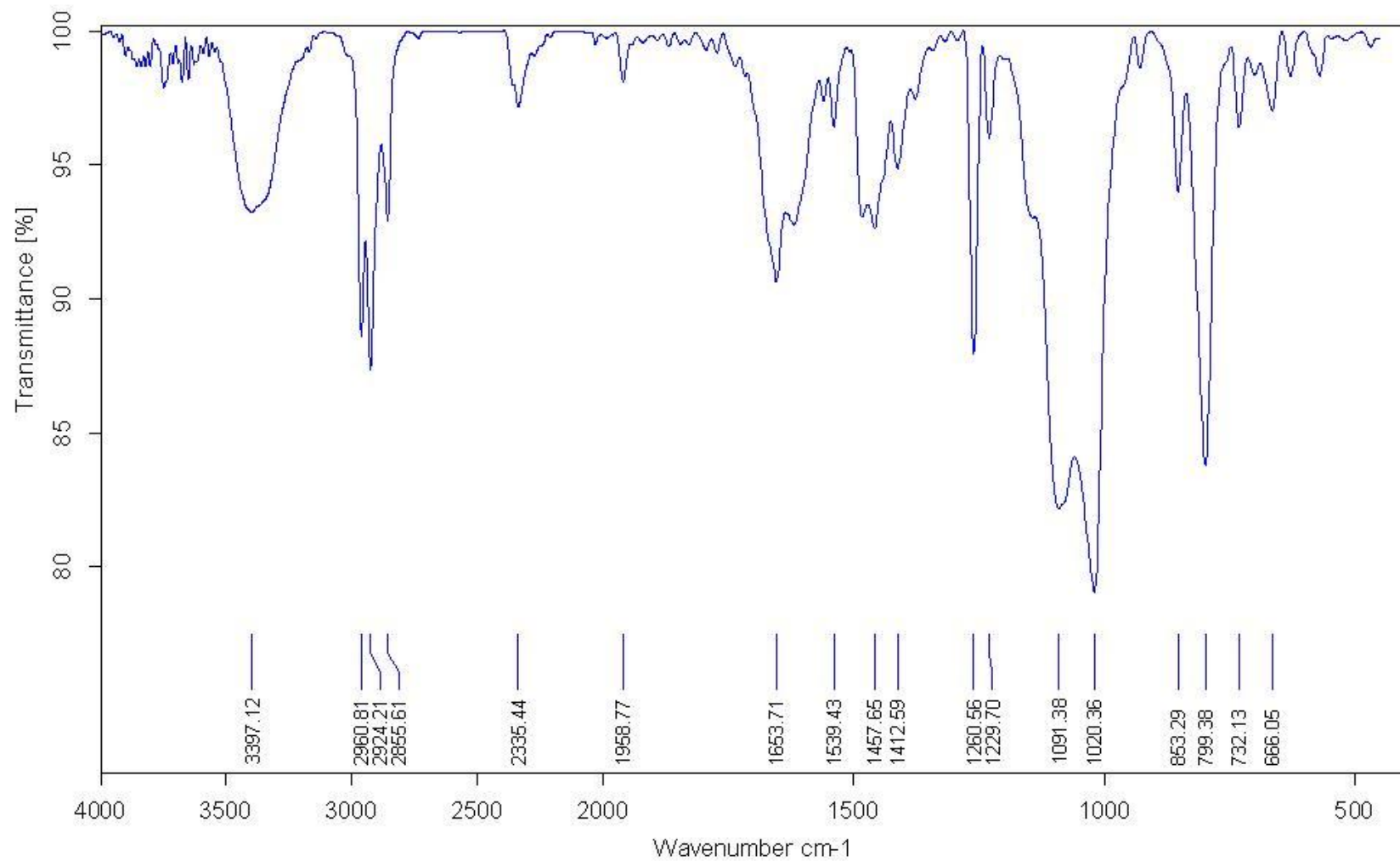


Figure B2: Tert-butylhydroxytoluene substituted carbon stabilized ylide (**3**) IR scan (CH₂Cl₂ solution)

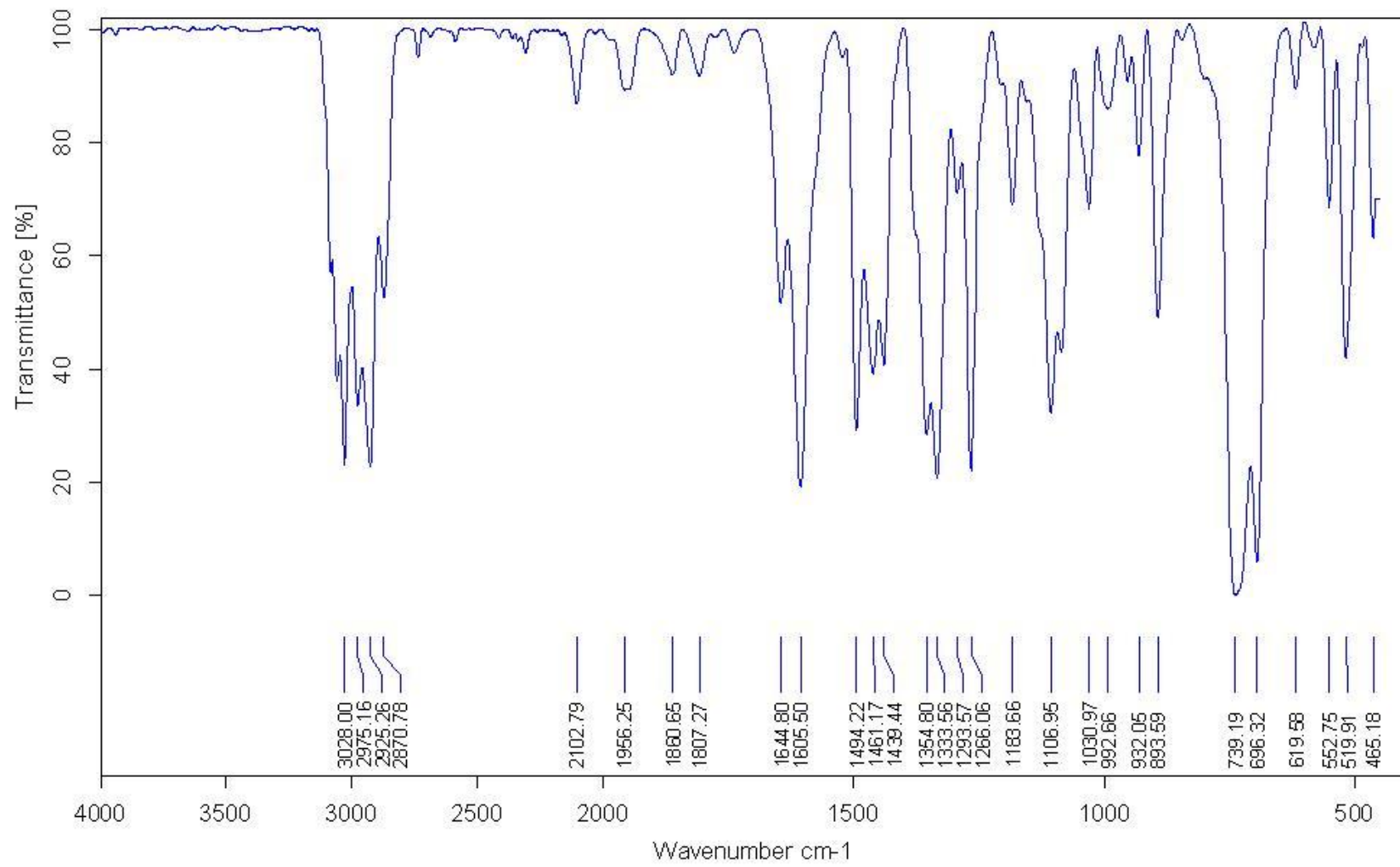


Figure B3: 1-hydroxyl-2,2,6,6-tetramethyl-piperidine substituted carbon stabilized ylide (**4**) IR scan (CH₂Cl₂ solution)

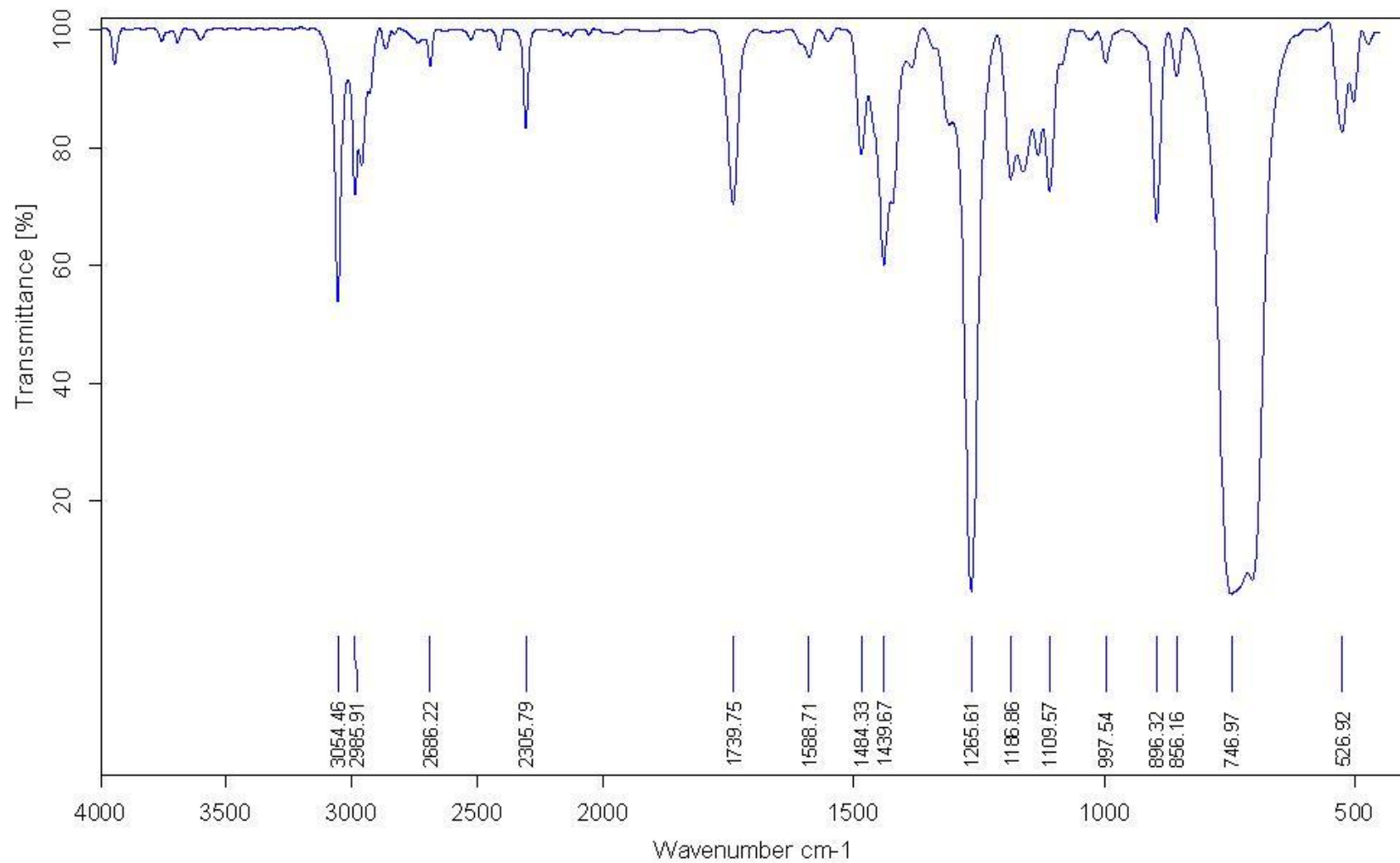


Figure B4: Methylated trimethylphenol substituted carbon stabilized ylide (**5**) IR scan (CH₂Cl₂ solution)

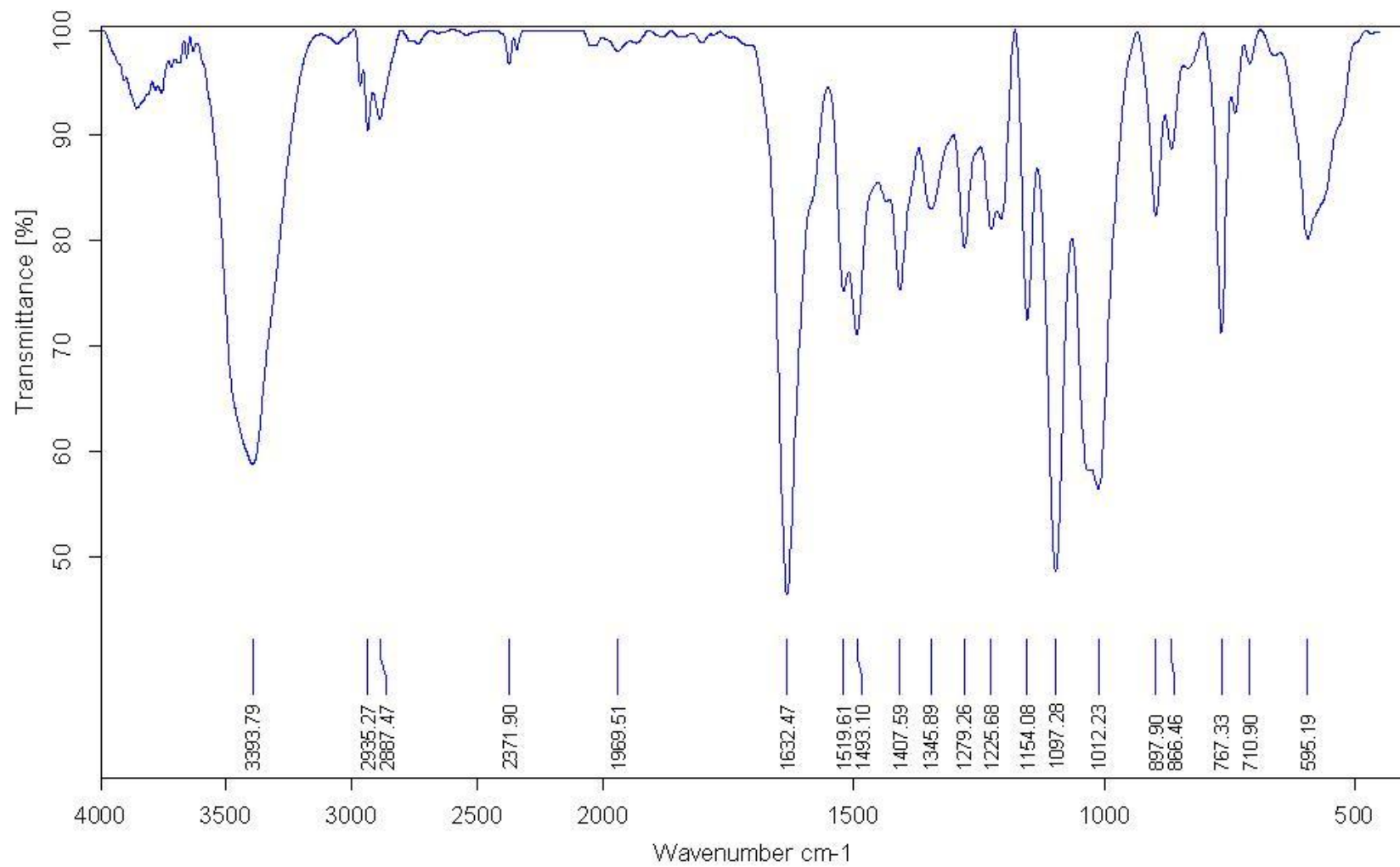


Figure B5: Choline oleate IR scan (NaCl plates)

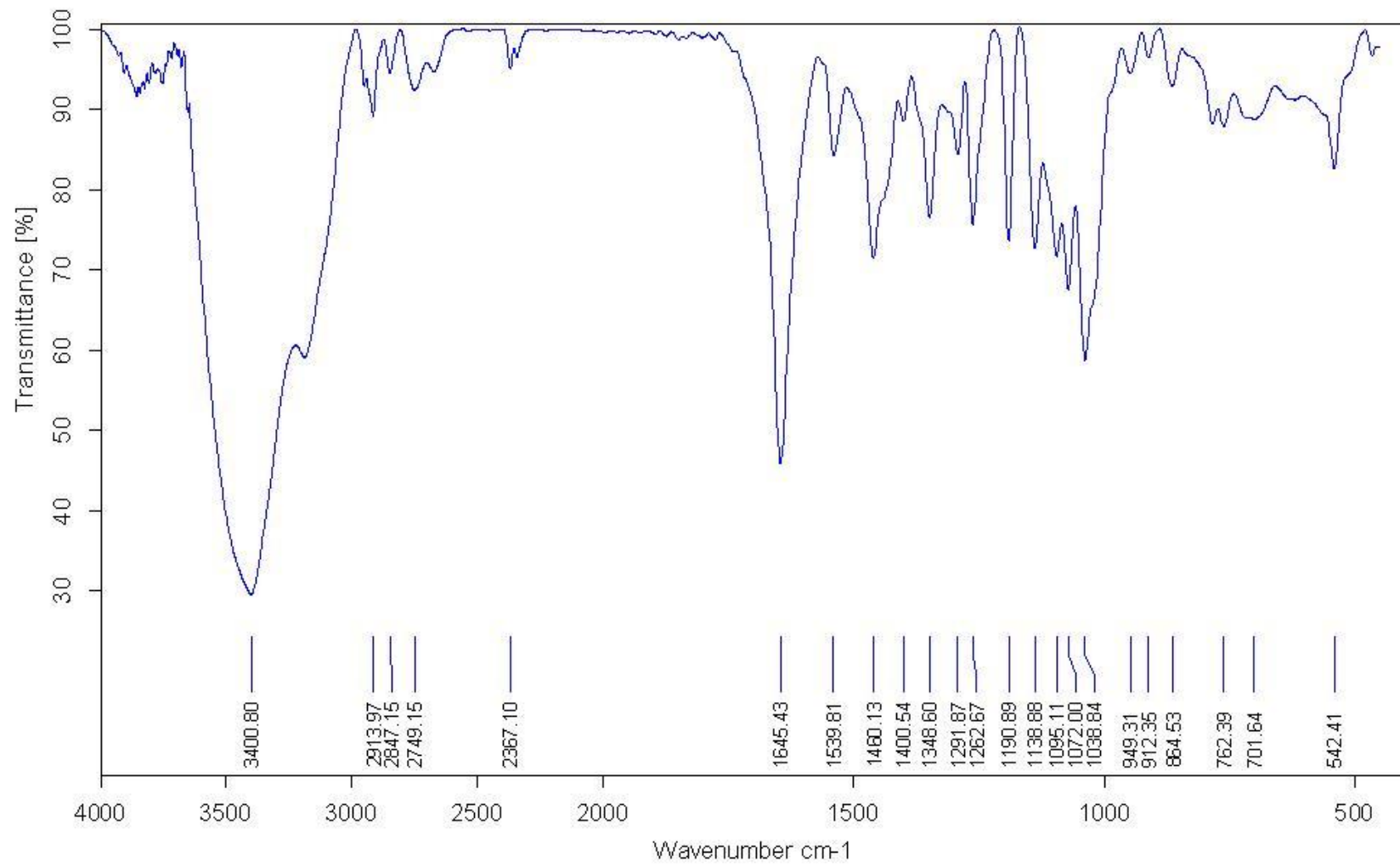


Figure B6: Choline erucate IR scan (NaCl plates)

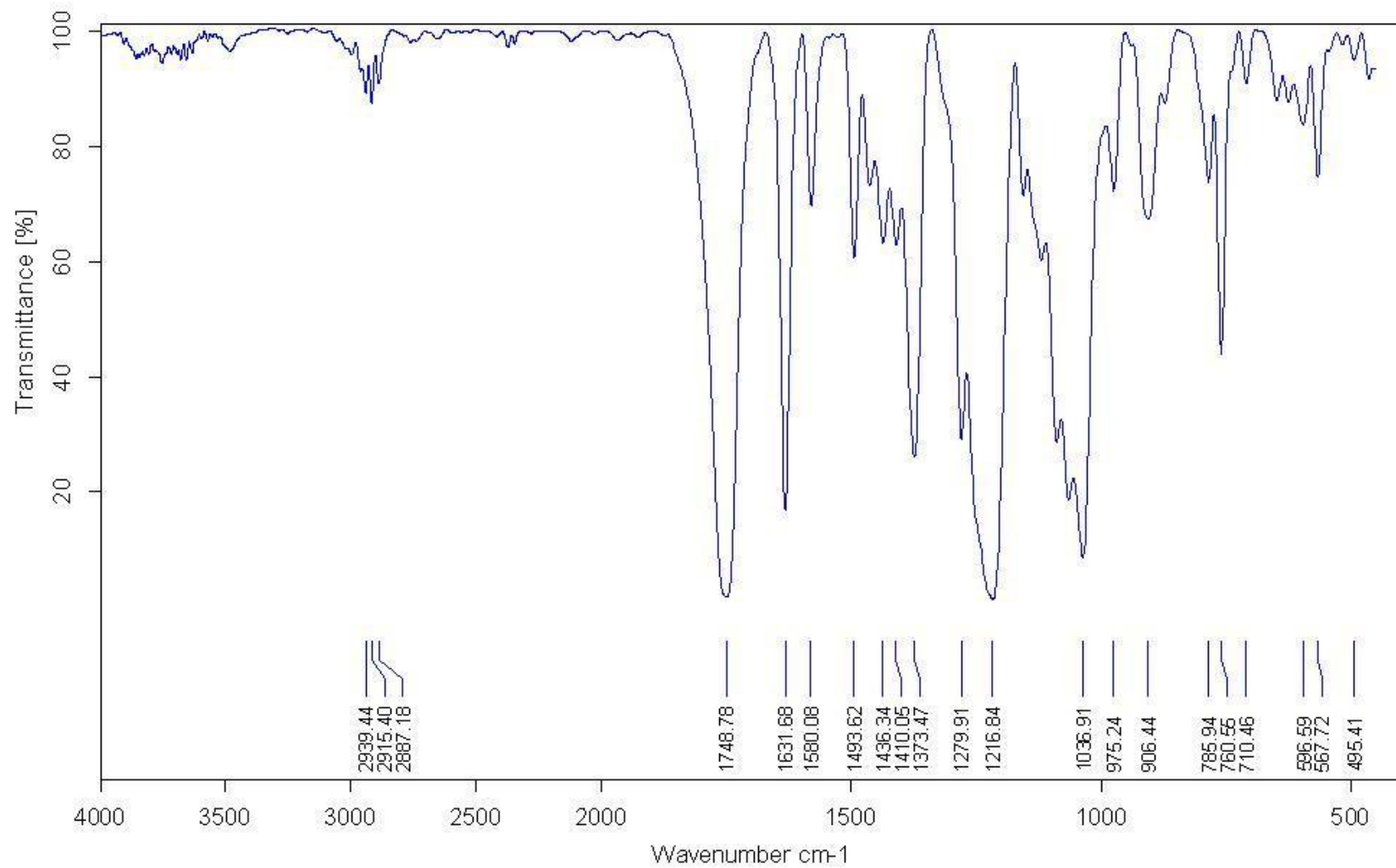


Figure B7: Choline linoleate IR scan (NaCl plates)

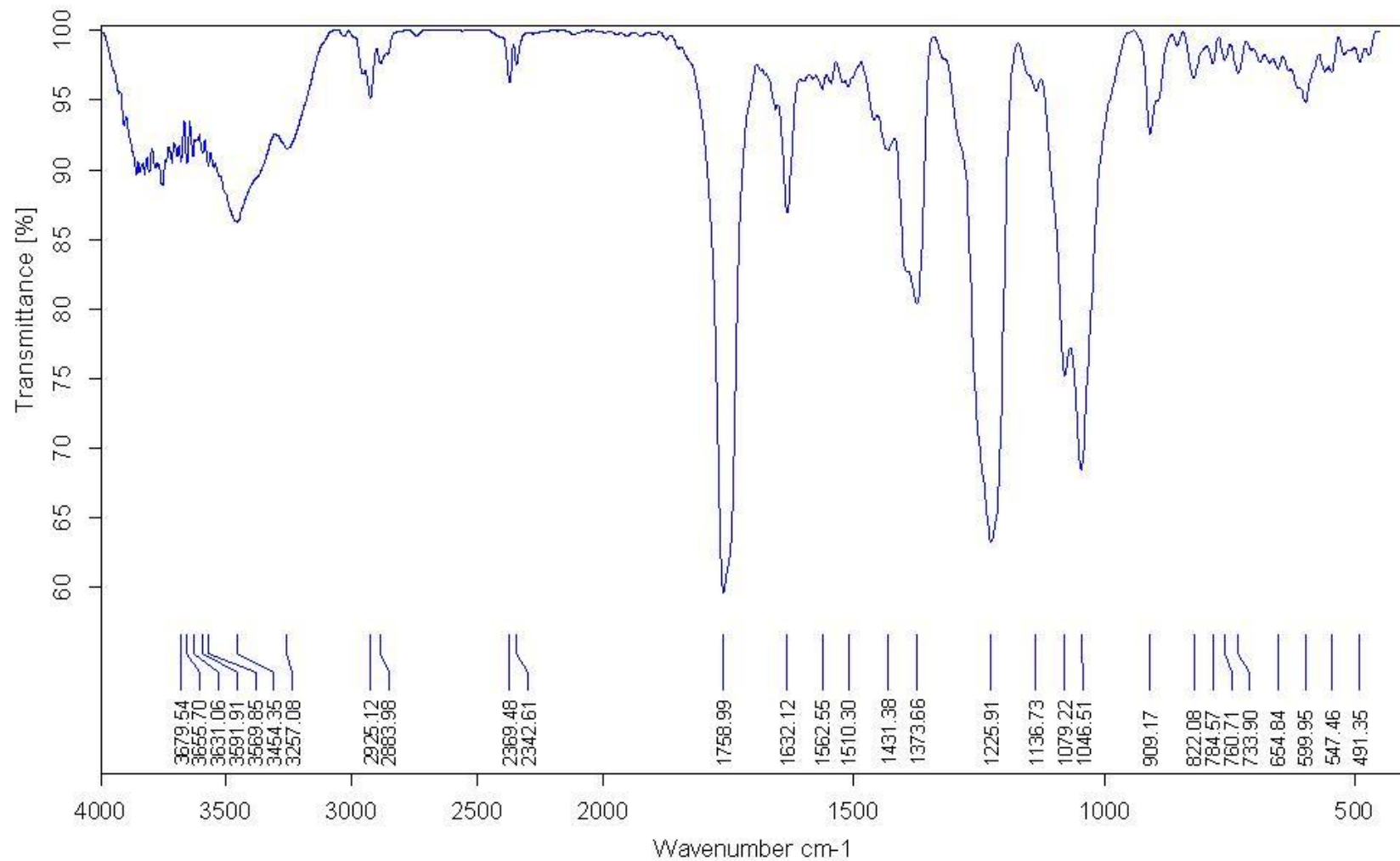


Figure B8: Choline laurate IR scan (NaCl plates)

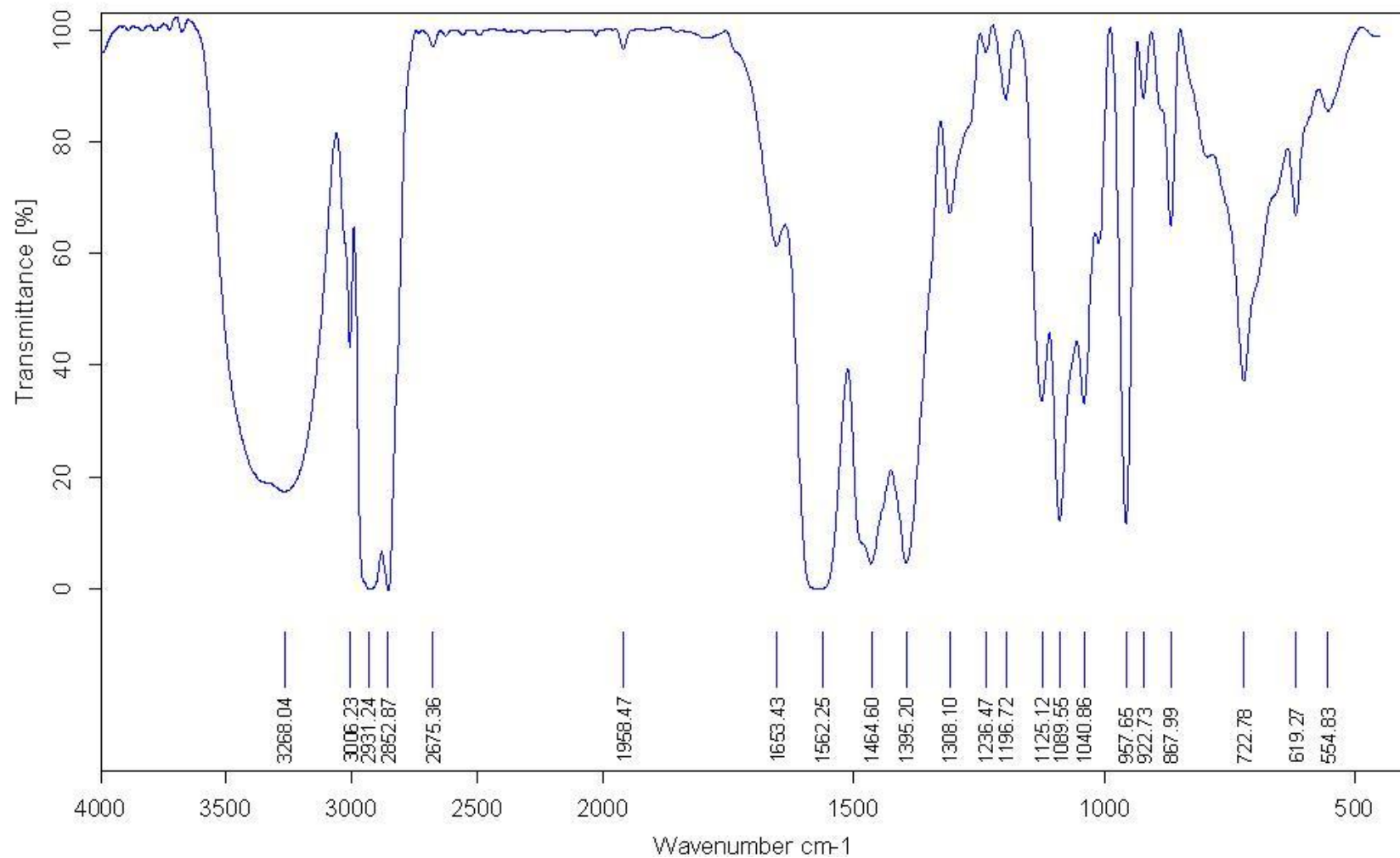


Figure B9: Glucosamine-salicylaldehyde Schiff's base (**6**) IR scan (KBr pellet)

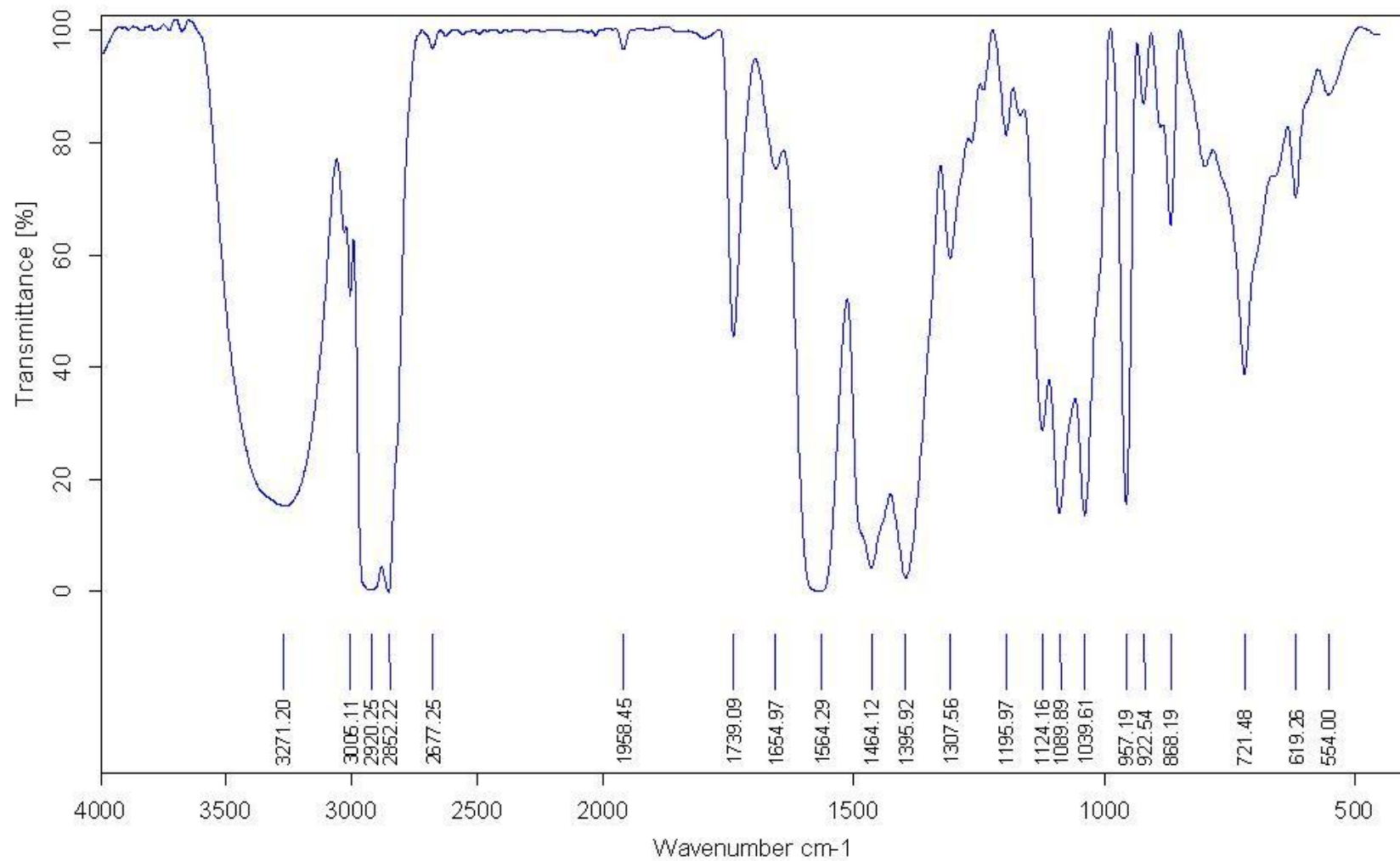


Figure B10: Glucosamine-pyridoxal Schiff's base (**7**) IR scan (KBr pellet)

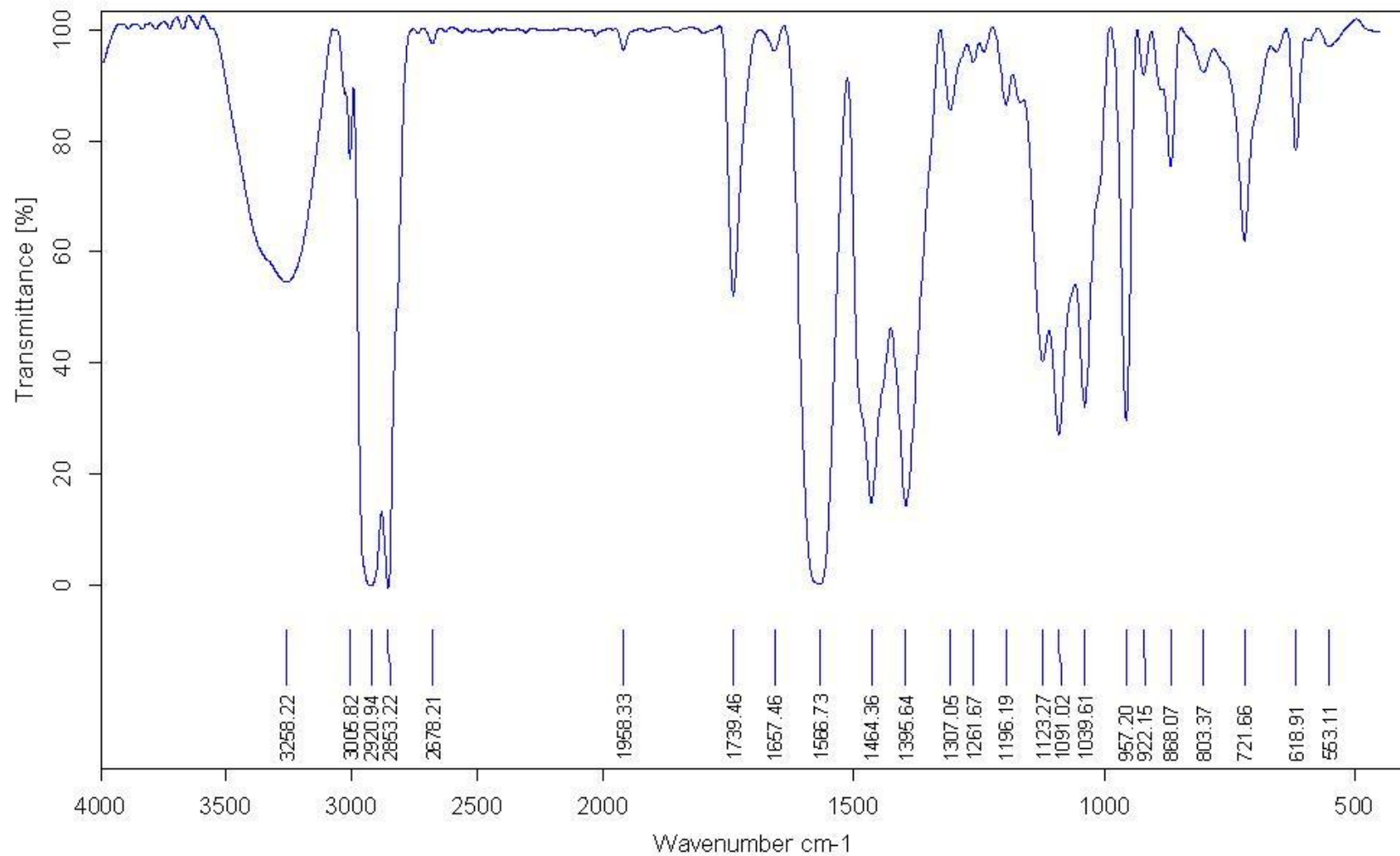


Figure B11: Tetraacetylglucosamine-salicylaldehyde Schiff's base (**8**) IR scan (KBr pellet)

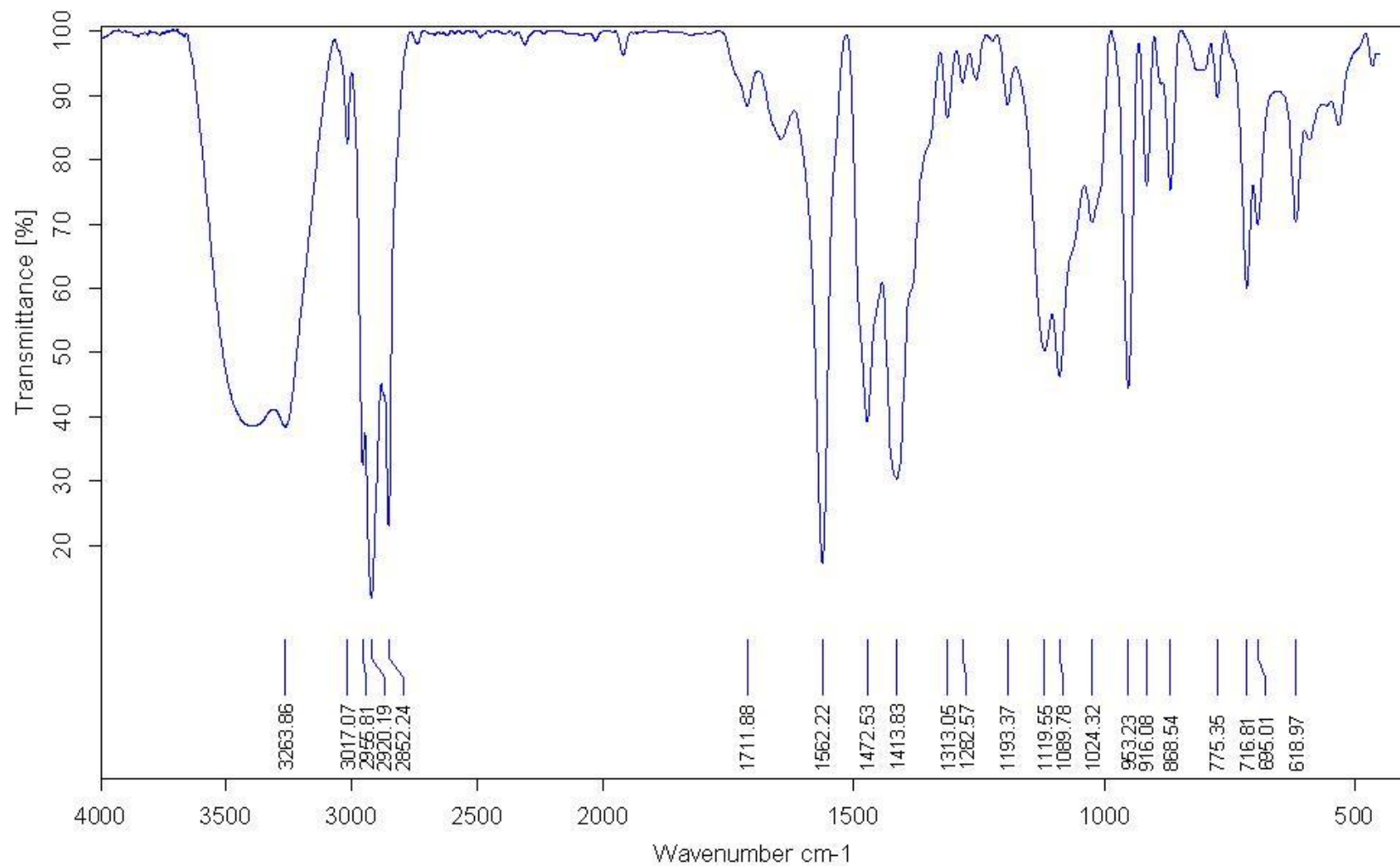


Figure B12: Tetracetylglucosamine-pyridoxal Schiff's base (**9**) IR scan (KBr pellet)